Active tectonics, Quaternary stress regime evolution and seismotectonic faults in southern central Hispaniola: implications for the quantitative seismic hazard assessment

J. Escuder-Viruete [1], F.J. Fernández [2], F. Pérez Valera [3], F. McDermott [4]

[1]Instituto Geológico y Minero España - CSIC, C. La Calera 1, 28760 Tres Cantos, Madrid. Spain
[2]Departamento de Geología, Universidad de Oviedo. C. Jesús Arias de Velasco, 33005 Oviedo. Spain
[3]Departamento de Ciencias de la Tierra y del Medio Ambiente, Universidad de Alicante. 03080 Sant Vicent de Raspeig, Alicante. Spain
[4]School of Earth Sciences. University College Dublin, Belfield. Dublin 4. Ireland.

(*) Corresponding author: Javier Escuder-Viruete.

E-mail addresses: javier.escuder@csic.es (J. Escuder-Viruete), fjfernandez@uniovi.es (F.J. Fernández), fperez@ua.es (F. Pérez Valera), frank.mcdermott@ucd.ie (F. McDermott)

Key Points:

- Active faults in central southern Hispaniola are controlled by NE-directed shortening
- Quaternary stress regime evolution includes a compressional D1 followed by a strike-slip D2, locally coeval with an extensional D3.
- Modeling establishes a very high seismic hazard zone centered in the Ocoa Bay

Abstract

Present-day convergence between Caribbean and North American plates is accommodated by subduction zones, major active thrust and strike-slip faults, which are probably the source of the historical large earthquakes on Hispaniola. However, little is known of their geometric and kinematic characteristics, slip rates and seismic activity over time. This information is important to understand the active tectonics in Hispaniola, but it is also crucial to estimate the seismic hazard in the region.

Here we show that a relatively constant NE-directed shortening controlled the geometry and kinematics of main active faults in central southern Hispaniola, as well as the evolution of the Quaternary stress regime. This evolution included a pre-Early Pleistocene D1 event of NE-trending compression, which gave rise to the large-scale fold and thrust structure in the Cordillera Central, Peralta Belt, Sierra Martín García and San Juan-Azua basin. This was followed by a near pure strike-

slip D2 stress regime, partitioned into the N-S to NE-SW transverse Ocoa-Bonao-La Guácara and Beata Ridge fault zones, as well as subordinate structures in related sub-parallel deformation corridors. Shift to D2 strike-slip deformation was related to indentation of the Beata Ridge in southern Hispaniola from the Early to Middle Pleistocene and continues today. D2 was locally coeval by a more heterogeneous and geographically localized D3 extensional deformation. Defined seismotectonic fault zones divide the region into a set of simplified seismogenic zones as starting point for a seismic hazard modeling. Highest peak ground acceleration values computed in the Ocoa Bay establish a very high seismic hazard.

1. Introduction

The present-day convergence between the Caribbean and North American plates is partially accommodated within Hispaniola Island (Dominican Republic and Haiti). As consequence, this region contains a number of major active faults with lengths of up to several hundred kilometres that stand out as geomorphological and tectonic features (Mann et al., 1991a, 2002; Hernaiz Huerta & Pérez-Estaún, 2002; Calais et al., 2016) and have been the source of some of the larges earthquakes documented in the past 250 years (Calais et al., 2010; Prentice et al., 2010; Bakun et al., 2012; Mercier de Lépinay, 2011). For example, the strike-slip system of the Enriquillo-Plantain Garden Fault Zone (EPGFZ) produced the Mw 7.0 Leogâne 12/01/2010 and Mw 7.2 Nippes 14/08/2021 earthquakes, as well as probably other historical earthquakes such as 03/06/1770 (estimated Mw 7.5; SISFRANCE Antilles, 2009) and 08/04/1860 (estimated Mw 6.3; Bakun et al. 2012).

The current tectonics in this densely populated and rapidly developing region are broadly understood (e.g., Mann et al., 1995, 2002; Hernaiz Huerta & Pérez-Estaún, 2002; Pérez-Estaún et al., 2007; Granja Bruña et al., 2014; Calais et al., 2016; Courbeau et al., 2016; Wang et al., 2018; Saint Fleur et al., 2019; Escuder-Viruete & Pérez, 2020), with underthrusting/subduction zones, major active thrust and oblique strike-slip faults identified in several clearly defined zones. However, little is known of detailed geometric and kinematic characteristics, Quaternary offsets and slip rates on these active fault systems, and its seismic activity over time is poorly constrained by geochronological data. This information is essential for understanding the present-day tectonics of Hispaniola, but it is also crucial to establish an inventory of potential seismogenic sources, a seismotectonic zonation model, and an estimate of the seismic hazard in the region.

The focus of this study is threefold: (1) to characterize the active deformation pattern and the main seismotectonic faults in southern central Hispaniola, based on tectonic and geomorphologic field observations, complemented with regional gravimetric and magnetic data analysis; (2) to determine the Quaternary to present-day stress regime evolution by inversion of geologically determined slip vectors on minor and major faults throughout the zone; and (3) to divide the region into a set of simplified seismogenic zones as a starting point for a subsequent quantitative seismic hazard modeling in terms of the peak ground acceleration (PGA).

2. Geological setting

2.1. From intra-oceanic subduction to arc-continent collision and subduction polarity reversal in the northern Caribbean plate

Located on the northern edge of the Caribbean plate, the Hispaniola Island is a tectonic collage produced by the SW-dipping Cretaceous subduction to Eocene oblique collision of the Caribbean intra-oceanic arc with the southern continental margin of North America (Mann et al., 1991a; Draper et al., 1994; Pérez-Estaún et al., 2007; Escuder-Viruete et al., 2011a, 2011b, 2013, 2016b). The main consequence of the arc-continent collision were the blocking of the suture zone, the transfer of deformation to the back-arc region in southern Hispaniola and subduction polarity reversal, with renewed subduction beginning along a new NE-dipping subduction zone (e.g., Kroehler et al., 2011).

The geodynamic modeling software *GPlates* V2.3 (Müller et al., 2018; www.gplates.org) and observations presented in this paper allows the reconstruction of this relative movement between the

Caribbean and North American plates, distinguishing three main stages of evolution from the lower Campanian to the present-day. In the lower Campanian (80 Ma), the Lower Cretaceous Caribbean island-arc is moving to the northeast at a rate of about 4-5 cm/yr (Fig. 1a). By this time, the Caribbean arc had overridden the Galapagos hotspot, giving rise to a period of vigorous submarine oceanic plateau volcanism that began as early as 139 Ma and was widespread by 88 Ma, building the Caribbean Large Igneous Province (CLIP). In a SW-dipping subduction zone, the intra-oceanic arc consumed through subduction the large area occupied by the proto-Caribbean oceanic crust in the current central part of the Caribbean, and obliquely collided with the Maya block of the southeastern margin of the North American plate (Mann et al., 2007).

By the middle Eocene (40 Ma) the collision and suturing of the Caribbean island-arc against North America had finished the forward motion of the oceanic arc (Fig. 1b). Arc-continent collision caused the extinction of the volcanism, the emplacement of supra-subduction zone ophiolites and developed a zone of NE-directed foreland thrusting on the lower plate (Mann et al., 1991a; Pindell & Kennan, 2009; Pérez-Estaún et al., 2007; Escuder-Viruete et al., 2013, 2016b). Because the arc can no longer subduct the more continental crust of North America, convergence was accommodated by back-thrusting and the initiation of a new, NE-dipping subduction zone (Kroehler et al., 2011). In southern Hispaniola, the arc-continent collision in the middle to upper Eocene resulted in a reversal of subduction polarity in the back-arc region, as well as deformation by back-thrusting at the resulting Peralta-Muertos accretionary prism (Witschard & Dolan, 1990; Mann et al., 1991b; Dolan et al., 1991; Hernáiz-Huerta & Pérez-Estaún, 2002). The new subduction zone separated the Venezuela basin from the upper island-arc crust of central Hispaniola.

Since the lower Miocene, the ENE movement of the Caribbean plate gave rise to the oblique collision/accretion of the northern sector of the Caribbean oceanic plateau of transitional crust with the Peralta accretionary prism, resulting in the formation of the SW-directed Haitian-Neiba fold-and-thrust belt and the San Juan-Azua basins in the foreland (Fig. 1c; Mercier de Lépinay, 1987;

Witschard & Dolan, 1990; Dolan et al., 1991; Heubeck & Mann, 1991; Pubellier et al., 2000; Hernáiz-Huerta & Pérez-Estaún, 2002; Granja Bruña et al., 2014; Escuder-Viruete et al., in press). During the Pliocene and until the present-day, convergence gave rise to the accretion of the central sector of the Caribbean oceanic plateau of thickened crust, causing in southern Hispaniola the uplift and folding of the Massif de la Serre-Sierra Bahoruco and the tectonic individualization of the Enriquillo-Cul de Sac basin. The blue star and line in the Fig. 1c represents the reconstructed location and path of a point of the Sierra Bahoruco as it travels with the Caribbean plate. *GPlates* reconstruction shows that the point started traveling to the NE at a rapid rate of 3-5 cm/yr and changed to a ENE direction in middle Eocene times (45 Ma) with a slow rate of 0.7-2.1 cm/yr. This change coincides with the arc-continent collision in northern Hispaniola and the start of subduction by back-thrusting in the Peralta-Muertos belts of southern Hispaniola.

2.2. Present-day geodynamic configuration of southern Hispaniola

Oblique collision has also led to the fragmentation of the northern Caribbean plate into several microplates, which are Septentrional (or North Hispaniola), Hispaniola-Puerto Rico and Gônave (Fig. 2; Mann et al., 1995; Calais et al., 2016; Rodríguez-Zurrunero et al., 2019). Microplates are limited by large-scale fault zones that, as reflected by the associated seismicity and modeled displacement rates, accommodate part of the relative movement between them (Mann et al., 2002; Manaker et al., 2008; Benford et al., 2012; Symithe et al., 2015; Calais et al., 2016; Corbeau et al., 2019).

In northern Hispaniola, the Septentrional microplate is a wedge-shaped tectonic forearc sliver, limited offshore to the north by the Northern Hispaniola Fault Zone (NHFZ, or western extension of the Puerto Rico Trench) and onshore to the south by the Septentrional Fault Zone (SFZ; Dolan et al., 1988; Mann et al., 2002; Escuder-Viruete and Pérez, 2020; Escuder-Viruete et al., 2020).

The Hispaniola-Puerto Rico microplate is an arc-crust block, limited to the north by the SFZ and to the south by the Muertos Trough (MT). To the west, the boundary between the Hispaniola block and Gonâve microplate is generally placed in the San Juan-Los Pozos fault zone (SJPFZ; e.g., Mann et al., 1991). From N to S (Fig. 2), the Hispaniola microplate includes the Cordillera Central domain and the Peralta-Muertos deformed belts. The Cordillera Central in the Dominican Republic and its prolongation in the Massif du Nord in Haiti is an Upper Jurassic-Upper Cretaceous basement composed mainly of Pacific-derived oceanic units, structurally limited to the northeast by the Hispaniola fault zone (HFZ) and to the southwest by the SJPFZ (Mann et al., 1991). It comprises fragments of oceanic lithosphere, plutono-volcanic complexes related to subduction, and basaltic units related to a mantle-plume magmatism (Escuder-Viruete et al., 2008). It also comprises the Quaternary intramountain basins of Cibao, Jarabacoa, Bonao, Constanza, Rancho Arriba and San José de Ocoa (Fig. 3).

The Peralta Belt (PB) is a NW-trending and SW-verging fold-and-thrust belt, structurally sandwiched between the San José-Restauración (SJRFZ) and the San Juan-Pozos fault zones (Mann et al., 1991b). The belt evolved from a back-arc basin for the Caribbean island-arc, with deposition of Campanian to Eocene turbidites (Trois Rivières and Las Palmas Formations), through a transpressive fold-and-thrust belt in the middle Eocene to early Miocene (Mercier de Lépinay, 1987; Witschard & Dolan, 1990; Dolan et al., 1991; Hernáiz-Huerta et al., 2007b). In the SE sector, the lithostratigraphic units of the Peralta Belt have been grouped into three thick sedimentary sequences, separated from each other by major unconformities: the Paleocene-Eocene Peralta Group; the middle Eocene-early Miocene Río Ocoa Group; and the middle Miocene-Pleistocene Ingenio Caei Group (Heubeck et al., 1991; Dolan et al., 1991; Díaz de Neira & Solé Pont, 2002; Hernaiz Huerta & Pérez-Estaún, 2002; Hernáiz-Huerta et al., 2007a; Pérez-Valera, 2010).

The Muertos Trough (MT) marks the boundary between the subducting/underthrusting floor of the Caribbean plate and the overlying deformed belt south of eastern Hispaniola and Puerto Rico (Fig.

2). The thrust focal mechanism of the 24/06/1984 earthquake (Mw 6.7) indicates subduction along the MT (Byrne et al., 1985). Seismic reflection profiles across the MT image an N-dipping low-angle thrust structure, with folded and faulted sedimentary rocks on top forming an accretionary prism (Driscoll & Diebold, 1998; Dolan et al., 1998; Mauffret & Leroy, 1999; Granja Bruña et al., 2009, 2014). Convergence across the Muertos Trough probably begins with the end of the arc-continent collision and the onset of back-thrusting. *GPlates* reconstruction shows that the amount of oblique subduction of the Caribbean plate beneath southern Hispaniola at the westernmost Muertos Trench has been about 100 km (Fig. 1).

The Gonâve microplate is limited to the north by the Oriente Fault Zone and to the south by the Enriquillo-Plantain Garden fault zone (EPGFZ). The nature of the crust of the Gonâve microplate is not well established, having been proposed as a Cretaceous-Eocene remnant arc (Heubeck et al., 1991), back-arc (Mann et al., 1991a) or the rifted crust of the eastern Cayman continental passive margin (Corbeau et al., 2017, 2019). From the lower Miocene onwards, the oblique collision/accretion processes have formed the Haitian-Neiba deformed belt in the microplate. It consists of a NW-trending and SW-verging fold-and-thrust belt, bounded to the north by the NE-dipping SJPFZ (Mann et al., 1995; Pubellier et al., 2000; Hernáiz Huerta et al., 2007a). The thrust bounding the NE Montagnes Noires-Sierra de Neiba thrust sheet was activated during the lower-middle Miocene and the thrust bounding the SW Chaîne des Matheux-southern Sierra de Neiba thrust sheet was developed from the middle-upper Miocene (Pubellier et al., 2000). Tilting and faulting of Quaternary age deposits in the northern margin of the Enriquillo basin indicate that the thrust belt is still active (Hernáiz Huerta et al. 2007), which is consistent with the seismic activity recorded by Corbeau et al. (2019).

The Beata Ridge is a prominent NE-trending bathymetric high of about 450 km long built on the Caribbean plate (Mauffret and Leroy, 1999; Mauffret et al., 2001; Granja Bruña et al., 2014). It separates the Haiti basin to the west, from the Venezuelan basin to the east (Fig. 2). The width of this structure in the zone of interaction with the Hispaniola-Puerto Rico microplate is about 120 km. The ridge comprises an unusually thick oceanic crust, essentially made up of mafic igneous rocks (gabbros, dolerites and basalts) of the Cretaceous CLIP (Sinton et al., 1998; Révillon et al., 2000; Dürkefälden et al., 2019). The Cretaceous basement of the Sierra Bahoruco and Hotte-Selle Massifs is made up of submarine volcanic rocks with similar petrological and geochemical characteristics, indicating that the Southern Peninsula of Hispaniola is an emerged fragment of the CLIP (Escuder-Viruete et al., 2016a).

Onshore/offshore seismic refraction and wide-angle reflection studies indicate a crustal thickness of 26 to 32 km in the Sierra Bahoruco, 20 to 22 km at the Beata Ridge, 10 to 15 km in the Venezuelan basin and only 5 to 10 km in the Haitian basin (Nuñez et al., 2016, 2019; Kumar et al., 2020). The crustal thickness of the Beata Ridge is controlled mainly by NNE to NE-striking faults, such as the Beata Ridge fault zone (BRFZ) that follows its axial trend (Mauffret et al., 2001). According to Granja Bruña et al. (2014), this fault acted in pre-Neogene times as a normal fault. The BRFZ continues to the NE, abruptly limiting the Sierra Bahoruco and Sierra Martín García to the southeast, until it intersects the SJPFZ in the western Ocoa Bay.

The NE-directed collision and impingement of the thickened crust of the Beata Ridge with the Hispaniola microplate in the Neogene gave rise to a recess of the Muertos accretionary prism and the clockwise rotation of fold and thrust structures of the Peralta Belt east of the Ocoa Bay (Mercier de Lépinay et al. 1988; Mann et al., 1991b; Hernaiz Huerta and Pérez-Estaún, 2002; Granja Bruña et al., 2014). Part of the present-day stress-field induced by the Beata Ridge collision is accommodated by the Ocoa-Bonao-La Guacara Fault Zone (OBFZ) within the Hispaniola microplate (Escuder-Viruete et al., in press). This fault zone is an active, NNE to NE-striking large-scale fault system that crosses the southern central sector of Hispaniola along more than 250 km (Pérez-Estaún et al., 2007). In the eastern Ocoa Bay, the OBFZ bends the fold and thrust structures of the Peralta Belt, the SJPFZ and the lower Miocene to Early Pleistocene sedimentary fill of the Azua basin (Fig. 2). This fault zone has recently been proposed as the onland transition between oceanic subduction and arc-oceanic plateau collision (Escuder-Viruete et al., in press).

3. Methodology

3.1. Bathymetric, gravimetric and magnetic data sets

Maps shown in this study were created using several topographic and bathymetric data sets: (1) digital elevation models (DEMs) from the Shuttle Radar Topography Mission-30 Plus (https://www2.jpl.nasa.gov/srtm/) with a resolution of 30 m (Tozel et al., 2019); (2) DEMs obtained from ALOS Global Digital Surface Model with a resolution of 25 m (Takaku et al., 2020); (3) satellite images from *Google Earth Pro*® (http://earth.google.com) with a resolution from 1 km to 10 m; and (4) topographic and bathymetric profiles obtained from the GMRT data-set (available with *GeoMapApp*; www.geomapapp.org; Ryan et al., 2009).

The gravity data are from the compilation by the National Geospatial-Intelligence Agency (https://www.nga.mil). This compilation includes data from various campaigns conducted onland between 1939 and 1991 by IFREMER, Royal Astronomical Society, Cambridge University, Lamont-Doherty Geological Observatory and Woods Hole Oceanographic Institution. This compilation contains 3012 stations with a resolution of ±2 mGal and a density reduction of 2.67 g/cm^3.

The magnetic data come from the magnetic and radiometric flight carried out between 1995 and 1997 by the Compagnie Générale de Géophysique (CGG) in the onland territory of the Dominican Republic, with 500 m of separation of lines and a nominal height of 120 m, in the context of the SYSMIN Program of the EU of *Cartografía geotemática de la República Dominicana* (García Lobón & Rey Moral, 2004). Data were gridded at 250 m and several procedures were followed to ensure data quality, such as micro-levelling and filtering of frequencies greater than Nyquist.

3.2. Regional analysis of potential field data

In this work, lithological, structural, gravimetric and magnetic data were analyzed together to constrain the crustal structure underlying southern central Hispaniola, to establish the distribution of different crustal blocks with specific geophysical properties at the surface and to identify their tectonic boundaries (even when they are hidden by a recent sedimentary cover). The analysis of the potential field data was carried out with the *Geosoft Oasis Montaj*® software. Gravity data has been gridded using a minimum curvature algorithm, resulting a grid cell size of 250 x 250 m.

Magnetic grids were calculated from raw data provided by CGG. Qualitative interpretation of the magnetic data has been made using a reduction technique to the pole of the total magnetic field. This reduction to the pole was calculated assuming a local inclination of 48° N and declination of 10° W. This process removes the inclination effect of the total magnetic field by transforming the anomaly into the vertical component of the field produced as if the source were at the North magnetic pole - 90° inclination. The inclination and declination used in the reduction to the pole were calculated from the International Geomagnetic Reference Field subroutine in *Oasis Montaj*® based on the latitude and longitude. Gravimetric and magnetic grids were interpreted on variations in amplitude, wavelength character, lineament distribution, texture, and structural discontinuities. More details of the methodology of acquisition and analysis of the potential field data are included in García-Lobón & Rey-Moral (2004), García-Lobón & Ayala (2007) and Ayala et al., (2017).

3.3. Seismicity

Compilation of an earthquake catalog allowed us to determine the spatial and temporal distribution of earthquakes, their relationships with the main active fault zones, and the characterization of the seismotectonic structures in terms of their seismic parameters. For southern central Hispaniola, the catalog was compiled by collecting and analyzing historical data (SISFRANCE-Antilles 2009; Bertil et al., 2010; Flores et al. 2011; McCann et al. 2011; ten Brink et al. 2011; Bakun et al., 2012; and references herein) and instrumental/experimental data (Russo & Villaseñor 1995; Alvarez et al.

1999; Tanner & Shepherd 1997; Terrier-Sedan & Bertil, 2021; ISC 2014; RSPR-Puerto Rico catalogue, and USGC-NEIC catalogue). Access the local network, constituted by the *Instituto Sismológico de la Universidad Autónoma de Santo Domingo* (ISU; uasd.edu.do), the *Observatorio Sismológico Politécnico Loyola* (OSPL; ospl.ipl.edu.do) and the Projet Ayiti-Seismes performed by Laboratoire Mixte International CARIBACT (ayiti.unice.fr/ayiti-seismes; BME, UEH/FDS/URGéo, ENS and Géoazur partnership), enabled information on earthquakes in ghost areas of the global seismic network to be obtained. Following Bertil et al. (2010, 2015), the catalogue was revised for data quality, duplication, and foreshocks or aftershocks, and then homogenized the magnitudes using the moment magnitude scale (*Mw*). The most contemporary sources describing the historical earthquakes were investigated to establish the focal characteristics of each seismic event.

Due to the high uncertainty related to the magnitude and location of historical earthquakes, the earthquakes in the catalogue were classified into three groups following Terrier-Sedan and Bertil (2021): historical data before 1750 of unreliable magnitude and location; historical data between 1750 and 1960 of intermediate quality; and instrumental data after 1960 generally of high quality. More than 12 epicentres of earthquakes of magnitude at least Mw 6.0 are located in the study area, or the immediate surroundings, including the earthquakes of 1562 (destroyed La Vega and Santiago de los Caballeros), 1615 (destroyed Santo Domingo), 1684 (affected Azua and Santo Domingo), 1691 (destroyed Azua, affected Santo Domingo), 1751 (destroyed Azua) and 1911 (affected San Juan).

3.4. U-Th geochronology

Fossil coral reefs provide a snapshot of the ocean environment and sea level during their growth. As uranium is incorporated into the coral calcium carbonate skeleton during its growth, the U-Th geochronology method is appropriate for dating geological and oceanographic events in the Quaternary (e.g., Hibbert et al., 2016). To limit the effects of element mobility during diagenesis and/or any chemical alteration, coral samples were collected in apparently unaltered sectors on top of fossil wave-cut platforms and paleo-cliffs of the topographically lower terraces, as well as on the sides of small narrow gorges cut through the higher terraces. Fragments of corals that preserve the pristine growth structure were selected in the field. Subsequently, thin sections of these fragments were examined under the petrographic microscope to characterize the crystalline habit, the mineralogy as indicated by staining for carbonate minerals, and the degree of neomorphism. Coral fragments with an excellent preservation of the original skeleton and primary pore spaces void of cement and sediment were selected. Fragments were ground and the resulting powder analyzed by X-ray diffraction analysis at the IGME Laboratories in Madrid. Samples selected for U-Th dating yielded more than 95% aragonite during diffraction analysis. This test eliminated most samples of the topographically higher coral reef terraces.

U-series measurements were carried out using a high-resolution multi-collector inductively coupled plasma mass-spectrometer (ThermoFisher Neptune® multi-collector equipped with an Aridus® desolvation nebuliser) at the National Centre for Isotope Geochemistry, University College Dublin. Samples were spiked with a mixed ^{229}Th-^{233}U-^{236}U spike and were slowly dissolved in 7M HNO_3. Following overnight sample-spike equilibration, U and Th fractions were separated using anion ion-exchange columns using standard methods (Fankhauser et al., 2016). ^{238}U/^{236}U and ^{233}U/^{236}U isotope ratios were measured simultaneously using Faraday collectors, and the lower intensity of the ^{234}U ion beam was measured using a Faraday collector equipped with a low-noise 10^^{13} Ohm resistor. A mass-fractionation correction was applied to the measured uranium and thorium isotope ratios based on the certified near-unity ^{233}U/^{236}U ratio of the mixed spike (sufficient uranium carry over into the thorium fraction permitted this for all thorium analyses). For thorium, ^{230}Th/^{232}Th and ^{230}Th/^{223}Th ratios were measured separately from the uranium runs, using the 10^^{13} Ohm equipped Faraday collector in the axial position for ^{223}Th. A detrital (inherited initial non-radiogenic ^{230}Th) correction was applied to all U-Th analyses, assuming that the inherited component had a (^{230}Th/^{232}Th) ratio of 0.8 ± 0.4 (parentheses denote activity ratios). Whilst the choice of (^{230}Th/^{232}Th) for the detrital component is somewhat arbitrary, the calculated ages for all are quite insensitive to this correction (Supporting Information S1). All ages were calculated using the following decay constants ($\lambda^{234}U$ = 2.826E-6, $\lambda^{230}Th$ = 9.1577E-6, $\lambda^{238}U$ = 1.551E-10 and $\lambda^{232}Th$ = 4.9475-11; Jaffey et al., 1971; Cheng et al., 2000). Laboratory blanks for ^{238}U and ^{232}Th were typically in the 1 to 10 pg range, and no blank corrections were applied.

3.5. Fault-slip data analysis

Stress or strain can be evaluated using brittle fault-slip data inversion methods (Angelier, 1994). It involves collecting faults data such as plane orientations, fault striae directions and sense of slip from kinematic indicators at the outcrop scale. The methodology of fault-slip data inversion to determine stress fields and to demonstrate temporal and spatial changes in the late Cenozoic stress states has been used in many active tectonic areas around the world over the past three decades (Angelier, 1994; Twiss & Unruh, 1998; Célérier et al., 2012; and references therein). It consists of obtaining from a population of fault-slip data the principal stress axes that best fit the reduced stress tensor at a given measurement site. Inversion results include the orientation (azimuth and plunge) of the principal stress axes ($\sigma_1 > \sigma_2 > \sigma_3$) of a reduced stress tensor as well as the stress ratio R = (σ_2-σ_3/σ_1-σ_3), a parameter describing relative stress magnitudes. The stress tensor provides information on the stress regime, i.e., compressional (with σ_3 vertical), strike-slip (with σ_2 vertical), transpressional (σ_2 or σ_3 vertical and σ_2 close to σ_3 in magnitude), or extensional (with σ_1 vertical).

Several inversion methods have been proposed in the literature (see reviews by Célérier et al., 2012). Using multiple methods, hence different algorithms, increases the accuracy of the results by reducing the effect of systematic errors. In this study, the fault-slip data analysis and principal stress axes calculation were first performed with the kinematic right-dihedra method (RDM; Angelier, 1994), which shows the distribution of the percentage of compression or extension dihedra in stereographic projection. Next, fault-slip data were inverted with two independent methods: direct inversion (DIM) and numeric dynamic analysis (NDA). All inversion methods were performed with *TectonicsFP* v1.7.9 software of Reiter & Acs (2000) and Ortnet et al. (2002). Statistically stable stress tensors were obtained from 10 to 30 fault-slip data measured in each structural site. A further explanation of the fault-slip data acquisition and analysis is included in the Supporting Information S2.

The main goal of the fault-slip data analysis was to characterize the Quaternary to present-day stress regime evolution in southern central Hispaniola. Unfortunately, it is generally challenging to date the striations more precisely than by simply recording that they are younger than the rocks deformed by the faults. In this study, we included results from fault-slip data measured in igneous and sedimentary rocks of upper Cretaceous to Early Pleistocene age, as well as in dated Middle to Late Pleistocene coral reef terraces and alluvial fan deposits.

On occasions, more than one set of striae are present on a fault plane at the same measurement site, which were formed by different stress tensors. For example, reverse dip-slip and oblique reverse striations caused by an NE-trending compression are crosscut by low-pitch angle striations resulting from a NE-trending σ_1 strike-slip stress regime. The discrimination of striae belonging to each fault set was conducted by numerical checking of compatibility with an inversion method and geological arguments. Fault crosscutting relationships, the overprinting of several striations in the same fault plane and the absolute age of the faulted rocks have also been used as geological criteria to date faults and thus discriminate paleostress tensors and tectonic events.

4. Neotectonics of southern central Hispaniola

4.1. Large-scale structures

The geology of southern central Hispaniola consists of five main elements: (1) an Upper Jurassic to Upper Cretaceous igneous and metamorphic basement of the Cordillera Central domain; (2) a group of latest Cretaceous-lower Eocene sedimentary rocks of the Peralta fold-and-thrust belt, that locally unconformable overlie the basement; (3) an unconformable cover of folded and faulted middle

Eocene to lower Miocene sedimentary rocks of the Rio Ocoa Group; (4) a sequence of slightly faulted and tilted Neogene sediments of the San Juan-Azua and Enriquillo basins; and (5) an unconformable cover of Quaternary alluvial, fluvial and shallow marine deposits. The spatial distribution of these elements is included in the geological map and cross-sections of Fig. 2.

The neotectonic structures of southern central Hispaniola are compiled in the map of the Fig. 3, which results from integrating of new field data with the geologic map obtained by the SYSMIN Project in the Dominican Republic (e.g., Pérez-Estaún et al., 2007). This map covers the eastern half of the Cordillera Central, the Sierra Martín García, the southeastern part of the San Juan basin and the whole Azua basin including the Baní pediment. This fieldwork area was selected because contains the main active structures of the arc-plateau collision in the southern Dominican Republic.

The neotectonic structures of this area show three main trends: NW to WNW-striking folds and thrusts; N to NE-striking right-lateral strike-slip faults; and ENE to E-striking left-lateral strike-slip faults. Combined detailed structural analysis, fault-slip data inversion, and geochronology show that these structures were generated during three main tectonic events (see below). The NW to WNW-trending D1 structures are parallel to the structural grain of the Cordillera Central, as the folds and thrusts of the Peralta belt. Located in the southern and eastern parts of the study area, the N-S to NE-SW transverse D2 structures are the strike-slip fault segments of the Ocoa-Bonao-La Guácara and Beata Ridge fault zones, as well as second-order structural elements of the related sub-parallel deformation corridors. The ENE to E-striking faults are also transverse D2 structures concentrated in the northwestern sector of the studied area, which also deform the boundary with the Cibao basin. The previous structures appear locally cut by two families of D3 extensional faults, which have a different trend depending on their geographic location: WNW to W in the Ocoa Bay sector; and NE in the Cordillera Central sector.

The Ocoa-Bonao-La Guácara fault zone represents the structural transition between the Muertos oceanic accretionary prism and the Beata Ridge-Peralta Belt collision zone (Fig. 3; Escuder-Viruete et al., in press). This fault runs along a N to NNE-striking band, 2 to 12 km wide and 120 km long, extending from the western termination of the Muertos Trough in the south to the Cibao basin in the north. Northward, the fault zone connects to the Hispaniola fault zone and changes its trend, curving from N-S to W-E over a distance of ~30 km. Based on discontinuities in its trace (such as step-overs, relays and bends), the fault zone comprises four major segments which are, from south to north (Fig. 3): Offshore (O-OBFZ), Southern (S-OBFZ), Central (C-OBFZ) and Western (W-OBFZ). These active segments are variably oblique with respect to the regional convergence direction and, therefore, they exhibit strike-slip, oblique reverse and thrust fault movements. Along the eastern margin of Ocoa Bay, the O-OBFZ segment produces offshore a clockwise rotation of the folded sediments of the Muertos accretionary prim, and bends and deforms onshore the fold and thrust structures of the Peralta Belt, the SJPFZ, the sedimentary fill of the Azua basin and the Late Pleistocene to Holocene alluvial fans (Escuder-Viruete et al., in press).

The Beata Ridge fault zone (BRFZ) is part of the Beata Ridge. Mauffret and Leroy (1999) and Mauffret et al. (2001) suggested that the Beata Ridge fault zone (BRFZ) is a recent major NE-striking right-lateral strike-slip fault that limits the Beata Ridge to the west and would continue to the NE along the Beata Ridge summit and the eastern termination of the Sierra Bahoruco. On the basis of swath bathymetry and offshore seismic reflection data (Granja Bruña et al., 2014), the northern part of the BRFZ can be divided in two fault segments which are, from south to north (Fig. 3): Central (C-BRFZ) and Northern (N-BRFZ). The N-BRFZ segment shows a constant NE-SW trend along 55 km, parallel to the east coast of the Sierra Bahoruco and Martín García and extends onland through the Azua Basin. The linearity of the fault segment indicates that it is a nearly vertical structure that accommodates a predominantly strike-slip displacement. Field data obtained in onland sub-parallel faults (see below) indicate a left-lateral strike-slip displacement characterizes the N-

BRFZ. This fault segment cuts the post-middle Miocene macrostructure of NW-trending folds in the Sierra Bahoruco and Martín García, as well as the post-Early Pleistocene folds and thrusts that deform the Arroyo Seco Formation in the Azua Basin. This segment connects at its northern end with the OBFZ.

4.2. Regional gravimetric data

The regional pattern of the Bouguer anomaly reflects the main lithological and structural characteristics of southern central Hispaniola (Fig. 4), even though the distribution of the stations of gravity data is sparse and the used grid cell size is 250 x 250 m. Areas with positive anomalies ranging from 40 to 134 mGal (yellow and orange tones) are present in the northern and eastern sectors of the Cordillera Central, the northern sector of Sierra Bahoruco, Sierra Martín García and the western Ocoa Bay, as well as the eastern Cordillera Septentrional. These anomalies have a general NW-SE to WNW-ESE trend and are interpreted as areas of variably thickened island arc crust of mafic to intermediate composition, with average densities around 2.95 g/cm^3 (Ayala et al., 2007). Varying textures of the gravity field within these areas include smooth parallel lineaments associated with bands of foliated amphibolites, elongated gabbro-dioritic batholiths and CLIP-related basaltic units of the Upper Cretaceous basement. In contrast, long wavelength gravity anomalies between -60 and 14 mGal (dark and light blue tones) characterize the Cibao basin, the southern sector of the Cordillera Central (Peralta belt) and the San Juan-Azua basin. These areas comprise silicilastic and carbonate rocks of the late Cenozoic sedimentary cover, with average densities around 2.55 g/cm^3 (Ayala et al., 2007). These negative anomalies present a smooth texture and are elongated in the NW-SE to WNW-ESE direction, subparallel to the positive anomalies of the Cretaceous basement.

Therefore, the regional gravity field defines an alternance of NW to WNW-striking long wavelength anomalies, reflecting the contrast between the high-density Cretaceous igneous and metamorphic basement of the northern Cordillera Central and the low-density Cenozoic sedimentary rocks of the southern Cordillera Central, Cibao and San Juan-Azua basins (Fig. 4). The positive gravity anomaly of the Cordillera Central is disturbed by intermediate anomalies between 20 and 50 mGal (light green tones), along the the arcuate trace of the Ocoa-Bonao-La Guacara fault zone. This pattern seems to reflect a NE-directed thick-skinned thrust structure in the basement, composed of tonalitic batholiths and intermediate volcanic rocks of the Tireo Group, over the Cibao and Bonao sedimentary basins.

The northern boundary of the Cibao Basin is linear and defined by a steep gradient in the gravity field towards the positive anomaly of the eastern Cordillera Septentrional, coinciding with the surface trace of the Septentrional fault zone. The southern limit of the Cibao basin with the Cordillera Central is also marked by a strong gradient and coincide with the northern branch of the Hispaniola fault zone. In turn, the southern boundary of the San Juan-Azua basin is marked by a transition towards a NE-striking long wavelength positive gravity anomaly, which suggests the existence of high-density basaltic rocks of the CLIP forming the basement of the Sierra Bahoruco, the Sierra Martín García and the Ocoa Bay.

4.3. Regional magnetic data

The large-scale structure of southern central Hispaniola can be deduced by the orientation of the regional magnetic field in NW to WNW-trending subparallel bands, which are often characterized by a distinctive textural pattern (Ayala et al., 2017). In the reduced to the pole grid (Fig. 4a), short-wavelength magnetic signatures generally correspond to areas where the magnetic sources in the basement are located close to the surface. These areas are characterized by a pattern of NW to WNW-trending sub-parallel anomalies, related to the late Cretaceous regional structure of amphibolites, gabbro-tonalitic batholiths and ridges of basalts in the Cordillera Central. The strong ferromagnetic character of the gabbros produces positive anomalies between 100 and 250 nT, which delineate the intrusive contact of the Arroyo Caña, Jumunuco and El Río batholiths. In the eastern Cordillera Central, the Hispaniola fault zone defines a strong NW-trending positive magnetic anomaly between 150 and 270 nT, separating the Loma Caribe Peridotite outcrops and the mafic volcanic rocks of the Los Ranchos Formation. This strong anomaly is related to the titanomagnetite growth during serpentinization by tectonic exhumation and surficial alteration of the peridotites in the late Cenozoic. A part of the southern Cordillera Central is characterized by scattered short-wavelengths anomalies, roughly elongated along a NE-SW trend and related to the extrusion of mafic to intermediate calc-alkaline to alkaline volcanic rocks during the Quaternary.

By contrast, long-wavelength magnetic signatures correspond to areas where the magnetic source is located farther from the surface, or where the magnetic rock intensity in the basement is weak. In the reduced to the pole grid (Fig. 4b), the Cibao and San Juan-Azua sedimentary basins generally display long-wavelength negative magnetic anomalies between -10 and -350 nT. These negative anomalies are related to the 1 to 5 km-thick overburden of paramagnetic sediments that fill these basins and reduces the basement magnetic intensity. In turn, the pattern of NW-striking negative magnetic anomalies that characterize the southern sector of the Cordillera Central is associated with the fold and thrust structure of the Peralta belt sedimentary rocks. Nevertheless, the sedimentary carbonate massifs of the Sierra Bahoruco, Sierra Martín García and coastal sectors of the Ocoa Bay shows long-wavelengths of relatively high magnetic intensity between 0 and 100 nT, suggesting a magnetic source that is shallower than the surrounding areas. A possible explanation for this high magnetic intensity is that the basement in these areas comprises magnetite-rich basalts typical of the late Cretaceous CLIP.

In general, the main magnetic discontinuities in the reduced to the pole magnetic grid correlate well with the large-scale fault zones and the regional macrostructure of southern central Hispaniola (Fig. 4b). These discontinuities juxtapose areas of long and short-wavelength magnetic anomalies and define tectonic blocks bounded by the segments of the Septentrional, Hispaniola, Ocoa-Bonao-La

Guácara and Beata Ridge fault zones (Fig. 4b). In detail, low magnetic values mark the surface trace of the main fault zones, suggesting that the deformed fault rocks are partially demagnetized. The reduced to the pole magnetic grid also shows the truncation and displacement of the NW to WNW-striking D1 structures in the Cordillera Central by the transverse D2 strike-slip fault system of the Ocoa-Bonao-La Guácara fault zone.

4.4. Late Neogene and Quaternary lithostratigraphy

In southern central Hispaniola, neotectonic activity is recorded by the sedimentary fill of the San Juan-Azua and Enriquillo basins, and by the growing of a system of coral reef terraces overlain by alluvial fans. The San Juan-Azua and Enriquillo basins have been defined as syn-tectonic flexural basins limited to the NE by SW-verging thrust systems, although the Enriquillo basin is also limited by opposite-vergence thrusts directed to the NE (Mann et al., 1991b, 1995; Hernáiz Huerta & Pérez-Estaún, 2002; Díaz de Neira, 2004; Hernaiz Huerta et al., 2007b). These basins form the southeastern extension of the Plateau Central and Cul-de-Sac basins in Haiti (Pubellier et al., 2000). The basins are filled by a ~4 km-thick upward shallowing and coarsening mega-sequence composed of Miocene to Early Pleistocene marine sediments (McLaughlin et al., 1991; Díaz de Neira & Solé Pont, 2002; Pérez-Valera, 2010).

The megasequence includes initial sedimentation on a regionally extensive open marine carbonate platform in the lower to middle Miocene (Sombrerito Formation). The deposition of turbiditic-type clastic sediments in a deep marine environment occurred in the middle to upper Miocene (Trinchera Formation) and in a shallow-water platform in the lower Pliocene (Quita Coraza Formation). The regressive character of sedimentation gave rise in the Pliocene to shallow-marine clastic and coral reef deposits (Arroyo Blanco Formation) and, in the Enriquillo basin, the deposition of halite and gypsum evaporites (Angostura Formation), and fine-grained clastic sediments of a bay with excess salinity (Las Salinas Formation). The change to continental deposition took place in the late

Pliocene-Early Pleistocene in the Azua basin, with the sedimentation of coarse-grained clastic sediments (Arroyo Seco Formation), and in the Early-Middle Pleistocene in the Enriquillo basin, with an upward change from reef limestones and supralittoral marls to alluvial-fan breccias and conglomerates (Jimaní Formation).

From the uppermost Pliocene, tectonic indentation of the southern margin of Hispaniola by northeastward displacement of the Beata Ridge (Heubeck & Mann, 1991; Mann et al., 1991b; Hernaiz Huerta & Pérez-Estaún, 2002), destroyed the foreland configuration developed in the southern margin, uplift and erosion of the Cordillera Central and emergence of the Azua and Enriquillo basins. After a sedimentary hiatus, uplift is recorded by the formation and progressive elevation of coral reef terraces in the southernmost coastal area during the Middle to Late Pleistocene. These coral terraces were probably organized in a staircase marine terrace system, which has only been partially preserved by later erosion and tectonics (see below).

Continued uplift and erosion were also accompanied by syn-tectonic sedimentation of coarse-grained alluvial fan systems directed towards Ocoa Bay (Díaz de Neira, 2000; Pérez-Valera, 2010). Recently, three alluvial fans systems developed at different topographic levels have been distinguished on the southern slope of the Cordillera Central during the Late Pleistocene to the Holocene (Fig. 3; Escuder-Viruete et al., in press). The upper alluvial fan system forms small relict plateaus inclined towards the S and SE, over the surface of the intermediate alluvial fan system. The intermediate alluvial fan system forms a more extensive and better-preserved deposit, which connects the foot of the Cordillera Central relief with the southern coast. The current lower alluvial fan system is spatially restricted to the Sabana Buey valley and small coastal plains of southwestern Baní (Fig. 3). Its incision in the intermediate alluvial fans implies a change in the geometry of the drainage network, which has been attributed to fluvial capture processes (Díaz de Neira, 2000; Pérez-Valera, 2010), triggered by the activity of the OBFZ (Escuder-Viruete et al., in press).

5. Fault-slip data inversion and late Cenozoic stress regimes

This work calculated stress tensors from a population of 562 fault-slip data, measured in 32 sites covering an area of approximately 100 × 50 km^2 in southern central Hispaniola. Geological characteristics of these sites are reported in the Supporting Information S3. Stress inversion of the fault-slip data yields 44 stress tensors and their respective plots are shown in the Figs. 5 to 14. The orientation of their maximum horizontal stress, stress regime, kinematic type of faults and the immersion method used in each site, which are generally consistent with each other, are included in the Supporting Information S4.

5.1. Fault-slip data inversion in the Peralta Belt

Sites 21JE94, 21JE95 and 21JE96 are located along the highway between San José de Ocoa and Nizao, within the Peralta Belt (Fig. 5). Both the mudstone-rich siliciclastic rocks of the lower Eocene Peralta Group and the turbiditic sediments and conglomerates of the late Eocene Ocoa Group exhibit 1 to 100 m-thick zones of intense stratal disruption, which were interpreted by Witschard & Dolan (1990) as thrust surfaces formed during the late Eocene in the Peralta accretionary prism. Disrupted zones are mesoscopically characterized by boudinaged sandstone beds and pich-and-swell structures defining lozenged blocks. Mudstone interbeds and argillaceous cataclastic bands have a WNW to NW-striking pervasive scaly clay fabric (Sp) and occasionally contain tight to isoclinal folds with rootless limbs (Fig. 5). The planar fabric (Sp) often contains a N to NE-trending calcite stretching lineation (Lp) subparallel to the fold axes. In this Sp-Lp fabric, kinematic indicators such as the asymmetry of the boudins or the S-C structures establish a general top-to-the W and SW shear sense. All these structures are typical of a block-in-matrix fabric of a mélange, essentially produced by syn-sedimentary deformation during the Late Eocene (see below). Stratally disrupted zones in the Ocoa Group rocks are cut by WNW-striking D1 thrust surfaces that typically dip 5° to 30° more deeply than the Sp fabric, when they are restored to the original horizontal position. Both the block-in-matrix fabric and the thrusts are cut by NNW to NE-striking strike-slip faults D2 and by high-dip angle normal faults D3 (Fig. 6).

The inversion of fault-slip data collected in several localidades throughout the Peralta Belt enables the separation of populations related to three distinct stress regimes (Fig. 6). The first population is represented by variably oblique reverse slip vectors in NW-striking and NE-dipping faults (sites 20JE09, 21JE94, 22JE12 in Yayas de Viajama, and 22JE13 in Tabera Arriba). It corresponds to a compressional stress regime D1 characterized by a NE-SW to ENE-WSW trending σ_1. The second population contains strike-slip to oblique reverse left-lateral slip vectors in NE-striking subvertical faults (sites 22JE13 and 21JE93). It is related to a near pure strike-slip stress regime D2 characterized by a NNE to NE-trending σ_1. The third population includes normal vectors along dip-slip and oblique normal striae in NE-striking high-angle faults (site 21JE96), and corresponds to an extensional stress regime D3 with a N136°E trending σ_3 (Fig. 13).

Sites 21JE123 and 21JE125 are located in the southernmost outcrops of the Peralta Belt, on the road Azua-Baní in the northern sector of the Ocoa Bay (Fig. 7). In this sector, the macrostructure in the Peralta Belt consists of a fold system of the lower to middle Eocene limestones of the Peralta Group and the upper Eocene turbidites with olistoliths of the Ocoa Group, related to a D1 deformation in a fold-and-thrust belt of NW-SE trend and SW-directed vergence. Towards the SE, the NW-trending D1 folds and thrusts of the Peralta Belt turn progressively towards a N-S trend and are cut and displaced by the O-OBFZ right-lateral D2 strike-slip fault. In the geological cross-section of Fig. 7, the Eocene rocks of the Peralta Belt overthrust through the SJPFZ the lower to middle Miocene limestones of the Sobrerito Formation, and the assemblage overthrust in turn the conglomerates of the upper Pliocene to Early Pleistocene Arroyo Seco Formation. Therefore, D1 thrusting continued in this sector until the Early Pleistocene times.

Site 21JE123 is located along the Loma Vieja frontal thrust, which corresponds to the thrust ramp associated with the NNW to NW-trending D1 Loma Vieja anticline (Fig. 7). The related D1 structures in the limestones of the Sobrerito Formation consist of SW-verging asymmetric folds, associated with mid-dip angle faults inclined to the NE and SW, subparallel to the Loma Vieja thrust. The mesoscopic S-C structures and other kinematic indicators imprinted on the fault planes establish a top-to-the-SW reverse movement. Predominant dip-slip striae in reverse fault planes define a population compatible with a thrust faulting stress regime and a N204°E trending compressional axis (Fig. 7). On the other hand, the orientation of calcite veins and T-planes in clasts of the conglomerates of the Arroyo Seco Fm establish a consistent NNE trend of D3 subhorizontal extension.

Site 21JE125 is located at the northwest end of the Ocoa Bay, 3.5 km southeast of the town of Azua, on the southern flank of a W-trending D1 anticline build-up in the limestones of the Sombrerito Formation (Fig. 7). The anticline is affected by a system of high-dip angle (> 60°) strike-slip faults D2 composed by NE-striking left-lateral strike-slip faults and antithetic N-striking right-lateral strike-slip faults. The assemblage is truncated by E to WNW-trending D3 normal faults, exhibiting a high-dip angle towards the N and S. Fault-slip measurements define two contrasting subsets (Fig. 7). The first subset includes striations with a low-pitch angle in NE-striking strike-slip faults. Normal and oblique normal dip-slip vectors in WNW-striking and NE and SW-dipping conjugate faults represent the second subset. The first population corresponds to a purely strike-slip stress regime D2 with a N200°E trending σ_1 and the second population to an extensional stress regime D3 characterized by a N020°E trending σ_3.

5.2. Fault-slip data inversion in the Ocoa Bay

The limestone outcrops of the Sombrerito Fm located on the eastern coast of Loma Vigía, about 6 km southeast of Azua (Fig. 7) exhibit folds, reverse faults and thrusts related to D1 deformation. In the 21JE112 site, these D1 structures consist of NW to WNW-trending and SW-verging asymmetric folds, associated with low to mid-dip angle reverse faults inclined to the NE, subparallel to the SJPFZ. The mesoscopic S-C structures and other kinematic indicators imprinted on these fault planes establish a top-to-the-SW reverse movement. Striae on the fault planes define a reverse slip consistent with a thrust faulting stress regime and a N222°E trending compressional axis (Fig. 8). In the 21JE120 site, several WNW-striking and NE-verging asymmetric anticlines correspond to the folds associated with a D1 back-thrust (Fig. 8). Slip measurements on the limbs of a decameter-scale anticline define a population of WNW-striking and SW-dipping reverse faults. This population corresponds to a purely compressional stress regime with a N026°E trending σ_1.

Throughout the Loma Vigia sector, D1 structures appear truncated by NW to W-trending D3 normal faults, which exhibit mid to high-dip angles towards the NE and SW (Fig. 8). For instance, the SW limb of a D1 anticline is cut by a D3 normal fault, causing the dragging of the limestone layers in the hanging-wall block (site 21JE120), or the stratification appears displaced by a system of ENE to E-striking normal faults with associated intrusion of mafic magmas (site 21JE113). In general, dip-slip striae in these fault planes define normal faults populations compatible with extensional stress regimes D3, characterized by a SSW to SW trending σ_3 (Fig. 8).

5.3. Fault-slip data inversion in the eastern Sierra Martín García

In the limestone outcrops of the Sombrerito Formation located on the southeast coast of the Sierra Martín García, the D1 structures are strongly obliterated by the D2 deformation. This deformation has given rise to fault zones with a general NE-SW direction and several kilometres in length, parallel to the trace of the Beata Ridge fault zone, which runs offshore about 1.5 km to the SE. Fault zones are marked by the development of bands of fault-gouge and fine crush breccia several tens of meters thick (Fig. 9). Individual fault planes are very steep (dip > 70°) and have low-pitch angle (< 20°) striations that indicate a dominant strike-slip displacement.

At the Playa Caobita (site 21JE126), the Miocene limestones appear to be unconformably overlain by a ~50 m-thick Quaternary sequence composed from bottom to top of (Fig. 9): reef limestones of a basal fossil coral terrace; poorly consolidated conglomerates of an intermediate alluvial fan, that includes reworked corals and cobbles at the base; and gravels and sands rich in limestone cobbles of a younger alluvial fan. A gastropod *Strombus* sp. collected at the highest stratigraphic levels of the coral terrace has provided a U-Th age of 118.47 ± 0.52 ka (21JE126C), so its growth took place in the interglacial marine oxygen isotope stage (MIS) 5e, in the Middle to Late Pleistocene boundary. Two specimens of coral *Diploria* sp. collected towards the basal and intermediate levels of the terrace have provided U-Th ages of 476.99 ± 23.6 ka (21JE126B) and 331.92 ± 4.51 ka (21JE126A), respectively. These ages indicate growth of the coral terrace during MIS 9c and 11 stages in the Middle Pleistocene, although a reworking of the corals is not ruled out because the terrace intercalates clastic levels.

Observations made in outcrops along the coast indicate that D2 strike-slip faults cut both reef terrace limestones and intermediate alluvial fan conglomerates. These relationships establish a Late Pleistocene age at least for the D2 deformation. On the other hand, the whole sequence of the coral terrace and the overlying alluvial fans is tilted 10-18° towards the SE and appear deformed by a system of E to ENE-striking D3 normal faults, which exhibits a high-dip angle (>60°) towards the N and S (Fig. 9). Therefore, the D3 deformation has taken place in the Late Pleistocene to Holocene. Fault-slip data measurements allow discrimination of a first population characterized by striations with a low-pitch angle in subvertical fault planes and a second population of normal dip-slip vectors in high-dipping faults. These populations represent two successive stress regimes: the first corresponds to a near strike-slip stress regime D2 with a N020°E trending σ_1 (21JE127); and the second matches with a near purely extensional regime D3 with a N008°E trending σ_3 (22JE15; Fig. 9).

5.4. Fault-slip data inversion in the northeast Sierra Bahoruco

The northwestern end of the Sierra Bahoruco shows a very sharp NE-SW trending coastline, subparallel to the trace of the central segment of the Beata Ridge fault zone, which runs offshore about 2.5 km to the SE (Fig. 3). Swath bathymetry and seismic reflection data suggest that fault segment constitutes the active boundary between the 1500 m elevated mountains of the Sierra Bahoruco to the NW and the -2500 m submerged slope of the Dominican sub-basin to the SE (Mauffret and Leroy, 1999; Granje Bruña et al., 2014).

Sites 21JE137 and 22JE26 are located in Playa Azul, about 6 km southeast of Barahona (Fig. 10). Along the coast, the limestone outcrops of the Sombrerito Formation define the northern limb of a D1 thrusting anticline of WNW trend and kilometric scale, which constitutes the internal structure of the Sierra Bahoruco in this sector. Limestones are strongly karstified and are unconformably overlain by a fossil coral reef 6 to 10 m-thick that defines a discontinuous morphological terrace along the coast. A *Diploria* sp. collected in the stratigraphically highest levels of the coral terrace has provided a U-Th age of 123.23 ± 0.70 ka (22JE26B), so its growth took place in the MIS 5e. The assemblage is also unconformably overlain by the poorly consolidated conglomerates and red clays of a >20 m-thick alluvial fan (Fig. 10).

Both the karstified limestones and the overlying coral terrace and clastic deposits are faulted and tilted by a system of N to NE-striking D2 strike-slip faults, subparallel to the trace of the Beata Ridge fault zone (see cross section in Fig. 10). Fault planes are generally very steep (dip > 65°) and the striae show left- and right-lateral conjugate motion with a low reverse component (pitch < 25°). Fault-slip data inversion reveals a strike-slip D2 stress-field with a N046°E trending σ_1 stress axis (Fig. 10). Therefore, the central Beata Ridge fault segment has been active for at least the Late Pleistocene. In turn, the internal structure in the alluvial fan deposit defines a system of open anticlines and synclines of WNW-ESE trend and decametric to hectometric wavelength, which appears faulted on the flanks by WNW to W-trending D3 normal faults. These folds are interpreted as roll-over structures related to the D3 extensional faulting. Striations measured in decametric-scale fault planes and T-planes open in clasts are compatible with an extensional D3 regime, characterized by a N010°E trending σ_3 (Fig. 10).

5.5. Fault-slip data inversion in the southwestern Sierra Martín García

In the southwestern sector of the Sierra Martín García, the limestones of the Miocene Sombrerito Formation overthrust the sandstones, marls and gypsum of the upper Pliocene La Salina Formation, and the ensemble regionally overthrusts the continental conglomerates and mundstones of the upper Pliocene to Early Pleistocene Arroyo Seco Formation. These WNW-trending structures constitute the SW-directed D1 frontal thrust, which juxtaposes the anticline macrostructure of the Sierra Martín García to the poorly consolidated alluvial, floodplain and deltaic Quaternary deposits of the Enriquillo basin (Fig. 3).

Site 21JE130 is located in the hanging-wall block, about 300 m northward of the frontal thrust, where the gypsum and marl beds of the La Salina Formation exhibit structures related to D1 deformation (Fig. 11). These structures consist of WNW-trending and SW-verging asymmetric folds, associated with mid-dip angle reverse faults inclined to the NE, subparallel to the basal thrust. The asymmetry of D1 folds and mesoscopic S-C structures establish a top-to-the-SW reverse movement. Oblique reverse striae measured in the reverse fault planes define a fault population compatible with a D1 thrust faulting stress regime and a N047°E trending compressional axis (Fig. 11). In the site 21JE129, the D1 frontal thrust is locally fossilized by a coral reef terrace, where a *Strombus* sp. collected near its stratigraphic base has provided a U-Th age of 124.65 ± 0.85 ka. A *Diploria* sp also collected in the same basal levels has given a similar U-Th age of 128.89 ka (Fig. 11), thus the coral terrace grew in the MIS 5e stage.

Both the D1 thrust-related folds and the coral terrace are affected by a system of high-dip (> 60°) strike-slip faults D2. This fault system comprises NE to ENE-striking left-lateral strike-slip faults filled by subvertical calcite veins and antithetical N to NNE-striking right-lateral strike-slip faults, establishing a strike-slip stress D2 regime characterized by a NE-trending σ_1 axis (Fig. 11). Therefore, the thrust-related D1 deformation reaches the Middle Pleistocene and the strike-slip-related D2 deformation continues after the Middle to Late Pleistocene boundary. Finally, a set of E to ENE-trending and high-dip angle D3 normal faults locally truncate the assemblage. Normal dip-slip striae measured in these fault planes cutting the gypsum beds are compatible to an extensional regime with a N355°E trending σ_3 axis (Fig. 11).

5.6. Fault-slip data inversion in the San José de Ocoa basin

The southern segment of the Ocoa-Bonao-La Guácara fault zone is a roughly 50 km-long, N-striking right-lateral strike-slip fault system, that cuts at a high-angle and clockwise rotate the NW-SE trending folds and thrusts of the Peralta Belt and the structure of the late Cretaceous basement of the Cordillera Central (Figs. 3, 5). The segment is geometrically characterized by separating the fault trace into two branches south of San José de Ocoa town, giving rise to a right-hand releasing-bend and the San José de Ocoa pull-apart sedimentary basin (Escuder-Viruete et al., in press). Both branches rejoin about 35 km northward into the C-OBFZ segment in the Bonao basin.

Site 21JE102 is located near the eastern branch of the S-OBFZ segment, in the town of Naranjal, 2.5 km east of San José de Ocoa (Fig. 5). At outcrop scale, N to NNE-striking right-lateral D2 strike-slip faults cut D1 thrust surfaces inclined to the NE, defined by sheared bands of mudstones in the upper Eocene Ocoa Formation, characterized by a SW-directed penetrative S-C fabric. Fault-slip measurements define two contrasting subsets (Fig. 12): the first subset is reverse to oblique reverse and is associated to striations with a high-pitch angle in NW-striking fault planes; the second subset has oblique reverse and strike-slip vectors in conjugate right- and left-lateral faults. The first population corresponds to a compressional stress regime D1 with a N243°E trending σ_1 and the second population establishes a purely strike-slip stress regime D2 characterized by a N047°E trending σ_1.

Site 21JE100 is also located along the eastern strand of the S-OBFZ segment, 2 km north of San José de Ocoa, on the road to Constanza (Fig. 5). The fault segment tectonically juxtaposes the folded and faulted volcanic rocks of the Tireo Group and the gravels and sands of the Quaternary fill of the San José de Ocoa basin. Volcanic rocks have developed hectometer-scale subvertical fault planes sub-parallel to the S-OBFZ, characterized by a 5 m-wide brecciated damage zone and striations with a low-pitch angle (Fig. 12). These striae define a vector population compatible with a D2 strike-slip stress regime and a N226°E trending compressional axis. South of San José de Ocoa town, the eastern strand juxtaposes the folded and faulted mudstones of the Numero Fm and the gravels and sands of the basin through a subvertical D2 fault system, that also tilts westward the Quaternary deposits. Striations measured in NNW-striking oblique reverse right-lateral faults of the 20JE15 site are compatible with a D2 strike-slip regime and a N186°E σ_1 axis (Fig. 12)

The D2 strike-slip deformation is also very penetrative along the western branch of the S-OBFZ segment, which is morphologically marked by an east facing 200 m-high scarp. This strand juxtaposes the folded and faulted rocks of the Peralta Belt to the W with poorly consolidated gravels and sands that fill the San José de Ocoa basin to the E (Fig. 5). In several sites (20JE14, 21JE97, 21JE98 and 21JE99), striations measured on metric to decametric-scale faults subparallel to the S-OBFZ segment define a population of pure strike-slip to oblique reverse slip vectors, compatible with a D2 strike-slip regime and a predominant NE trending σ_1 stress axis (Fig. 12). The subvertical orientation of calcite veins and T-planes in clasts of the Quaternary conglomerates consistently establishes a WNW to NW trend of subhorizontal extension.

However, the effects of D3 extensional deformation are limited in this sector and geographically localized to the right-hand releasing-bend that forms the San José de Ocoa basin. Site 21JE99 is located between the two branches of the S-OBFZ segment, where the mafic to intermediate tuffs of the Tireo Group are in tectonic contact with the well-bedded limestones of Maastrichtian age. Slip measurements show two different populations: oblique reverse righ-lateral and dip-slip reverse vectors (Fig. 12); and oblique normal vectors (Fig. 13). The overlap relationships between striaes establish that these two populations represent two successive stress fields: the first corresponds to a transpressional D2 stress regime with a N270°E trending σ_1; and the second corresponds to a more purely extensional D3 regime characterized by a N121°E trending σ_3. Also related to local D3 extensional tectonics, NW to N-striking normal faults have also been observed at sites 21JE103 and 21JE108 (Fig. 5). Dip-slip striations measured on these fault planes establish an extensional D3 regime characterized by a W-trending σ_3 (Fig. 13).

5.7. Fault-slip data inversion in the Cordillera Central

The Cordillera Central is characterized by the development of crustal shortening structures, topographic uplift and exposure of the late Cretaceous volcano-plutonic basement in the core of large-scale WNW to NW-trending D1 anticlines (Fig. 3). In the Constanza-Sabana Quéliz area, the macrostructure consists of D1 folds and thrusts of WNW-ESE trend and usually SW-directed vergence, built up in a sequence composed by Cenomanian limestones and siliceous-rich sediments, Turonian to early Campanian mafic tuffs of the Constanza Formation, late Campanian mudstones of the El Convento Formation and Maastrichtian shallow-water platform limestones, as well as plutonic rocks (Escuder-Viruete et al., 2008). This macrostructure is locally cut and displaced by a system of high-dip angle strike-slip D2 faults, which includes NW to NNE-striking right-lateral strike-slip faults and conjugate NE to ESE-striking left-lateral strike-slip faults. NE to E-trending D3 normal faults locally truncated the assemblage exhibiting a high-dip angle towards the NW and SE.

This deformative sequence is well recorded at the 21JE80 site, located ~10 km east of the Constanza town in the Tireo river valley (Fig. 5). Fault-slip data measurements and cross-cutting relationships show three contrasting subpopulations (Fig. 14): reverse and oblique reverse left-lateral faults; subvertical faults with low-pitch angle striations; and normal and oblique normal right-lateral faults. These subsets represent three successive stress regimes: the first corresponds to a compressional stress regime D1 characterized by a N213°E trending σ_1; the second adjusts to a near strike-slip stress regime D2 with a N321°E trending σ_1; and the third matches with a purely extensional regime D3 with a N183°E trending σ_3 (Fig. 14).

Field observations at various points in the Cordillera Central show that D3 extensional faults overlap D1 thrusts. For example, the various kinematic types of faults that deform green mafic tuffs at sites 21JE78 and 21JE79, where the fault-slip data inversion enables the separation of populations related to two distinct stress regimes (Figs. 13, 14). The first population is represented by dip-slip to variably oblique reverse slip vectors in low to mid-dip faults; the second population includes normal slip vectors along dip-slip striae in predominantly NNE to NE-striking high-dip faults. Both fault types define a NE-SW to W-E compressional D1 regime and a NW-SE extensional D3 regime, respectively.

A similar deformative sequence is recognized in the southeastern Cordillera Central, located east of the S-OBFZ segment (Fig. 3). In this sector, the S-OBFZ exhibits a fresh N-S scarp and represents the boundary between the >2000 m elevated mountains of the Cordillera Central to the W and the 650 m elevated Rancho Arriba valley to the E. Along this morphological step, the fault zone produces triangular facets, perched valleys, and dextral offsets of streams that testify its recent activity. Deformation related to this segment produced the local clockwise rotation of the D1 fold and thrust structure and the formation of the Rancho Arriba intramountain basin, which is filled by the Quaternary alluvial fans fed by the erosion of the surrounding relief.

Site 21JE70 is located at the Rancho Arriba basin southern bound. The basin exhibits an ENE-WSW elongated rectangular shape controlled by a southern active master fault (Fig. 5). Fault-slip measurements on hornblende-bearing tonalities of the Arroyo Caña batholith define two contrasting subsets (Figs. 13, 14): oblique reverse to strike-slip vectors in NE to ENE-striking faults; and oblique normal slip vectors in conjugate ENE and WSW-striking high-angle faults. The first set corresponds to a strike-slip stress regime D2 with a N022°E trending σ_1 and the second set establishes a near pure extensional stress regime D3 characterized by a N023°E trending σ_3, related to the formation of the basin. Observations carried out in the volcanic rocks of the Tireo Group at sites 21JE72 and 21JE73 allow us to establish similar temporal relationships: younger NE to E-striking D3 normal faults cut older D2 strike-slip and D1 reverse faults. Striations measured in decametric-scale fault planes subparallel to the NW to WNW-trending regional macrostructure in these sites are compatible with a compressional D1 regime, characterized by a general NNE to NE-trending σ_1 (Fig. 14).

The NW-SE to W-E directed D3 extensional tectonics has also been detected in other sites located close to the OBFZ. Site 21JE99 is located between the two branches of the S-OBFZ segment, north of San José de Ocoa town (Fig. 5), where Maastrichtian limestones exhibit a penetrative brecciation associated with decametric-scale NE-striking fault surfaces, dipping a high-angle to the NW and SE. Slip measurements establish an oblique normal left-lateral movement on these planes and their inversion establishes an extensional D3 regime characterized by a N121°E trending σ_3 (Fig. 13). Site 21JE103 is located ~1.5 km east of the S-OBFZ (Fig. 5), where decametric-scale fault planes measured in basalts of the Tireo Group contain striations of an oblique normal kinematics in NW to NE-trending and E-dipping faults. Inversion of these fault-slip data yields an extensional stress regime characterized by a N256°E trending σ_3 (Fig. 13). Finally, slip measurements in N- to NNW-striking fault planes at site 21JE108 (Fig. 5) indicates a predominance of dip-slip normal vectors, compatible with a purely extensional regime with a N069°E trending σ_3 (Fig. 13).

6. Discussion

6.1. Relations between neotectonics and Quaternary sedimentation in southern central Hispaniola

Several researchers have previously described the uplift, folding and thrusting of the Cordillera Central basement and the Peralta Belt during the lower Miocene to upper Pliocene time interval (Heubeck & Mann, 1991; Mann et al., 1991a, b; Pubelier et al., 2000). The style of this D1 deformation consisted of a SW-directed fold-and-thrust belt, which was developed above a basal detachment horizon following a forward propagating sequence (Heubeck & Mann, 1991; Hernaiz Huerta & Pérez-Estaún, 2002; this work). D1 is superimposed on a deformation produced during the upper Eocene in the Peralta accretionary prism (Witschard and Dolan, 1990). Data obtained in this study indicate that a large part of this deformation is syn-sedimentary and characterized by the formation of a block-in-matrix fabric typical of a heterogeneous mélange. Syn-sedimentary deformation was very probably produced by submarine gravitational processes, triggered by instability in the basin slope and/or tectonics (e.g., Alonso et al., 2014; Escuder-Viruete & Baumgartner, 2014; Súarez Rodríguez et al., 2017).

In this tectonic context, the San Juan-Azua basin constitutes the foreland flexural basin developed in front of the SW-directed Peralta fold-and-thrust belt, and bounded to the NE by SW-directed thrusts (Hernaiz Huerta & Pérez-Estaún, 2002; Díaz de Neira, 2004; this work). These basins were filled by shelf marine, turbiditic, and continental sediments giving rise to a 4-km thick, shallowing and coarsening upward regressive megasequence of lower Miocene to Lower Pleistocene age. D1 deformation propagated to the Azua basin sediments and continued until Early to Middle Pleistocene times, which is the age of the Arroyo Seco Formation deformed in the footwall of the Peralta frontal thrust (Díaz de Neira & Solé Pont, 2002). As documented in the present work, these coarse-grained continental deposits were folded and thrusted in the footwall of the San Juan-Pozos fault zone, current frontal thrust of the Peralta Belt.

After a sedimentary hiatus, uplift and erosion of the resulting relief fed several staircase alluvial fan systems, developed at different topographic levels on the southern slopes of the Cordillera Central probably since the Early Pleistocene (Díaz de Neira, 2000; Pérez-Valera, 2010). The ages obtained by optically stimulated luminescence (OSL) geochronology between 43.8 ± 8.3 ka and 5.9 ± 0.6 ka for the intermediate and young alluvial fan systems indicate the uplift continued, at least, during the

Late Pleistocene to the Holocene (Escuder-Viruete et al., in press). The older alluvial fan is not yet been dated, but probably also records uplift and erosion during the Middle Pleistocene.

In both the eastern and western sectors of the Ocoa Bay, these alluvial fan systems unconformably overlie a fossil coral reef terrace developed during the MIS 5e (118-128 ka) and 5c (~105 ka) stages in the Last Interglacial. Therefore, the fluvial incision and the progradation/aggradation of the intermediate and young alluvial fans were also controlled by the global sea level fall and its variations during the Last Glacial. The coral terrace also includes reworked corals grown during MIS 7 and 9 stages. However, no remains have been found of coral terraces built during these stages in the Ocoa Bay, so erosion might eliminated them.

On the other hand, the Quaternary coral reef terrace and the alluvial fans unconformably overlie the D1 large-scale structure of NW-trending and SW-verging folds and thrusts that affect the NE margin of the Azua basin. Therefore, the regional pervasive D1 deformation ends, at least in southern central Hispaniola, during the Lower Pleistocene. Late Pleistocene to Holocene alluvial fan and pediment deposits are all offset by strike-slip faults of the D2 event, implying that the more recent tectonic activity is mainly partitioned in the Ocoa-Bonao and Beata Ridge fault zones, as well as by faulting in related structures. Finally, both the coral reef terraces of the MIS 5e and 5c stages and the overlapping alluvial fan systems of Late Pleistocene to Holocene age appear deformed by the normal faults of the D3 event in the Ocoa Bay sector.

6.2. Evolution of the Quaternary stress regime in southern central Hispaniola

The geometric characteristics of the faults at all scales, the striae sets in their planes, the compatible stress tensors and their chronological succession, constrained by offset relations with dated lithostratigraphic units, define three types of neotectonic fault kinematics in southern central Hispaniola. These types are: thrust and reverse faulting with horizontal σ_1 and σ_2; strike-slip faulting with horizontal σ_1 and σ_3; and extensional faulting with vertical σ_1 (Fig. 15; see also Supporting

Information S5). Each type of fault kinematics is related to a different deformation event, characterized by a specific state of stress, whose development changes geographically throughout southern central Hispaniola (Fig. 16).

Throughout the Cordillera Central domain, Sierra Martín García and San Juan-Azua basin there is evidence of slip on thrust and reverse faults related to a NNE to NE-trending compressional D1 stress regime (Fig. 16). These NW-trending D1 structures deform the middle Eocene-lower Miocene sedimentary rocks of the Río Ocoa Group, as well as its substrate of the Peralta Belt accretionary prism, the early/middle Miocene to middle Pliocene marine turbiditic and platform sediments of the San Juan-Azua foreland basin, and the upper Pliocene to Early Pleistocene clastic continental deposits of the Arroyo Seco Formation (Heubeck & Mann, 1991; Díaz de Neira & Solé Pont, 2002; Hernáiz Huerta & Pérez-Estaún, 2002; among others). A similar structural relationship has been described along the southern border of the Chaîne des Matheux in Haiti, where SW-directed thrusts deform rocks of middle to upper Miocene age (Pubellier et al., 2000). Upper Miocene to lower Pliocene onset of uplift in the Cordillera Central is simultaneous with uplift in the Sierra de Neiba, with both ranges providing the clastic sedimentary source for the eastern San Juan and Azua (piggyback) basins. The pre-Early Pleistocene folding and thrusting D1 event has been related to the collision between CLIP-related units of the Southern Hispaniola Peninsula and the island-arc crust of the Cordillera Central (Heubeck & Mann, 1991; Mann et al., 1991b).

Stress tensors obtained for D1 event indicate a general NE-trending σ_1 axis, ranging between N017°E and N070°E directions, with a relatively well-constrained maximum value in the count-contours stereoplot at N202°E, plunging 06° to the SW (Fig. 15). In the calculations, the orientation of σ_1 has been restored at sites in the eastern Ocoa Bay that have undergone a post-D1 clockwise rotation. The vertical arrangement of σ_3 axis in the computed stress tensors is consistent with deformation by thrusting. The R stress ratio has values of 0.50 ± 0.25, indicating stress tensors close to pure compression. Therefore, the regional D1 stress regime consisted of a NE-trending subhorizontal compression. However, R ratio presents some values of 0.87 and 0.92 (21JE73 and 21JE79 sites), which means that the maximum and minimum σ_H axes are close in magnitude and higher that σ_V ($\sigma_1 \approx \sigma_2$). These R values suggest that a D1 deformationlocally characterized by a radial compression regime. On the other hand, the WSW-directed GPS motions measured in JUAN, CONS and BARA stations, located away from important D2 structures, are suborthogonal to the strike of the San Juan-Pozos and Barahona fault zones, as well as the thrust structures in the Cordillera Central and Peralta Belt domains. Therefore, present-day reverse faulting dominates active D1 structures (Fig. 16). This argument agrees with thrust kinematics and reverse stress regime obtained for D1 from field permanent deformation.

The NNE to NE-trending strike-slip D2 stress regime has been deduced near the Ocoa-Bonao-La Guácara fault zone, particularly in the eastern sector of the Ocoa Bay and in the margins of the San José de Ocoa and Rancho Arriba intramountain basins (Fig. 16). This strike-slip deformation has also been observed in the vicinity of the Beata Ridge fault zone, in the western sector of the Ocoa Bay, and in relation to NE to ENE-striking left-hand strike-slip faults that cut and displace D1 thrusts in the Cordillera Central. Therefore, D2 strike-slip faults cut and displace the D1 fold-and-thrust structures, as described in previous works (Hernáiz Huerta & Pérez-Estaún, 2002; Pérez-Valera, 2010).

D2 strike-slip faults deform the Quaternary deposits in several places, as the fossil coral reef terrace built during the MIS 5e and 5c stages in the SW and NE flanks of the Sierra Martín García and Bahoruco. Recent field-data collected in the eastern sector of Ocoa Bay (Escuder-Viruete et al., in press), indicate that D2 strike-slip faults subparallel to the O-OBFZ segment deform an alluvial fan of latest Pleistocene age, but are locally fossilized by a younger alluvial fan of Holocene age. Nonetheless, the Ocoa-Bonao-La Guácara fault zone cuts geomorphic features along its path, such as Late Pleistocene-Holocene alluvial fans, fluvial terraces and streams in the San José de Ocoa and Rancho Arriba intramountain basins, which collectively evidence active D2 deformation. Therefore, the D2 stress-field continues through the latest Pleistocene and most likely today. This interpretation is consistent with the moment tensor solutions of strike-slip faulting calculated for the 1977 and 1988 earthquakes (CMT catalogue; Ekströn et al., 2012), whose epicenters are located very close to the OBFZ trace.

The change from a D1 compressional to a D2 strike-slip stress regimes took place during the Early and Middle Pleistocene (or sometime in the Early Pleistocene). This change could be related to the indentation of the eastern sector of the Beata Ridge in southern Hispaniola, as part of the Caribbean oceanic plateau collision in the back-arc region of the Hispaniola microplate. This processes could produced the large-scale drag of the pre-existing D1 structures in the eastern Ocoa Bay and generated large-scale conjugate D2 strike-slip faults on the margins of the aseismic ridge indenter. In this sense, the geometric characteristics of the D2 deformation, such as landward deflection of the Muertos trench axis and development of conjugate strike-slip faults and back-thrusts, are analogous to those produced above a subducted conical seamount or submarine aseismic ridge (Ranero and von Huene, 2000; Sak et al., 2009; Gardner et al., 2013), as it has been faithfully reproduced by sandbox analogue models of such convergent margins (Dominguez et al., 2000).

Stress tensors of D2 event indicate a general NE-trending σ_1 axis, comprised between N015°E and N055°E directions, with a relatively well-constrained maximum value at N045°E, plunging 01° to the NE (Fig. 15). The dispersion of σ_1 axes is due to fault-slip measures in sites located in the San José de Ocoa Basin, where the S-OBFZ trends N-S, or probably due to the reorientation of the regional stress field that occurs around this large-scale strike-slip fault. The subvertical arrangement of the σ_2 axes indicates that the D2 deformation took place in a strike-slip regime, characterized by a NE-trending subhorizontal shortening for R-values ranging between 0.21 and 0.60, with prevalence of values close to 0.5. These R-values suggest a deformation mode close to pure strike-slip, consistent with the low-pitch angle of the displacement vectors observed in D2 strike-slip faults and some focal mechanism solutions. Note that the SW-directed GPS motion measured in the TORT station is parallel to the NE-SW strike of the nearby Beata Ridge fault segment, implying a present-day pure strike-slip faulting along this D2 structure (Fig. 16).

D3 faults can be grouped into two geometric families: D3a and D3b. The first family includes NE-SW to NNE-SSW trending normal and oblique normal D3a faults. Although the number of computed stress tensors is limited, inversion of fault-slip data establishes a general NW-SE trending extensional stress regime D3a (Fig. 15). This extensional stress regime has only been detected in the western Cordillera Central-Peralta Belt domains and in sectors close to the S-OBFZ segment, as the San José de Ocoa and Rancho Arriba intramountain basins (Fig. 16). The orientation of σ_3 axes has a high dispersion, ranging between N103°E and N168°E, for values of the R ratio very close to 0.5, establishing stress tensors of pure extension. The age of the D3a event could not be precisely established. However, these normal faults affect the volcanic rocks of Pleistocene age of the Valle Nuevo area whose K-Ar ages are 0.5 ± 0.3 and 0.3 ± 0.2 Ma (Vespucci, 1988; Kamenov et al., 2011; and references herein) and, therefore, its age is at least post-Middle Pleistocene. The alignment of the emissive centers of the Quaternary calc-alkaline to mafic alkaline volcanism in the region follows a NE-SW strike (Fig. 16), so the NW-directed extension during D3a could have favoured the opening of NE-SW striking planes and the rise of magmas. Alternatively, the rise of magmas could have taken place in favour of releasing bends formed during D2 deformation. Hot springs and associated travertine deposits in the volcanic region indicate that geothermal activity continues today.

The second family includes WNW to W-striking dip-slip normal faults that established an N to NNE-trending extensional D3b stress regime. Its development is geographically limited to the surroundings of Ocoa Bay (Fig. 16). D3b normal faults deform the coral reef terraces of the MIS 5e and 5c stages (22JE26, Playa Azul; 21JE126, Playa Las Caobitas; and 20JE04, Palmar de Ocoa sites) and the overlapping alluvial fan of Late Pleistocene to Holocene? age (21JE127 and 22JE15 sites). Inversion of 12 fault-slip data sets gives rise to NNE-trending σ_3 axes, comprised between N003°E and N023°E directions, with a relatively well-constrained maximum value at N022°E, plunging 6° to the NE (Fig. 15). The subvertical arrangement of the σ_1 axes and the obtained R-values close to 0.5 indicate stress tensors close to pure extension.

In summary, a relatively constant NE-trending horizontal shortening, parallel to the current direction of plate convergence established by GPS measurements, controlled the evolution of the Quaternary stress tensor in southern central Hispaniola. This evolution included a D1 event of compression followed by a D2 near pure strike-slip event, which was locally coeval by a more heterogeneous and geographically localized D3 regime of pure extension. The successive changes in the stress regime were related to a permutation of σ_3 by σ_2 vertical stress between D1 and D2 events, and to a permutation of σ_2 by σ_1 vertical stress between D2 and D3 events (Fig. 15).

6.3. Origin of the extensional tectonics localized in the Ocoa Bay

Figure 13 shows the coast of southern central Hispaniola intermittently covered by the fossil coral reef terrace that grew as a fringing reef during MIS 5e/5c stage and currently ranges in elevation from 0 to 20 m above sea level. The MIS 5e stage corresponds to a relatively long period of high-sea level that took place during the 118–128 ka interval in the Last Interglacial, when the sea level was between 2 and 6 m above the current level (e.g., Schellmann and Radtke, 2004). The existence of coral reef terraces of the MIS 5e/5c stage at elevations between 1 and 25 m above the current sea level can be explained by active tectonics that has uplifted in variable amounts the southeastern margin of Cordillera Central, the Sierra Martín García and the Sierra Bahoruco. Assuming a *Diploria* sp. growth depth of ~2 m and an average sea level height during the MIS 5e of +2.0 m (see details in Escuder-Viruete et al., 2020), the minimum uplift rates for the terrace range between 0.01 and 0.22 m/ka. The absence of the coral terrace, as well as of other coral terraces presumably built up during older MIS stages, can be explained as due to erosion or to being located at elevations below present sea level as a consequence of later subsidence. In our case, the absence of the coral terrace of the MIS 5c/5e stage coincides with the reentrant of the Ocoa Bay affected by D3b extensional tectonics.

Figure 13 also shows two outcrops of the modern fringing reef raised between 0.5 and 3 m above sea level, which are currently subjected to strong marine erosion. An specimen of coral *Diploria* sp. collected in the uppermost levels of the terrace at Playa Caracoles (21JE124 site) have provided an U-Th ages of 0.730 ± 0.01 ka. This age indicates growth of the coral terrace during MIS 1 stage in the Middle Holocene. The calculated minimum uplift rate for the terrace is 4.11 m/ka.

Thus, the spatial distribution of the topography in the Ocoa Bay, the D3b extensional deformation, outcrops of the coral reef terraces and uplift rates are, to the first order, controlled by the subducting Beata Ridge of the Caribbean plate. This is because the Muertos accretionary prism that makes up the margin wedge on the Ocoa Bay must deform around this indenting bathymetric feature. The topographically low area of the Ocoa Bay lines up along the relative plate motion vector with the Beata Ridge indenter. The highest uplift rates are recorded along the central northern coast of the Ocoa Bay and decrease parallel to the trench and perpendicular to the Beata Ridge to the E (southeast coast of the Cordillera Central) and the W (Sierra Martín García).

This pattern in the distribution of the D3b deformation and vertical motions can be interpreted as a wave of rapid uplift followed by subsidence that propagates parallel to the current plate motion vector in the Ocoa Bay, as a response to the subduction of bathymetric irregularities in the Beata Ridge. Following the deformation mechanism proposed for seamount subduction in the New Hebrides and Solomon Arcs (e.g., Taylor et al. 2005), the passage of a subducting bathymetric high produces a history of rapid uplift and subsequent collapse and subsidence in a block of similar dimensions of the upper plate.

Along the Ocoa Bay, where the Beata Ridge indenter currently entering the Muertos Trench, macroscale WNW to W-striking dip-slip normal faults and mesoscale fault-slip data, are consistent with SSW to S-directed extension perpendicular to the margin (Fig. 16). These steeply-dipping normal faults may be a consequence of the collapse of the margin, constituted by relatively soft sedimentary rocks of the Muertos accretionary prism, in the wake of the stronger mafic igneous rocks of the subducting Beata Ridge that produce a basal erosion of the upper plate (Ramero & von Huene, 2000; Sak et al., 2009; Gardner et al., 2013; Vannucchi et al., 2013). The subvertical and NE-striking faults formed during D2, such as the N-BRFZ and O-OBFZ segments, are arranged at high angles to the margin and may have accommodated differential displacements during D3, acting as transfer faults. Ocoa Bay would therefore be an embayment of ~20 km wide and ~25 km length, formed by the passage of a bathymetric high in the subducting Beata Ridge. A similar mechanism has been proposed along the northern Hispaniola-Puerto Rico margin, where subduction/collision of bathymetric highs built on the Atlantic oceanic crust has resulted to basal erosion in the upper plate and forearc collapse (Grindlay et al., 2005; Escuder-Viruete and Pérez, 2020).

This interpretation is favored by the absence of the coral terrace of the MIS 5e/5c inboard of the Beata indenter (Fig. 13), which must have been uplifted and eroded or sunk by D3b extensional tectonics. In turn, the gravimetric and magnetic anomaly produced by the CLIP magnetic basalts that characterizes the surroundings of Ocoa Bay (Fig. 4) suggests a thinning of the upper plate wedge in the submarine portion of the margin. In this tectonic context, the high uplift rates detected in the uplifted modern coral terrace indicate a new episode of rapid uplift and future subsidence of the margin during continued subduction of the Beata Ridge.

Although the role of seamounts/aseismic ridge subduction in the plate-margin seismicity is disputed, e.g. enhancing seismic coupling (e.g., Bangs et al., 2015) versus decreasing the degree of coupling and limiting the lateral propagation of megathrust-earthquake rupture planes (e.g., Bonnet et al., 2019), the 1751 earthquake occurred in the vicinity of the Ocoa Bay and destroyed the city of Azua. The presence of the subducting Beata Ridge in high-resolution bathymetric swath maps of the Caribbean-Hispaniola plate boundary region and in seismic reflection profiles across the Muertos Trench (e.g., Granja Bruña et al., 2014), together with the proposed location of the Azua earthquake intensity center in the Ocoa Bay (Bakun et al., 2012), suggest that this Mw=7.5 event may have resulted from the rupture of a ridge asperity in the subduction and can therefore be repeated in the future.

6.4. Definition of seismotectonic structures in southern central Hispaniola

The characterization of seismotectonic structures has been previously carried out in some sectors of Hispaniola Island (Frankel et al., 2010; Bertil et al., 2015; Escuder-Viruete et al., 2020; Terrier-Sedan and Bertil, 2021). Used criteria in the definition were: geodynamic situation; geological, stratigraphic and/or tectonic evidence of recent activity; kinematic type of fault and rate of displacement; and associated historical and/or instrumental seismicity. The definition of these large-scale active structures is critical since it allows for establishing seismotectonic zonation models of the area under consideration, which is fundamental for the quantitative seismic hazard assessment. However, this approach requires updating the inventory of active structures as tectonic and seismological knowledge increases.

The previous works and the new data presented in this work allow updating the main seismotectonic fault zones structures in southern central Hispaniola, including its adjacent offshore sector. They are: San Juan-Pozos (Mann et al., 1991a); Matheux-Sierra de Neiba (MAFZ, Hernaiz Huerta et al., 2007); Bahoruco (BAFZ or Barahona Thrust; Rodríguez et al., 2018); Beata Ridge (Mauffret and Leroy, 1999); Muertos Trough (Granja Bruña et al., 2009; 2014); Ocoa-Bonao-La Guacara (Pérez-Estaún et al., 2007; Escuder-Viruete et al., in press); and probably the eastern end of the Enriquillo-Plantain Garden (EPGFZ; Mann et al., 1995).

The attribute compilation of these seismotectonic structures is outlined in Table 1, including the fault or segment name, deformation mechanism, estimated maximum magnitude (Mw), known biggest earthquake (magnitude in Mw), estimated displacement rate, length, strike and dip, and width of the fault zone. Following Bertil et al. (2015) and Terrier-Sedan and Bertil (2021), the maximum magnitude of rupture for each fault/segment was estimated using the major recorded historical earthquake, or its geometric parameters (e.g. Wells and Coppersmith, 1994), taking into account its degree of uncertainty. Displacement rates for each seismogenic structure were derived from geological mapping (SYSMIN Project, 2010; this work), geodetic GPS measurements (Calais et al., 2002; Manaker et al., 2008), or calculated in the present study through empirical relationships (e.g. Wells and Coppersmith, 1994).

From this information, a simplified seismotectonic model was built that considers two types of seismic sources: subduction and strike-slip fault zones in which the seismicity of greater magnitude is concentrated; and superficial/upper crustal areas located between them where the seismicity is of moderate to low magnitude and is more homogeneously distributed. This seismotectonic model is the starting point for the seismic hazard assessment in southern central Hispaniola presented below.

6.5. Seismic hazard assessment in southern central Hispaniola

The seismic hazard assessment carried out in this work follows a probabilistic approach. Following the Cornell-McGuire methodology, the R-CRISIS calculation code (Ordaz et al., 2014) builds a probabilistic model that takes into account the spatial distribution of seismogenic sources, the occurrence and magnitude of earthquakes in time, and the attenuation characteristics of the strong motion in the ground. Thus, the R-CRISIS code computes the seismic hazard in terms of the probability of exceeding a peak ground acceleration (PGA) value for a specific site in a given period.

For the seismic hazard assessment in southern Central Hispaniola, the previously described seismotectonic zonation model composed of subduction zones, main strike-slip fault zones and diffuse seismogenic zones located between them, was geometrically built as simplified 3-D polygonal surfaces of specific wildth. In these seismic sources, earthquakes can occur at any point of the source with equal probability (Ordaz et al., 2014). Functions selected to describe the attenuation of the ground motion acceleration with distance from the source are the same as those used by Frankel et al. (2010) and Benito et al. (2012) to evaluate the seismic hazard in Haiti after the

12/10/2010 earthquake. Parameters used to establish the seismic activity of each source and their uncertainties are included in Escuder-Viruete et al. (2020). The hazard analysis performed in this work did not take into account possible amplifications of the seismic parameters by site effects. Seismic hazard was computed in a rectangular point grid, framed by the coordinates: 17.960°N and 18.835°N of latitude; -70.175°W and -71.250°W of longitude (WGS-84 projection system), with a point spacing of 0.025° in both directions. Results were converted in a continuous surface using an inverse distance squared weighted interpolation algorithm.

Figure 17 includes the results of the seismic hazard assessment in southern central Hispaniola, expressed as PGA intervals (values in cm/s^2) and for a return period of 475 years (i.e., for a probability of exceedance of 10% in 50 years). Modeled minimum and maximum PGA values are 86 cm/s^2 and 857 cm/s^2, respectively, with a mean (and standard deviation) of 386.7 (148.0). Therefore, the regional seismic hazard values range from low to very high. PGA zoning defines an elongated pattern sub-parallel to the main fault zones. Seismic hazard is higher in the Ocoa Bay, along the San José de Ocoa valley in the southern Cordillera Central, and in the topographic transition between the northern Cordillera Central and the eastern Cibao Valley. It decreases towards the NW and SE regions. This seismic hazard zoning contrasts with the previously proposed by Frankel et al. (2010), Benito et al. (2012) and Bertil et al. (2010, 2015), which did not take into account all the seismic sources included in the present work, particularly the Ocoa-Bonao-La Guácara fault zone.

With this seismotectonic model, the highest PGA values (> 600 cm/s^2) are associated with the N-BRFZ, O-OBFZ and C-OBFZ segments. Branches of the S-OBFZ segment set intermediate to high values (500-650 cm/s^2). The C-OBFZ segment also has associated high PGA values (>650 cm/s^2), which decrease to intermediate and low values westward along the W-OBFZ segment (250-450 cm/s^2). The superficial trace of the O-MT segment of the Muertos Trough also has associated high PGA values (600 cm/s^2), which extend into depth following the subduction interface. The BAFZ has associated intermediate PGA values in its connection to the BRFZ, which also decrease westward.

The S-JPFZ presents high PGA values at its SE end (500-700 cm/s^2), where it is displaced by the N-BRFZ, decreasing towards the NW. The Hispaniola fault zone has also been included in the modeling, giving rise to intermediate values of the PGA that become high in its central segment. The E-EPGFZ segment also has associated intermediate to low PGA values (400-500 cm/s^2).

In summary, the highest PGA values in southern central Hispaniola are associated with N-BRFZ, O-OBGFZ and A-MT segments, whose traces frame a triangular zone centered on Ocoa Bay where the seismic hazard is very high. As described, this sector includes the intensity center estimated for the 1751 Azua earthquake (Mw 7.5), which according to some historical accounts gave rise to a tsunami in the bay. For Bakun et al., (2012), this event could be produced by the Enriquilo-Platain Garden fault zone or, as an alternative source, the Muertos deformation belt. The results of the PGA modeling rule out the EPGFZ as a source and indicate that the BRFZ, the O-MT and, less likely, the O-OBFZ, could have generated this earthquake.

Historical records indicate that the greatest effects of the 1615, 1684, 1691 and 1911 earthquakes (Mw from 6.0 to 7.5) were in the southern sector of the Central Cordillera. However, the determination of its seismic source could not be confidently established with the available data, since these strong earthquakes did not produce known surface ruptures. Future neotectonic and paleoseismological studies, together with the seismic hazard modeling, may shed light on the active fault zones that generated large earthquakes in the region and therefore allow updating the spatial distribution of the seismic hazard.

Acknowledgments

We would like to thank the support and infrastructures provided by the Servicio Geológico Nacional of the Dominican Republic, particularly to Yésica Pérez-Alejandro, Maria Betania Roque-Quezada and Edwin García. The research was funded through PID2019-105625RB-C22 project of the MCIN/AEI/10.13039/501100011033 of the Spanish Government. Some works also received funding from the FONDOCYT Project 2015-1b3-118 of the MESCyT of the Dominican Republic Government.

Data Availability Statement

The data for this paper are contained in the text, figures and supporting information and can also be found in the data repository DIGITAL.CSIC which is the institutional repository of the Spanish National Research Council (Escuder-Viruete et al., 2023).

Electronic supporting informationin also in Data Repository

Supporting Information S1. U-Th geochronological results of coral samples.

Supporting Information S2. Methodology of dynamic fault-slip analysis.

Supporting Information S3. Sites used to obtain stress tensors from the analysis of fault-slip data sets.

Supporting Information S4. Stress tensors obtained by methods of inversion of fault-slip data.

Supporting Information S5. Maximum horizontal stresses and tectonic regimes obtained by inversion methods.

References

Alonso, J.L., Marcos, A. Villa, E., Suárez, A., Merino-Tomé, O.A. & Fernández, L.P. (2014). Mélanges and other types of block-in-matrix formations in the Cantabrian Zone (Variscan Orogen, northwest Spain): origin and significance. International Geology Review. DOI: 10.1080 /00206814.2014.950608. 18 pp.

Alvarez L, Chuy T, Garcia J, Moreno B, Alvarez H, Blanco M, Exposito O, Gonzalez O, Fernandez AI (1999) An earthquake catalogue of Cuba and neighboring areas. The Abdus Salam International Centre for Theoretical Physics. Internal Report IC/IE/99/1, 62p. Trieste, Italy

Angelier, J. (1994). Fault slip analysis and paleostress reconstruction. In: Hancock, P. (ed.), Continental Deformation. Pergamon Press, United Kingdom, pp. 53–100.

Ayala, C., García-Lobón, J.L., Escuder-Viruete, J., Rey-Moral, C., Pérez-Estaún, A. & Padín-Debén, A. (2017). High-resolution magnetic, regional gravity and petrophysical characterization of the Dominican Republic tectonic domains with special focus on the Central Cordillera. Boletín Geológico y Minero 128 (3): 611-631.

Bakun, W.H., Flores, C.H. & Uri, S. (2012). Significant earthquakes on the Enriquillo fault system, Hispaniola, 1500–2010: Implications for seismic hazard. Bulletin of the Seismological Society of America 102, 18–30.

Bangs, N. L., McIntosh, K. D., Silver, E. A., Kluesner, J. W., & Ranero, C. R. (2015). Fluid accumulation along the Costa Rica subduction thrust and development of the seismogenic zone. Journal of Geophysical Research: Solid Earth, 120, 67–86.

Benford, B., Demets, C. & Calais, E. (2012). GPS estimates of microplate motions, northern Caribbean: evidence for a Hispaniola microplate and implications for earthquake hazard. Geophysical Journal International 191 (2), 481-490.

Benito, O.B., Cervera B.J., Molina P.S., Navarro B.M., Doblas L.M., Martínez D.J.J. and others, 2012. Évaluation de l'aléa et du risque sismique en Haïti dirigée vers la conception parasismique. Monografía E.T.S.I. en Topografía, Geodesia y Cartografía (UPM), 137pp. http://oa.upm.es/view/institution/Topografia/

Bertil, D., Lemoine A., Winter T. & Belvaux M. (2010). Microzonificación sísmica de Santiago – Republica Dominicana. Amenaza regional. Informe final. BRGM/RC-59107-FR, 100 pp.

Bertil, D., Terrier M., Belvaux M., 2015. Análisis de las fuentes sísmicas y evaluación de la amenaza sísmica regional del gran Santo Domingo. Estudio de la amenaza sísmica y vulnerabilidad física del Gran Santo Domingo. Actividad 1.1. BRGM/RP-65305-FR, 149 pp.

Bonnet, G., Agard, P., Angiboust, S., Fournier, M., & Omrani, J. (2019). No large earthquakes in fully exposed subducted seamount. Geology, 47, 407–410.

Byrne, D.B., Suarez, G., McCann, W.R., 1985. Muertos Trough subduction, microplate tectonics in the northern Caribbean? Nature 317, 420–421.

Calais, E., Freed, A., Mattioli, G., Amelung, F., Jonsson, S., Jansma, P., Hong, S.H., Dixon, T., Prépetit, C. & Momplaisir, R. (2010). Transpressional rupture of an unmapped fault during the 2010 Haiti earthquake. Nature Geoscience 3 (11), 1–6.

Calais, E., Symithe, S., Mercier de Lépinay, B.M. & Prépetit, C. (2016). Plate boundary segmentation in the northeastern Caribbean from geodetic measurements and Neogene geological observations. Comptes Rendus Geoscience 348, 42-51.

Célérier, B., Etchecopar, A., Bergerat, F., Vergely, P., Arthaud, F. & Laurent, P. (2012). Inferring stress from faulting: from early concepts to inverse methods. Tectonophysics 581,206-219.

Cheng, H., Edwards, R.L., Hoff, J., Gallup, C.D., Richardsm D.A., Asmerom,Y., 2000. The half-lives of uranium-234 and thorium-230. Chemical Geology 169, 17-33.

Corbeau, J., Rolandone, F., Leroy, S., de Lépinay, B.M., Meyer, B., Ellouz-Zimmermann, N., Momplaisir, R., 2016. The northern Caribbean plate boundary in the Jamaica Passage: structure and seismic stratigraphy. Tectonophysics 675, 209–226.

Corbeau, J., Rolandone, F., Leroy, S., Guerrier, K., Keir, D., Stuart, G., Clouard, V., Gallacher, R., Ulysse, S., Boisson, D., Bien-Aime Momplaisir, R., Saint Preux, F., Preprtit, C., Saurel, J.-M., de Lépinay, B.M., Meyer, B., 2017. Crustal structure of the western Hispaniola (Haiti) from teleseismic receiver function study. Tectonophysics 709, 9–19.

Corbeau, J., Gonzalez, O.L. Clouard, V., Rolandone, F., Leroy, S., Keir, D., Stuart, G., Momplaisir, R., Boisson, D. & Prépetit, C. (2019). Is the local seismicity in western Hispaniola (Haiti) capable of imaging northern Caribbean subduction? Geosphere, 15, 6, 1738–1750. https://doi.org/10.1130 /GES02083.1.

Díaz de Neira, J.A. (2000). Evolución geomorfológica del Llano de Azua (Sur de la República Dominicana). Acta Geológica Hispánica 37, 207-227.

Díaz de Neira, J.A. (2004). Mapa Geológico de la Hoja a E. 1:50.000 nº 5970-I (Barahona). Dirección General de Minería, Santo Domingo. 68 pp. https://www.sgn.gob.do

Díaz de Neira, J.A. & Solé Pont, F.J. (2002). Precisiones estratigráficas sobre el Neógeno de la cuenca de Azua (República Dominicana). Acta Geologica Hispanica 37, 163-181.

Dolan, J., Mann, P., De Zoeten, R., Heubeck, C. & Shiroma, J. (1991). Sedimentologic, stratigraphic, and tectonic synthesis of Eocene-Miocene sedimentary basins, Hispaniola and Puerto Rico. In: Mann, P., Draper, G., & Lewis, J.F. (Eds.), Geologic and Tectonic Development of the North America-Caribbean Plate Boundary in Hispaniola: Geological Society of America Special Paper 262, 17–26.

Dolan, J.F., Mullins, H.T. & Wald, D.J. (1998). Active tectonics of the north-central Caribbean region: oblique collision, strain partitioning and opposing slabs. In: Dolan, J. & Mann, P. (Eds.), Active Strike-Slip and Collisional Tectonics of the Northern Caribbean Plate Boundary in Hispaniola. Geological Society America Special Paper 326: 1-61

Dominguez, S., Malavieille, J. & Lallemand, S.E. (2000). Deformation of accretionary wedges in response to seamount subduction: Insights from sandbox experiments. Tectonics 19, 182-196.

Draper, G., Mann, P. & Lewis, J.F. (1994). Hispaniola. In: Donovan, S.K., Jackson T.A. (Eds.), Caribbean Geology: An introduction. Jamaica, University of the West Indies Publishers Association, 129-150.

Driscroll, N.W. & Diebold, J.B. (1998). Deformation of the Caribbean region: one plate or two? Geology 26 (11), 1043–1046.

Dürkefälden, A., Hoernle, K., Hauff, F., Wartho, J.A., Bogaard, P. van den & Werner, R. (2019). Age and geochemistry of the Beata Ridge: Primary formation during the main phase (~89 Ma) of the Caribbean Large Igneous Province. Lithos 328–329, 69-87.

Ekström, G., Nettles, M. & Dziewonski, A.M. (2012). The global CMT project 2004-2010: Centroid-moment tensors for 13,017 earthquakes. Physics of the Earth and Planetary Interiors 200-201, 1-9.

Escuder-Viruete, J. & Baumgartner, P.O. (2014). Structural evolution and deformation kinematics of a subduction-related serpentinite-matrix mélange, Santa Elena Península, northwest Costa Rica. Journal of Structural Geology 66, 356-381.

Escuder Viruete, J. & Pérez, Y., 2020. Neotectonic structures and stress fields associated with oblique collision and forearc sliver formation in northern Hispaniola: Implications for the seismic hazard assessment. Tectonophysics, 784, 228452.

Escuder-Viruete, J., Joubert, M., Urien, P., Friedman, R., Weis, D., Ullrich, T., Pérez-Estaún, A., 2008. Caribbean island-arc rifting and back-arc basin development in the Late Cretaceous: geochemical, isotopic and geochronological evidence from Central Hispaniola. Lithos, 104, 378-404. doi:10.1016/j.lithos.2008.01.003.

Escuder-Viruete, J., Pérez-Estaún, A., Gabites, J. & Suárez-Rodríguez, Á. (2011a). Structural development of a high-pressure collisional accretionary wedge: The Samaná complex, northern Hispaniola, Journal of Structural Geology 33, 928-950.

Escuder-Viruete, J., Pérez-Estaún, A., Booth- Rea, G. & Valverde-Vaquero, P. (2011b). Tectonometamorphic evolution of the Samaná complex, northern Hispaniola: Implications for the burial and exhumation of high-pressure rocks in a collisional accretionary wedge. Lithos 125, 190-210.

Escuder-Viruete, J., Valverde-Vaquero, P., Rojas-Agramonte, Y., Gabites, J. & Pérez-Estaún, A. (2013). From intra-oceanic subduction to arc accretion and arc-continent collision: Insights from the structural evolution of the Río San Juan metamorphic complex, northern Hispaniola. Journal of Structural Geology 46, 34-56.

Escuder-Viruete, J., Joubert, M., Abad, M., Pérez-Valera, F. & Gabites, J. (2016a). The basaltic volcanism of the Dumisseau Formation in the Sierra de Bahoruco, SW Dominican Republic: a record of the mantle plume-related magmatism of the Caribbean large Igneous Province. Lithos 254–255, 67–83.

Escuder-Viruete, J., Súarez, A., Gabites, J. & Pérez-Estaún, A. (2016b). The Imbert Formation of northern Hispaniola: a tectono-sedimentary record of arc-continent collision and ophiolite emplacement in the northern Caribbean accretionary prism. Solid Earth Discuss 6, 1-50.

Escuder Viruete, J., Beranoaguirre, A., Valverde-Vaquero, P. & Mcdermott, F. (2020). Quaternary deformation and uplift of coral reef terraces produced by oblique subduction and underthrusting of the Bahama Platform below the northern Hispaniola forearc. Tectonophysics, 796, 228631.

Escuder-Viruete, J., Fernández, F.J., Pérez Valera, F. & Medialdea, A. (2023, in press). Present-day accommodation of Caribbean-North American oblique plate convergence through the Ocoa-Bonao-La Guacara fault zone, southern central Hispaniola: a transition zone between oceanic subduction and arc-oceanic plateau collision. Tectonics. DOI: 10.1029/2022TC007618

Escuder-Viruete, J., Fernández, F.J., Pérez Valera, F. & McDermott, F. (2023). Active tectonics, Quaternary stress regime evolution and seismotectonic faults in southern central Hispaniola: implications for the quantitative seismic hazard assessment. DIGITAL.CSIC repository (temporary private link at).

Frankel, A., Harmsen, S., Mueller, Ch., Calais, E., Haase, J., 2011. Seismic Hazard Maps for Haiti. Earthquake Spectra, Volume 27, No. S1, pages S23-S41

Flores, C. H., U. S. ten Brink, and W. H. Bakun (2011), Accounts of damage from historical earthquakes in the northeastern Caribbean, to aid in the determination of their location and intensity magnitudes, U.S. Geol. Surv. Open File Rep., 2011–1133, 226 pp.

Fankhauser, A., McDermott, F., Fleitmann, D., 2016. Episodic speleothem deposition tracks the terrestrial impact of millennial-scale last glacial climate variability in SW Ireland. Quat. Sci. Rev. 152, 104-117. http://dx.doi.org/10.1016/j.quascirev.2016.09.019

García Lobón, J.L. & Rey Moral, C. (2004). Magnetismo y radiación gamma natural de la República Dominicana. Boletín Geológico y Minero 115 (1), 153-168.

García-Lobón J.L. & Ayala. C. (2007). Cartografía geofísica de la República Dominicana: datos de densidad, susceptibilidad magnética y magnetización remanente. Boletín Geológico y Minero, 118 (2), 175-194

Gardner, T. W., Fisher, D.M., Morell, K.D. & Cupper, M.L. (2013). Upper-plate deformation in response to flat slab subduction inboard of the aseismic Cocos Ridge, Osa Peninsula, Costa Rica. Lithosphere 5, 3, 247-264.

Granja Bruña, J.L., ten Brink, U.S., Carbó-Gorosabel, A., Muñoz-Martín, A. & Gómez Ballesteros, M. (2009). Morphotectonics of the central Muertos thrust belt and Muertos Trough (northeastern Caribbean). Marine Geology 263, 7–33.

Granja Bruña, J.L., Carbó-Gorosabel, a., Llanes Estrada, P., Muñoz-Martín, a., ten Brink, U.S., Gómez Ballesteros, M., Druet, M. & Pazos, A. (2014). Morphostructure at the junction between the Beata ridge and the Greater Antilles island arc (offshore Hispaniola southern slope). Tectonophysics 618, 138–163.

Grindlay, N.R., Mann, P., Dolan, J.F., van Gestel, J.P., 2005. Neotectonics and subsidence of the northern Puerto Rico–Virgin Islands margin in response to the oblique subduction of high-standing ridges. Geol. Soc. Am. Special Paper 385, 31–60.

Hernáiz-Huerta, P.P. & Pérez-Estaún, A. (2002). Estructura del cinturón de pliegues y cabalgamientos de Peralta, República Dominicana. Acta Geológica Hispánica 37, 183-205.

Hernáiz-Huerta, P.P., Díaz De Neira, J.A, García Senz, J., Deschamps, I., Lopera, E., Escuder Viruete, J., Ardévol Oró, Ll., Granados L., Calvo J.P. & Pérez Estaún, A. (2007a). La estratigrafía de la Sierra de Neiba, República Dominicana. Boletín Geológico y Minero 118, 313-336.

Hernáiz-Huerta, P.P., Díaz De Neira, J.A, García Senz, J., Deschamps, I., Genna, A., Nicole, N., Lopera, E., Escuder Viruete, J., Ardévol Oró, Ll. & Pérez Estaún, A. (2007b). La estructura de la sierra de Neiba, margen norte de la sierra de Bahoruco, Sierra de Martín García y cuenca de Enriquillo de la República Dominicana: un ejemplo de deformación transpresiva. Boletín Geológico y Minero 118, 337-357.

Heubeck, C. & Mann, P. (1991). Structural geology and Cenozoic tectonic history of the southeastern termination of the Cordillera Central, Dominican Republic. In: Mann, P., Draper, G., & Lewis, J.F. (Eds.), Geologic and Tectonic Development of the North America-Caribbean Plate Boundary in Hispaniola. Geological Society of America Special Paper 262, 315–336.

Heubeck, C., Mann, E, Dolan, J. & Monechi, S. (1991). Diachronous uplift and recycling of sedimentary basins during Cenozoic tectonic transpression, northeastern Caribbean plate margin. Sedimentary Geology 70: 1-32.

Hibbert, F.D., Rohling, E.J., Dutton, A., Williams, F.H., Chutcharavan, P.M., Mark, Ch.Z., Tamisiea, E., 2016. Coral indicators of past sea-level change: A global repository of U-series dated benchmarks. Quaternary Science Reviews 145, 1-56.

Jaffey, A.H., Flynn, K.F., Glendenin, L.E., Bentley, W.C., Essling, A.M., 1971. Precision measurement of half-lives and specific activities of 235U and 238U. Phys. Rev. C 4, 1889–1906.

Kamenov, G., Perfit, M., Lewis, J., Goss A.R, Arévalo, R. & Shuster, R.D. (2011). Ancient lithospheric source for Quaternary lavas in Hispaniola. Nature Geoscience 4, 554–557.

Kroehler, M.E., Mann, P., Escalona, E. & Christeson, G.L. (2011). Late Cretaceous-Miocene diachronous onset of back thrusting along the South Caribbean deformed belt and its importance for understanding processes of arc collision and crustal growth. Tectonics 30 (6), 1–31.

Manaker, D.M., Calais, E., Freed, A.M., Ali, S.T., Przybylski, P., Mattioli, G., Jansma, P., Prépetit, C. & De Chabalier, J.B. (2008). Interseismic plate coupling and strain partitioning in the Northeastern Caribbean. Geophysical Journal International 174, 889-903.

McCann, W. R., L. Feldman, and M. McCann (2011), Catalog of felt earthquakes for Puerto Rico and neighboring islands 1492–1899 with additional information for some 20th century earthquakes, Rev. Geofís. Num. 62, 141–293.

McLaughlin, P.P., van den Bold, W.A. & Mann, P. (1991). Geology of the Azua and Enriquillo basins, Dominican Republic; 1, Neogene lithofacies, biostratigraphy, biofacies, and paleogeography. In: P. Mann, G. Draper and J.F. Lewis (Editors), Geologic and Tectonic Development of the North America-Caribbean Plate Boundary in Hispaniola. Geol. Soc. Am., Spec. Pap., 262: 337-366.

Mann, P., Draper, G. & Lewis, J.F. (1991a). An overview of the geologic and tectonic development of Española. In: Mann, P., Draper, G. & Lewis, J.F. (Eds.), Geologic and Tectonic Development of the North America-Caribbean Plate Boundary in Española. Geological Society of America Special Paper 262, 1-28.

Mann, P., McLaughlin, P.P., Jr. & Cooper, J.C. (1991b). Geology of the Enriquillo-Azua basins, Dominican Republic, 2. Structure and tectonics. In: Mann, P., Draper, G. & Lewis, J.F. (Eds.), Geologic and Tectonic Development of the North America-Caribbean Plate Boundary in Española. Geological Society of America Special Paper 262, 367-389.

Mann, P., Taylor, F.W., Edwards, R.L. & Ku, T.L. (1995). Actively evolving microplate formation by oblique collision and sideways motion along strike-slip faults: an example from the northeastern Caribbean plate margin. Tectonophysics 246, 1-69.

Mann, P., Calais, E., Ruegg, J.C., Demets, C., Jansma, P.E. & Mattioli, G.S. (2002). Oblique collision in the northeastern Caribbean from GPS measurements and geological observations. Tectonics 21(6), 1-23.

Mann, P., Rogers, R., Gahagan, L., 2007. Overview of plate tectonic history and its unresolved tectonic problems. Bundschuh, J., and Alvarado, G.E. (eds) Central America: Geology, Resources and Hazards, v. 1. Leiden. The Netherlands, 201-237.

Mauffret, A. & Leroy, S. (1999). Neogene intraplate deformation of the Caribbean plate at the Beata Ridge, in: Hsü, K.J., (Series Ed.). Sedimentary Basins of the World, 4. Caribbean Basins. Mann, P. (Ed.), Elsevier Science, N. Y. 627–669.

Mauffret, A., Leroy, S., Vila, J.-M., Hallot, E., Mercier de Lepinay, B., Duncan, R.A., 2001. Prolonged magmatic and tectonic development of the Caribbean Igneous Province revealed by a diving submersible survey. Mar. Geophys. Res. 22, 17–45.

Mercier de Lépinay, B. (1987). L'évolution géologique de la bordure nord-caraïbe: L'exemple de la transversale del'île d'Hispaniola (Grandes Antilles). Thèse d'Etat, Université Pierre et Marie Curie, 366 p.

Mercier de Lépinay, B., Deschamps, A., Klingelhoefer, F., Mazabraud, Y., Delouis, B., Clouard, V., Hello, Y., Crozon, J., Marcaillou, B., Graindorge, D., Vallée, M., Perrot, J., Bouin, M.-P., Saurel, J.-M., Charvis, P. & St-Louis, M. (2011). The 2010 Haiti earthquake: A complex fault pattern constrained by seismologic and tectonic observations. Geophysical Research Letters, 38, L22305. https:// doi .org /10 .1029 /2011GL049799.

Müller, R. D., Cannon, J., Qin, X., Watson, R. J., Gurnis, M., Williams, S., et al. (2018). GPlates: Building a virtual Earth through deep time. Geochemistry, Geophysics, Geosystems, 19. doi:10.1029/2018GC007584

Ordaz M., Cardona O., Salgado-Gálvez M.A., Bernal G., Singh K. & Zuloaga D. (2014). Probabilistic seismic hazard assessment at global level. International Journal of Disaster Risk Reduction. 10(B):419-427.

Ortner, H., Reiter, F., Acs, P., 2002. Easy handling of tectonic data: the programs TectonicVB for Mac and TectonicsFP for Window. Computers & Geosciences 28, 1193-1200.

Pérez-Estaún, A., Hernaiz Huerta, P.P., Lopera, E., Joubert, M., Escuder Viruete, J., Díaz de Neira, A., Monthel, J., García-Senz, J., Urien, P., Contreras, F., Bernárdez, E., Stein, G., Deschamps, I., García-Lobón, J.L. & Ayala, C. (2007). Geología de la República Dominicana: De la construcción de arco-isla a la colisión arco-continente. Boletín Geológico y Minero 118, 157-174.

Pérez Valera, F. (2010). Mapa Geológico de la Hoja a E. 1:50.000 nº 6070-I (Sabana Buey). Dirección General de Minería, Santo Domingo, 96 pp. https://www.sgn.gob.do

Pindell, J. & Kennan, L. (2009). Tectonic evolution of the Gulf of Mexico, Caribbean and northern South America in the mantle reference frame: an update. In: James, K., Lorente, M.A. & Pindell, J. (Eds.), The geology and evolution of the region between North and South America, Geological Society of London Special Publication 328, 1-55.

Prentice, C.S., Mann, P., Crone, A.J., Gold, R.D., Hudnut, K.W., Briggs, R.W., Koehler, R.D. & Jean, P. (2010). Seismic hazard of the Enriquillo–Plantain Garden fault in Haiti inferred from palaeoseismology. Nature Geoscience 3, 789–793.

Pubellier, M., Mauffret, A., Leroy, S., Vila, J.M. & Amilcar, H. (2000). Plate boundary readjustment in oblique convergence: Example of the Neogene of Hispaniola, Greater Antilles. Tectonics 19, 4, 630–648.

Ranero, C.R., & von Huene, R. (2000). Subduction erosion along the Middle America convergent margin. Nature 404, 748–752.

Reiter, F. & Acs, P. (2000). TectonicsFP 1.6. Computer Software for Structural Geology. Operating Manual. 48 pp.

Révillon, S., Hallot, E., Arndt, N., Chauvel, C., & Duncan, R.A. (2000). A Complex History for the Caribbean Plateau: Petrology, Geochemistry, and Geochronology of the Beata Ridge, South Hispaniola. Journal of Geology 108, 641–661.

Rodriguez, J., Havskov, J., Botter Sorebseb, M. & Santos, L.F. 2018. Seismotectonics of south-west Dominican Republic using recent data. Journal of Seismology 22:883–896.

Rodríguez-Zurrunero, J.L. Granja-Bruña, A. Carbó-Gorosabel, A. Muñoz-Martín, J.M. Gorosabel-Araus, L. Gómez de la Peña, M. Gómez Ballesteros, A. Pazos, M. Catalán, S. Espinosa, M. Druet, P. Llanes, U. ten Brink, 2019. Submarine morpho-structure and active processes along the North American-Caribbean plate boundary (Dominican Republic sector). Marine Geology 407, 121-147.

Russo, R.M. & Villaseñor, A. (1995). The 1946 Hispaniola earthquake and the tectonics of the North America Caribbean plate boundary, northeastern Hispaniola. Journal Geophysical Research 100, 6265–6280

Ryan, W.B.F., Carbotte, S.M. Coplan, J. O'Hara, S. Melkonian, A. Arko, R. Weissel, R.A. Ferrini, V. Goodwillie, A. Nitsche, F. Bonczkowski, J. & Zemsky, R. (2009). Global Multi-Resolution Topography (GMRT) synthesis data set. Geochemistry, Geophysics, Geosystems 10, Q03014, doi: 10.1029/2008GC002332

Sak, P.B., Fisher, D.M., Gardner, T.W., Marshall, J.S., & LaFemina, P.C. (2009). Rough crust subduction, forearc kinematics, and Quaternary uplift rates, Costa Rican segment of the Middle American Trench. Geologival Society America Bulletin 121 (7-8), 992–1012.

Schellmann, G., Radtke, U., 2004. A revised morpho- and chronostratigraphy of the late and middle Pleistocene coral reef terraces on Southern Barbados (West Indies). Earth-Science Reviews, 64, 157–187.

Sinton, C.W., Duncan, R.A., Storey, M., Lewis, J. & Estrada, J.J. (1998). An oceanic flood basalt province within the Caribbean plate. Earth Planetary Science Letters 155, 221– 235.

SISFRANCE Antilles (2009). Sismicité historique de la France Antilles-Guyane-Mer des Caraïbes, BRGM Available online: https://sisfrance.irsn.fr/Antilles/

Suárez-Rodríguez, Á., Escuder-Viruete, J. & Colmenero-Hidalgo, E. (2017). La mélange de San Marcos, Cordillera Septentrional de la República Dominicana. Significado, origen y edad. The San Marcos mélange, Cordillera Septentrional of the Dominican Republic. Nature, origin and age. Boletín Geológico y Minero 128 (3), 633-656.

Symithe, S., Calais, E., de Chabalier, J.B., Robertson, R. & Higgins, M. (2015). Current block motions and strain accumulation on active faults in the Caribbean. Journal Geophysical Research Solid Earth 120, 3748-3774.

Taylor, F. W., Mann, P., Bevis, M. G., Edwards, R. L., Cheng, H., Cutler, K. B., et al. (2005). Rapid forearc uplift and subsidence caused by impinging bathymetric features: Examples from the New Hebrides and Solomon arcs. Tectonics, 24, 6. https://doi.org/10.1029/2004tc001650

Tanner JG, Shepherd JB (1997) Seismic hazard in Latin America and the Caribbean, Final Report. Volume I: Project Catalogue and Seismic Hazard Maps. Instituto Panamericano de Geografia y Historia (IPGH). Project n°89-0190. International Development Research Centre, Ottawa, Canada, 143 p

Takaku, J., T. Tadono, M. Doutsu, F. Ohgushi, and H. Kai, "Updates of 'AW3D30' ALOS Global Digital Surface Model with Other Open Access Datasets", The International Archives of the Photogrammetry, Remote Sensing and Spatial Information Sciences, ISPRS, Vol.XLIII-B4-2020, pp.183–189, 2020.

ten Brink, U.S., Bakun, W.H. & Flores, C.H. (2011). Historical perspective on seismic hazard to Hispaniola and the northeast Caribbean region. Journal Geophysical Research 116, b12318.

Terrier-Sedan, M. & Bertil, D. (2021). Active fault characterization and seismotectonic zoning of the Hispaniola island. Journal of Seismology 25, 499–520.

Tozer, B., Sandwell, D. T., Smith, W. H. F., Olson, C., Beale, J. R., & Wessel, P. (2019). Global bathymetry and topography at 15 Arc Sec: SRTM15+. Earth and Space Science, 6(10), 1847–1864. https://doi.org/10.1029/2019EA000658

Twiss, R.J. & Unruh, J.R. (1998). Analysis of fault slip inversions: do they constrain stress or strain rate? Journal of Geophysical Research 103 (6), 12.205–12.222.

Vannucchi, P., Sak, P. B., Morgan, J. P., Ohkushi, K., & Ujiie, K. (2013). Rapid pulses of uplift, subsidence, and subduction erosion offshore Central America: Implications for building the rock record of convergent margins. Geology, 41, 995–998.

Wells, D.L. & Coppersmith, K.J. 1994. New empirical relationships among magnitude, rupture length, rupture width, rupture area, and surface displacement. Bull Seismol Soc Am 84, 974–1002.

Vespucci, R.M. (1988). Petrology and Geochemistry of Late Cenozoic Volcanic Rocks of the Dominican Republic PhD thesis, George Washington University. 378 pp.

Witschard, M. & Dolan, J.F. (1990). Contrasting structural styles in siliciclastic and carbonate rocks of an offscraped sequence: The Peralta accretionary prism, Hispaniola. Geological Society of America Bulletin 102 (6), 792–806.

Figure Captions

Fig. 1. Geodynamic reconstructions made with *Gplates* 2.3.0 software for arc-continent and arc-oceanic plateau collisions in northern and southern Hispaniola, respectively. Different tectonic elements are color coded and described in the key. (a) Reconstruction at 80 Ma (lower Campanian): the large white area in the present-day location of the central Caribbean represents the proto-Caribbean oceanic crust that will be subducted by the NE motion of the intra-oceanic Caribbean island-arc. Dark grey areas represent zones of thickened Caribbean oceanic plateau (CLIP). (b) Reconstruction at 40 Ma (middle Eocene): at this time the Caribbean island-arc collided with the southern North American continental margin and is moving eastward. The small white area adjacent to southern Hispaniola will start to subduct due to back-thrusting in the Peralta-Muertos accretionary prism. (c) Present-day: the ENE-directed convergence led to Caribbean plate subduction and Beata Ridge collision in southern central Hispaniola. The blue line represents the path of a point (blue star) on the Sierra Bahoruco in the Caribbean plate since 80 Ma. *GPlates* reconstructions show that the direction of motion of the central Caribbean plate abruptly changes from northeastward to east-northeastward in the middle Eocene. This means that the direction of subduction/collision is highly oblique along the E-W-striking Peralta-Muertos deformed belt in southern Hispaniola. AVR, Aves Ridge; BR, Barbados Prism; BE, Beata Escarpement; BOFZ, Boconó Fault Zone; BOFZ, Bowin

Fault Zone; BFZ, Bucaramanga fault zone; CAT, Cayman Trough; CHO, Chortis block; CGFZ, Cerro Golden Fault Zone; CR, Costa Rica; CU, Cuba; EPFZ, El Pilar Fault Zone; EPGFZ, Enriquillo-Platain Garden Fault Zone; GRB, Grenada basin; H; Hispaniola (Dominican Republic and Haiti); HP, Haiti Plateau; HE, Hess Escarpement; HB, Hispaniola Basin; LA, Lesser Antilles; MB, Maracaibo basin; MES, Mesquito terranes; MAT, Middle America Trench; MC, Mona Canyon; MP, Mona Passage; MDB, Muertos Deformed Belt; MT, Muertos Trough; MPFZ, Motaguá Polochic fault zone; NHDB, North Hispaniola Deformed Belt; NHFZ, North Hispaniola Fault Zone; NPFB, Nothern Panamá Fold Belt; OFZ, Oriente fault zone; P, Panamá; PB, Peralta Belt; PR, Puerto Rico; PRT, Puerto Rico Trench; SFZ, Septentrional Fault Zone; SCDB, South Caribbean Deformed Belt; SFB, South Florida basin; TB, Tobago basin; VDB, Venezuela Deformed Belt; VI, Virgin Islands; YUC, Yucatán block.

Fig. 2. (a) Map of the northeastern margin of the Caribbean Plate showing the location of plate and microplate boundaries, as well as the main tectonic structures. The red arrow defines the movement vector of 18-20 mm/a in the direction N070ºE of the Caribbean Plate with respect to the North American Plate (mod. Mann et al., 2002). Relief in color scale has been made from the GMRT synthesis data set (Ryan et al., 2009) with *GeoMapApp* (www.geomapapp.org). The discontinuous red rectangle defines the situation of the study area in the Dominican Republic. (b) Schematic geologic map of southern Hispaniola (mod. from the SYSMIN Project; Pérez-Estaún et al., 2007). The discontinuous red line marks location of Fig. 3. (c) Geological cross-section of the study area. The location is shown in (b). Abbreviations as in Fig. 1, in addition: CFZ, Camú fault zone; HDB; Haiti Deformed Belt; OBFZ, Ocoa-Bonao-La Guacara fault zone; SFZ, Septentrional fault zone; SJPFZ, San Juan-Los Pozos fault zone; TBFZ; Trois Baies fault zone.

Fig. 3. Neotectonic map of southern central Hispaniola. Shaded relief in grayscale has been made from the GMRT synthesis data set (Ryan et al., 2009) with *GeoMapApp* (www.geomapapp.org). The neotectonic structures and late Neogene and Quaternary lithostratigraphic units compiled in the map

result from integrating new field data with the geologic map obtained by the SYSMIN Project in the Dominican Republic (Pérez-Estaún et al., 2007). The main neotectonic structures are: Offshore (O-OBFZ) and Southern (S-OBFZ) segments of the Ocoa-Bonao-La Guacara fault zone; Central (C-SFZ) segment of the Septentrional fault zone; Southern (S-HFZ), Central (C-HFZ) and Northern (N-HFZ) segments of Hispaniola fault zone; Southern (S-JPFZ) and Central (C-JPFZ) segments of the San Juan-Los Pozos fault zone; and Northern (N-BRFZ) and Central (C-BRFZ) segments of the Beata Ridge fault Zone. Other relevant structures are the Bahoruco fault zone (BAFZ) and the Ocoa segment of the Muertos Trust (O-MT).

Fig. 4. (a) Bouguer gravity anomaly map of southern central Hispaniola showing major tectonic features delineated by sharp gravity gradients. Areas of exposed or shallow igneous and metamorphic basement of Cretaceous age in the northern Cordillera Central and Sierra Bahoruco show higher anomalies (red to yellow tones), whereas areas with high sediment accumulation in the Cibao, San Juan and Azua basins are expressed by low anomalies (dark to light blue tones). (b) Reduced to the magnetic pole map showing major lithologic and tectonic features of southern central Hispaniola. The reduction to the pole of the whole magnetic field improves the spatial position of anomalies that help to define areas with long and short wavelengths, regional trends and tectonic boundaries between magnetic provinces. See explanation in the text.

Fig. 5. Structural analysis of the Peralta Belt. (a) Structural map of the eastern Peralta Belt in southern central Hispaniola (see location in Fig. 3), showing the tectonic domains, main Quaternary lithostratigraphic units, neotectonic structures, and sites of fault-slip data measurements. OBFZ, Ocoa-Bonao-La Guacara fault zone; SJ, San José de Ocoa intramountain basin; RA, Rancho Arriba intramountain basin. (b) Stereoplots of the non-coaxial Sp-Lp fabric produced by syn-sedimentary deformation during the upper Eocene in the Peralta and Ocoa Groups. (c) Field aspect of the syn-sedimentary deformation developed heterogeneously in the turbidites of the Ocoa Group. (d) Zone of stratal disruption in the Ocoa Group, characterized by boudinage of sandstone beds, tight to isoclinal

folds with rootless limbs, and a pervasive scary clay fabric (Sp) in mudstone interbeds. (e) Detail of the boudinaged sandstone beds and the S-C structures in the mudstones.

Fig. 6. Structural analysis of the Peralta Belt. (a) Stereoplots of the principal stress axes obtained from inversion of fault-slip data. n, number of data. Inversion methods: PTM, P–T Method; RDM, Right Dihedra Method; DIM (Direct Inversion Method); and NDA, Numerical Dynamic Analysis Method. (b) Asymmetric D1 folds of SW vergence, associated with mid-dip angle reverse faults, developed in the limestones of the lower Miocene Sobrerito Formation. (c) D1 reverse faults cutting the block-in-matrix fabric (Sp) and calcite veins in the Peralta Group.

Fig. 7. Structural analysis of the Peralta Belt. (a) Stereoplots of the principal stress-axes obtained from inversion of fault-slip data. (b) Structural map of the northern Ocoa Bay in southern central Hispaniola (see location in Fig. 3), showing main lithostratigraphic units, neotectonic structures, and sites of fault-slip data measurements. (c) Geological cross-section of the frontal part of the Peralta Belt. (d, e) Field aspect of the Loma Vieja frontal thrust (site 21JE123, see location in the cross-section), where the lower to middle Miocene limestones of the Sobrerito Formation overthrust the conglomerates of the late Pliocene to lower Pleistocene Arroyo Seco Formation. Acronyms as in Fig. 3.

Fig. 8. Structural analysis in the Loma Vigia sector of the Ocoa Bay. (a) Stereoplots of the principal stress axes obtained from inversion of fault-slip data. (b) D1 fold and reverse fault truncated by D3 normal faults, dragging the limestone layers in the hanging-wall block to the SW (site 21JE120). (c, d) Limestone beds of the Sombrerito Formation displaced by a system of ENE to E-striking normal faults along whose planes intrude locally mafic magmas (site 21JE113).

Fig. 9. Structural analysis in the Sierra Martín García. (a) Stereoplots of the principal stress axes obtained from inversion of fault-slip data. (b) Structural map of the eastern Sierra Martín García in southern central Hispaniola (see location in Fig. 3), showing main lithostratigraphic units,

neotectonic structures, and sites of fault-slip data measurements. (c) Stratigraphic logs in Cañada Arenazo and Playa Caobita sites. (d) Aspect of the bands of fault-gouge and fine crush breccia several tens of meters thick associated with the strike-slip D2 deformation. View width is 40 m. (e) D3 normal faults deforming the alluvial fans deposits of Late Pleistocene to Holocene? age. View width is 18 m. (f) Coral-reef terrace of Late Pleistocene boundary age (MIS 5c) deformed by D3 normal faults. (g) Field appearance of the calcite fill in the planes of the D3 extensional faults that deform the coral terrace. Gm, matrix-supported, muddy-sandy conglomerate; Gp, clast-supported, sandy conglomerate; Sc, medium-to-thick bedded coarse-grained sandstone and microconglomerates; Sm, thin-bedded, medium-to-fine-grained sandstone; Sf, fine-grained sandstone, siltstone and laminated mudstone; Ms, massive variocolored mundstone; Ls, coral reef limestone.

Fig. 10. Structural analysis in northeast Sierra Bahoruco. (a) Stereoplots of the principal stress axes obtained from inversion of fault-slip data. (b) Geological cross-section of the Playa Azul site (see location in Fig. 3). (c) Panoramic view of the geological cross-section outcrop. (d) Field relationships of the limestones of the Sombrerito Formation, coral-reef terrace of Middle to Late Pleistocene boundary age (MIS 5e stage) and gravels and red mudstones of the alluvial fan faulted by D2 strike-slip faults. (e) Field aspect of the gravels and red mudstones of the alluvial fan faulted by D3 extensional faults.

Fig. 11. Structural analysis in the Sierra Martín García. (a) Stereoplots of the principal stress axes obtained from inversion of fault-slip data. (b) Structural map of the southwestern Sierra Martín García (see location in Fig. 3), showing main lithostratigraphic units, neotectonic structures, and sites of fault-slip data measurements. (c) WNW-trending and SW-verging asymmetric D1 folds developed in the the marls and gypsum beds of the upper Pliocene La Salina Formation. (d) SW-verging asymmetric D1 folds associated with mid-dip angle reverse faults inclined to the NE developed in the gypsum deposits. The asymmetry of D1 folds and mesoscopic S-C structures establish a top-to-

the-SW reverse movement. (e) Field relationships of superposition of D3 normal fault striations (e2) over D2 strike-slip striations (e1) deforming stratified gypsum beds (S0). (f) Accumulation of *Diploria* sp. forming the reef-platform facies of a coral terrace grown during the MIS 5e stage that fossilizes the D1 frontal thrust of the Sierra Martín García.

Fig. 12. Structural analysis in the San José de Ocoa basin. (a) Stereoplots of the principal stress axes obtained from inversion of fault-slip data. (b) Folded and faulted mudstones of the Numero Formation juxtaposed to tilted and faulted San José de Ocoa basin deposits through subvertical oblique reverse right-lateral D2 faults of the eastern branch of the S-OBFZ segment. (c) Low-pitch angle striations developed in subvertical fault planes subparallel to the S-OBFZ segment deforming the volcanic rocks of the Tireo Group. (d) Brecciated damage fault zone with low-pitch angle striations developed in subvertical D2 fault planes sub-parallel to the S-OBFZ segment. (e) Field overlapping relationships between low-pitch angle strike-slip striaes deformed by dip-slip normal striaes in the same fault plane, establishing a temporal order between D2 and D3 deformations.

Fig. 13. Structural analysis of the extensional D3 deformation in the Cordillera Central. (a) Stereoplots of the principal stress-axes obtained from inversion of fault-slip data. (b) Map of distribution of fossil coral reef terraces of the MIS 5e/5c and 1 stages, as well as the area affected by the D3b extensional event. See explanation in text. Shaded relief as in Fig.3.

Fig. 14. Structural analysis in the Cordillera Central. (a) Stereoplots of the principal stress-axes obtained from inversion of fault-slip data. (b) Late Cretaceous green tuffs of the Tireo Group imbricated by WSW-directed D1 thrusts. (c) Detail of D3 extensional faults overlaping D1 thrusts in the green tuffs. (d) Panoramic view of Constanza mountainous area showing a D1 macrostructure of NW-striking thrusts built up on late Cretaceous volcano-plutonic rocks overthrusting the sedimentary fill of a Quaternary intramountaneous basin. Note the development of perched valleys and triangular

facets in the hanging-wall block. (e) Detail of the striae associated to the development of a D2 left-hand strike-slip fault in late Cretaceous tonalitic rocks.

Fig. 15. (a) Stereoplots of the principal stress-axes obtained from fault-slip data inversion grouped by deformation events and (b) their classification according to its kinematic regime (see Supporting Information S5). The orientation of σ_1 has been restored at sites that have undergone a post-D1 rotation. Contours in stereoplots at 1.0, 5.0, 10.0, 15.0, 20.0 and 25.0%. Computed mean stress axes for each deformation event are expressed in % and trend/plunge angles.

Fig. 16. Neotectonic diagrams showing the evolution of the Quaternary stress regime in southern central Hispaniola set up for (a) D1 reverse, (b) D2 strike-slip, and (c) D3 extensional events. Maximum horizontal stress axis trends were derived from fault-slip data inversion. Shaded relief in grayscale has been made as in Fig. 3, indicating the overlay colour different geological domains: green, the Cretaceous basement of the Cordillera Central; pink, the middle Eocene-lower Miocene Peralta fold-and-thrust belt and the overlying uplifted forearc basin; yellow, the Tertiary limestones of the Sierras de Neiba, Martín García y Bahoruco; and pale blue, the Neogene San Juan-Azua Basin. Vectors of GPS velocities relative to the Caribbean plate at stations located in the study area are from Symithe et al. (2015), Calais et al. (2016) and UNAVCO (https://coconet.unavco.org). Acronyms as in Fig. 3. See text for explanation.

Fig. 17. Result of the probabilistic seismic hazard modeling in southern central Hispaniola, as well as adjacent offshore sectors of the Ocoa Bay, expressed as iso-PGA (Peak Ground Acceleration) zones (in cm/s^2) for a return period of 475 years (i.e., an exceedance probability of 10% in 50 years). The modelled area is the same of Fig. 3 and framed by a discontinuous red box in Fig. 2. Figure also includes the trace of the main seismogenic structures described in Table 1. MDT. Shaded relief and acronyms as in Fig. 3. See text for explanation.

Figure1.

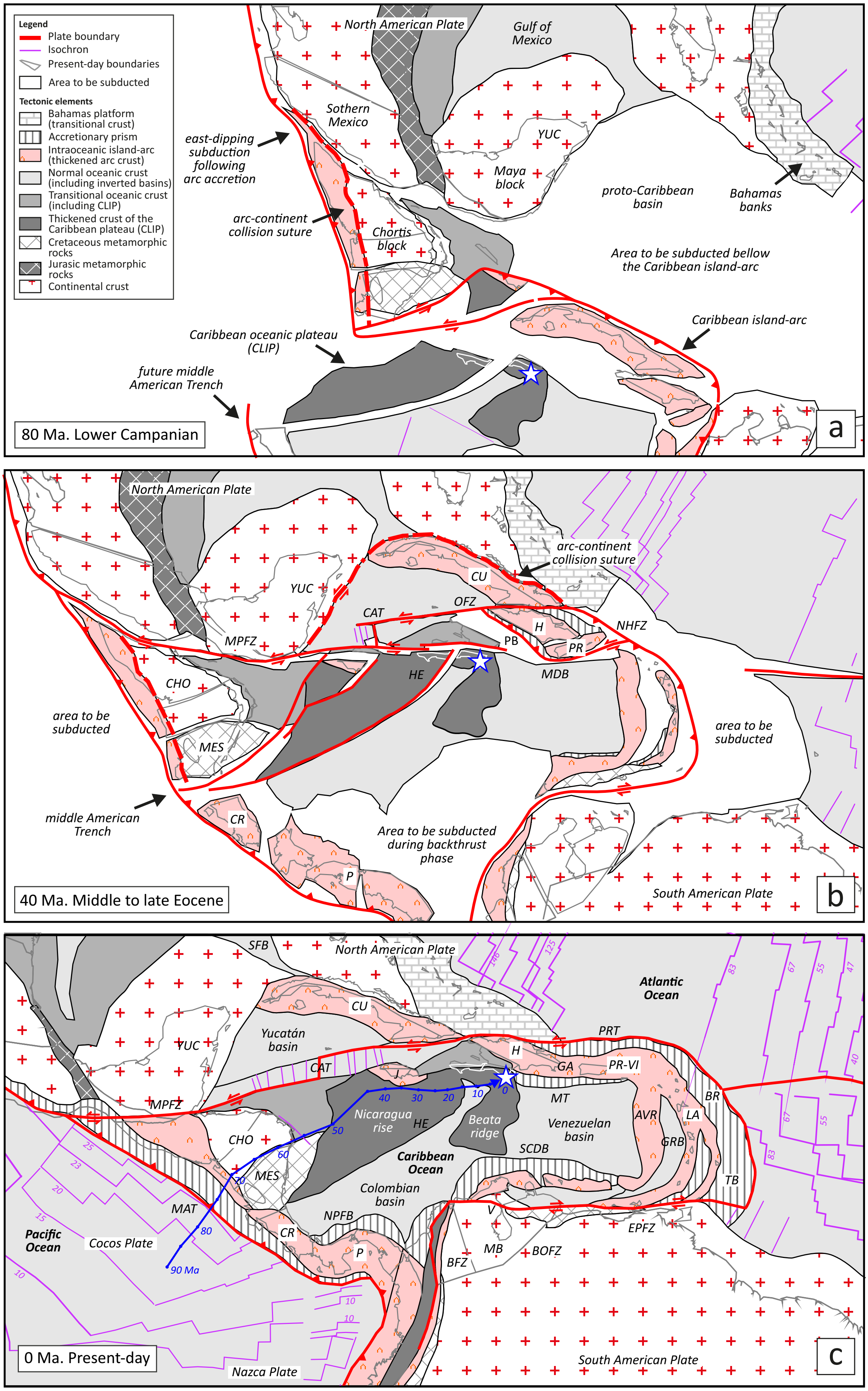
Legend
Plate boundary
Isochron
Present-day boundaries
Area to be subducted
Tectonic elements
Bahamas platform (transitional crust)
Accretionary prism
Intraoceanic island-arc (thickened arc crust)
Normal oceanic crust (including inverted basins)
Transitional oceanic crust (including CLIP)
Thickened crust of the Caribbean plateau (CLIP)
Cretaceous metamorphic rocks
Jurassic metamorphic rocks
Continental crust
North American Plate
Gulf of Mexico
Sothern Mexico
east-dipping subduction following arc accretion
arc-continent collision suture
Chortis block
YUC
Maya block
proto-Caribbean basin
Bahamas banks
Area to be subducted bellow the Caribbean island-arc
Caribbean island-arc
Caribbean oceanic plateau (CLIP)
future middle American Trench
80 Ma. Lower Campanian
a
North American Plate
arc-continent collision suture
YUC
CU
CAT
OFZ
H
NHFZ
PB
PR
MPFZ
HE
MDB
CHO
area to be subducted
MES
middle American Trench
CR
Area to be subducted during backthrust phase
P
area to be subducted
South American Plate
40 Ma. Middle to late Eocene
b
SFB
North American Plate
Atlantic Ocean
CU
Yucatán basin
YUC
CAT
H
PRT
GA
PR-VI
MPFZ
MT
BR
Nicaragua rise
HE
Beata ridge
Venezuelan basin
AVR
LA
GRB
CHO
SCDB
Caribbean Ocean
MES
Colombian basin
TB
MAT
NPFB
V
EPFZ
CR
Pacific Ocean
Cocos Plate
P
MB
BOFZ
BFZ
90 Ma
80
70
60
50
40
30
20
10
0
South American Plate
Nazca Plate
0 Ma. Present-day
c

Figure2.

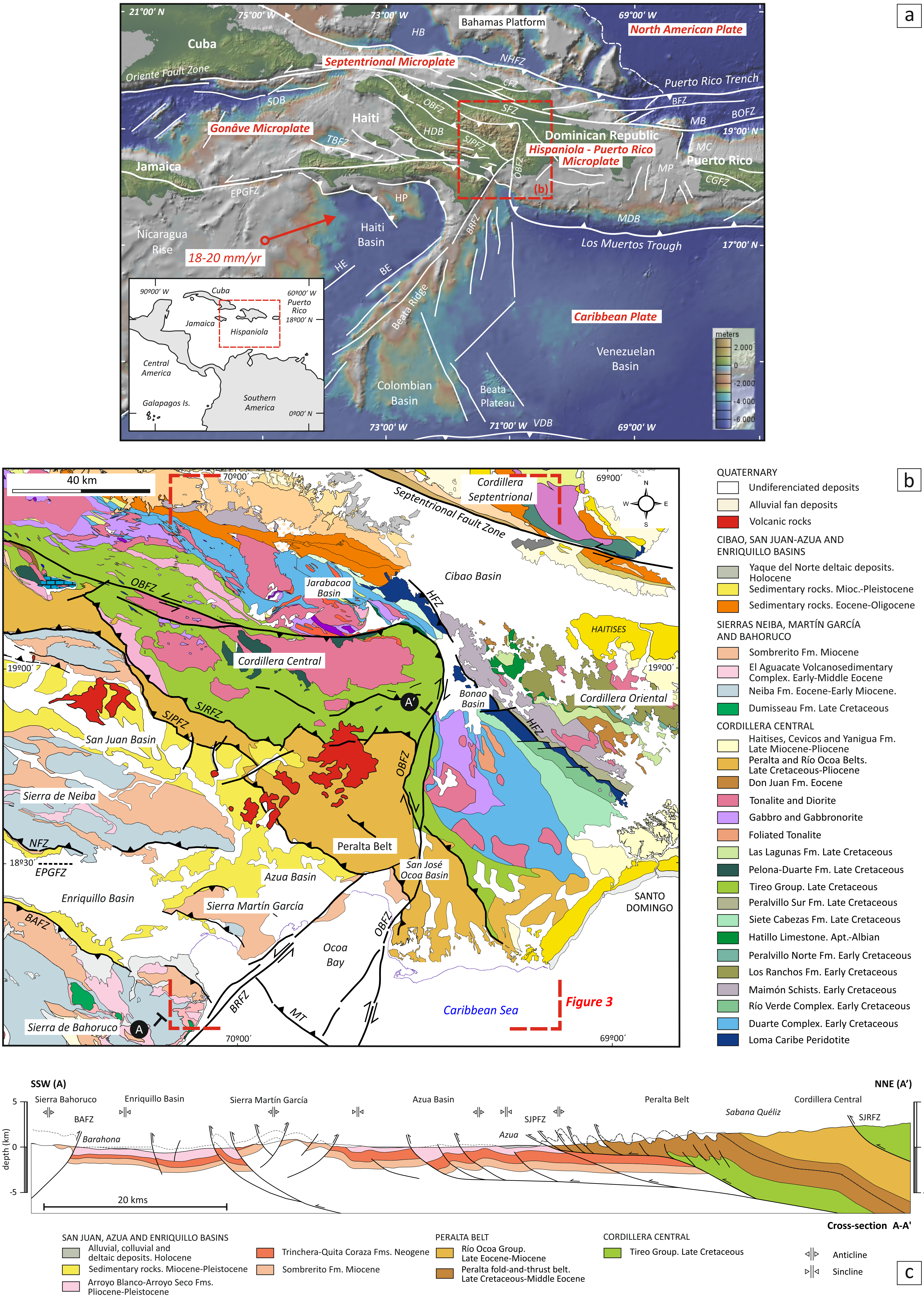

a
21°00' N
75°00' W
73°00' W
69°00' W
Bahamas Platform
North American Plate
HB
Cuba
Septentrional Microplate
NHFZ
Oriente Fault Zone
CFZ
Puerto Rico Trench
BFZ
SDB
OBFZ
SFZ
MB
BOFZ
Haiti
19°00' N
Gonâve Microplate
HDB
Dominican Republic
TBFZ
SJPFZ
Hispaniola - Puerto Rico Microplate
MC
Jamaica
OBFZ
MP
Puerto Rico
CGFZ
(b)
EPGFZ
HP
MDB
Haiti Basin
BRFZ
Nicaragua Rise
Los Muertos Trough
17°00' N
18-20 mm/yr
HE
BE
Beata Ridge
Caribbean Plate
Venezuelan Basin
Colombian Basin
Beata Plateau
73°00' W
71°00' W
VDB
69°00' W
meters
2.000
0
-2.000
-4.000
-6.000
90º00' W
Cuba
60º00' W
Puerto Rico
18º00' N
Jamaica
Hispaniola
Central America
Galapagos Is.
Southern America
0º00' N
b
40 km
70º00´
69º00´
Cordillera Septentrional
Septentrional Fault Zone
Cibao Basin
Jarabacoa Basin
OBFZ
HFZ
HAITISES
Cordillera Central
19º00´
Bonao Basin
Cordillera Oriental
A'
SJRFZ
SJPFZ
HFZ
San Juan Basin
OBFZ
Sierra de Neiba
NFZ
Peralta Belt
18º30´
EPGFZ
San José Ocoa Basin
Azua Basin
Enriquillo Basin
Sierra Martín García
SANTO DOMINGO
BAFZ
OBFZ
Ocoa Bay
BRFZ
MT
Caribbean Sea
Figure 3
Sierra de Bahoruco
A
70º00´
69º00´
QUATERNARY
Undiferenciated deposits
Alluvial fan deposits
Volcanic rocks
CIBAO, SAN JUAN-AZUA AND ENRIQUILLO BASINS
Yaque del Norte deltaic deposits. Holocene
Sedimentary rocks. Mioc.-Pleistocene
Sedimentary rocks. Eocene-Oligocene
SIERRAS NEIBA, MARTÍN GARCÍA AND BAHORUCO
Sombrerito Fm. Miocene
El Aguacate Volcanosedimentary Complex. Early-Middle Eocene
Neiba Fm. Eocene-Early Miocene.
Dumisseau Fm. Late Cretaceous
CORDILLERA CENTRAL
Haitises, Cevicos and Yanigua Fm. Late Miocene-Pliocene
Peralta and Río Ocoa Belts. Late Cretaceous-Pliocene
Don Juan Fm. Eocene
Tonalite and Diorite
Gabbro and Gabbronorite
Foliated Tonalite
Las Lagunas Fm. Late Cretaceous
Pelona-Duarte Fm. Late Cretaceous
Tireo Group. Late Cretaceous
Peralvillo Sur Fm. Late Cretaceous
Siete Cabezas Fm. Late Cretaceous
Hatillo Limestone. Apt.-Albian
Peralvillo Norte Fm. Early Cretaceous
Los Ranchos Fm. Early Cretaceous
Maimón Schists. Early Cretaceous
Río Verde Complex. Early Cretaceous
Duarte Complex. Early Cretaceous
Loma Caribe Peridotite
SSW (A)
NNE (A')
Sierra Bahoruco
Enriquillo Basin
Sierra Martín García
Azua Basin
Peralta Belt
Cordillera Central
BAFZ
Sabana Quéliz
SJPFZ
SJRFZ
Barahona
Azua
depth (km)
5
0
-5
20 kms
Cross-section A-A'
SAN JUAN, AZUA AND ENRIQUILLO BASINS
Alluvial, colluvial and deltaic deposits. Holocene
Sedimentary rocks. Miocene-Pleistocene
Arroyo Blanco-Arroyo Seco Fms. Pliocene-Pleistocene
Trinchera-Quita Coraza Fms. Neogene
Sombrerito Fm. Miocene
PERALTA BELT
Río Ocoa Group. Late Eocene-Miocene
Peralta fold-and-thrust belt. Late Cretaceous-Middle Eocene
CORDILLERA CENTRAL
Tireo Group. Late Cretaceous
Anticline
Sincline
c

Figure3.

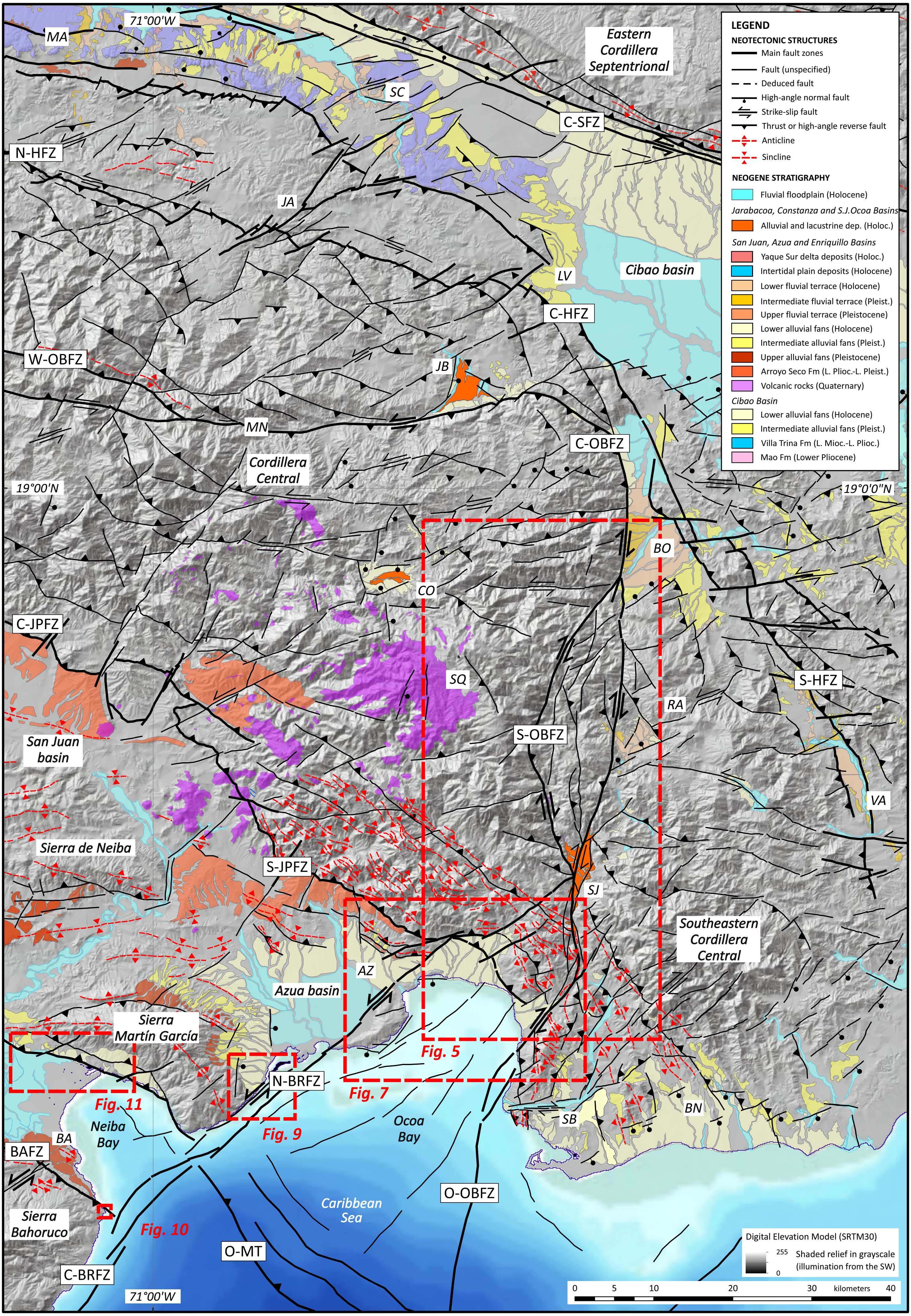

LEGEND
NEOTECTONIC STRUCTURES
Main fault zones
Fault (unspecified)
Deduced fault
High-angle normal fault
Strike-slip fault
Thrust or high-angle reverse fault
Anticline
Sincline
NEOGENE STRATIGRAPHY
Fluvial floodplain (Holocene)
Jarabacoa, Constanza and S.J.Ocoa Basins
Alluvial and lacustrine dep. (Holoc.)
San Juan, Azua and Enriquillo Basins
Yaque Sur delta deposits (Holoc.)
Intertidal plain deposits (Holocene)
Lower fluvial terrace (Holocene)
Intermediate fluvial terrace (Pleist.)
Upper fluvial terrace (Pleistocene)
Lower alluvial fans (Holocene)
Intermediate alluvial fans (Pleist.)
Upper alluvial fans (Pleistocene)
Arroyo Seco Fm (L. Plioc.-L. Pleist.)
Volcanic rocks (Quaternary)
Cibao Basin
Lower alluvial fans (Holocene)
Intermediate alluvial fans (Pleist.)
Villa Trina Fm (L. Mioc.-L. Plioc.)
Mao Fm (Lower Pliocene)
71°00'W
MA
Eastern Cordillera Septentrional
SC
C-SFZ
N-HFZ
JA
LV
Cibao basin
C-HFZ
W-OBFZ
JB
MN
C-OBFZ
Cordillera Central
19°00'N
19°0'0"N
BO
CO
C-JPFZ
SQ
S-HFZ
RA
San Juan basin
S-OBFZ
VA
Sierra de Neiba
S-JPFZ
SJ
Southeastern Cordillera Central
AZ
Azua basin
Sierra Martín García
Fig. 5
N-BRFZ
Fig. 7
Fig. 11
Neiba Bay
BA
BAFZ
Fig. 9
Ocoa Bay
SB
BN
O-OBFZ
Caribbean Sea
Sierra Bahoruco
Fig. 10
O-MT
C-BRFZ
71°00'W
Digital Elevation Model (SRTM30)
255
0
Shaded relief in grayscale (illumination from the SW)
0 5 10 20 30 kilometers 40

Figure4a.

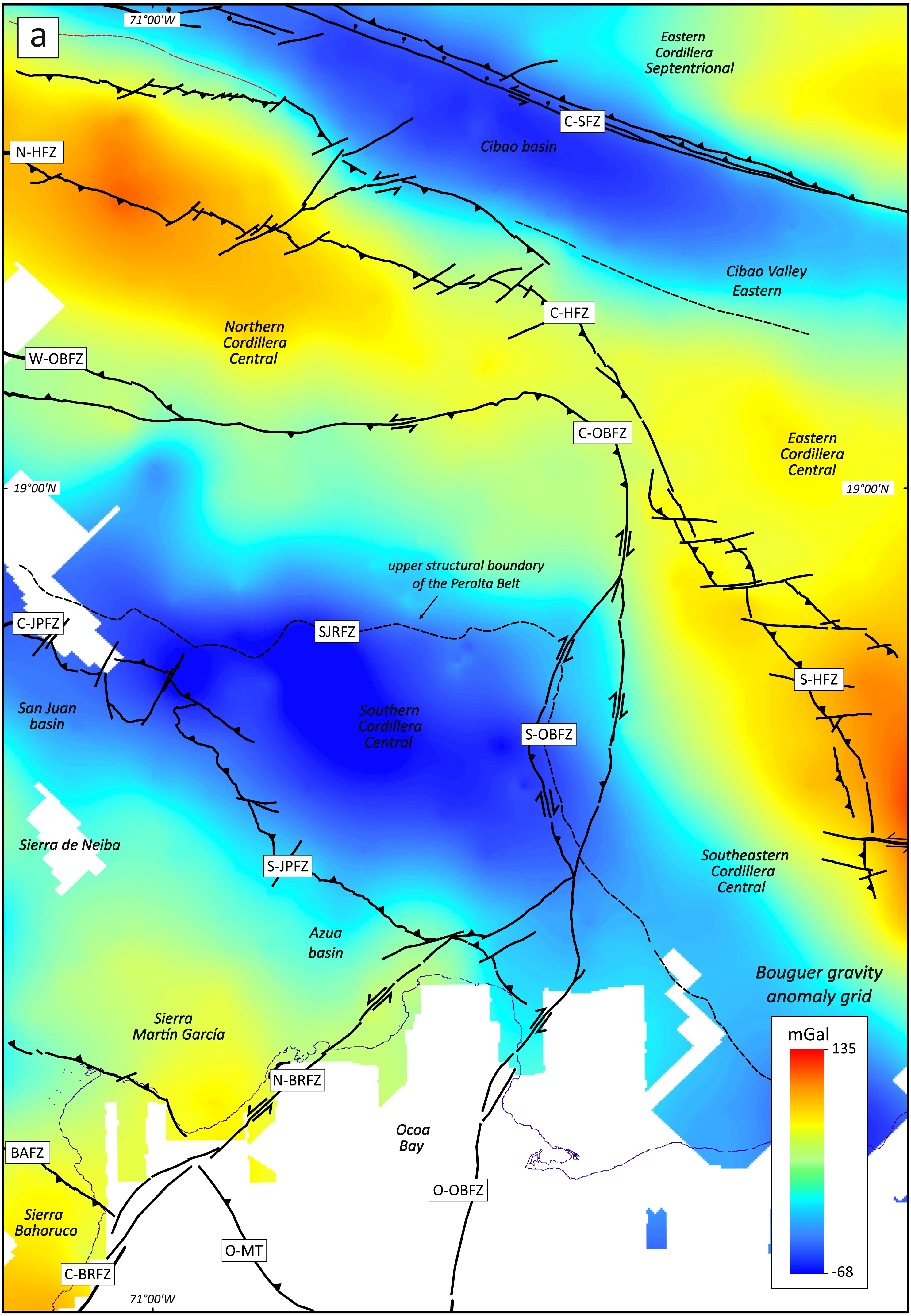

a
71°00'W
Eastern
Cordillera
Septentrional
C-SFZ
Cibao basin
N-HFZ
Cibao Valley
Eastern
C-HFZ
Northern
Cordillera
Central
W-OBFZ
C-OBFZ
Eastern
Cordillera
Central
19°00'N
19°00'N
upper structural boundary
of the Peralta Belt
C-JPFZ
SJRFZ
S-HFZ
San Juan
basin
Southern
Cordillera
Central
S-OBFZ
Sierra de Neiba
S-JPFZ
Southeastern
Cordillera
Central
Azua
basin
Bouguer gravity
anomaly grid
mGal
135
Sierra
Martín García
N-BRFZ
Ocoa
Bay
BAFZ
O-OBFZ
Sierra
Bahoruco
O-MT
C-BRFZ
-68
71°00'W

Figure4b.

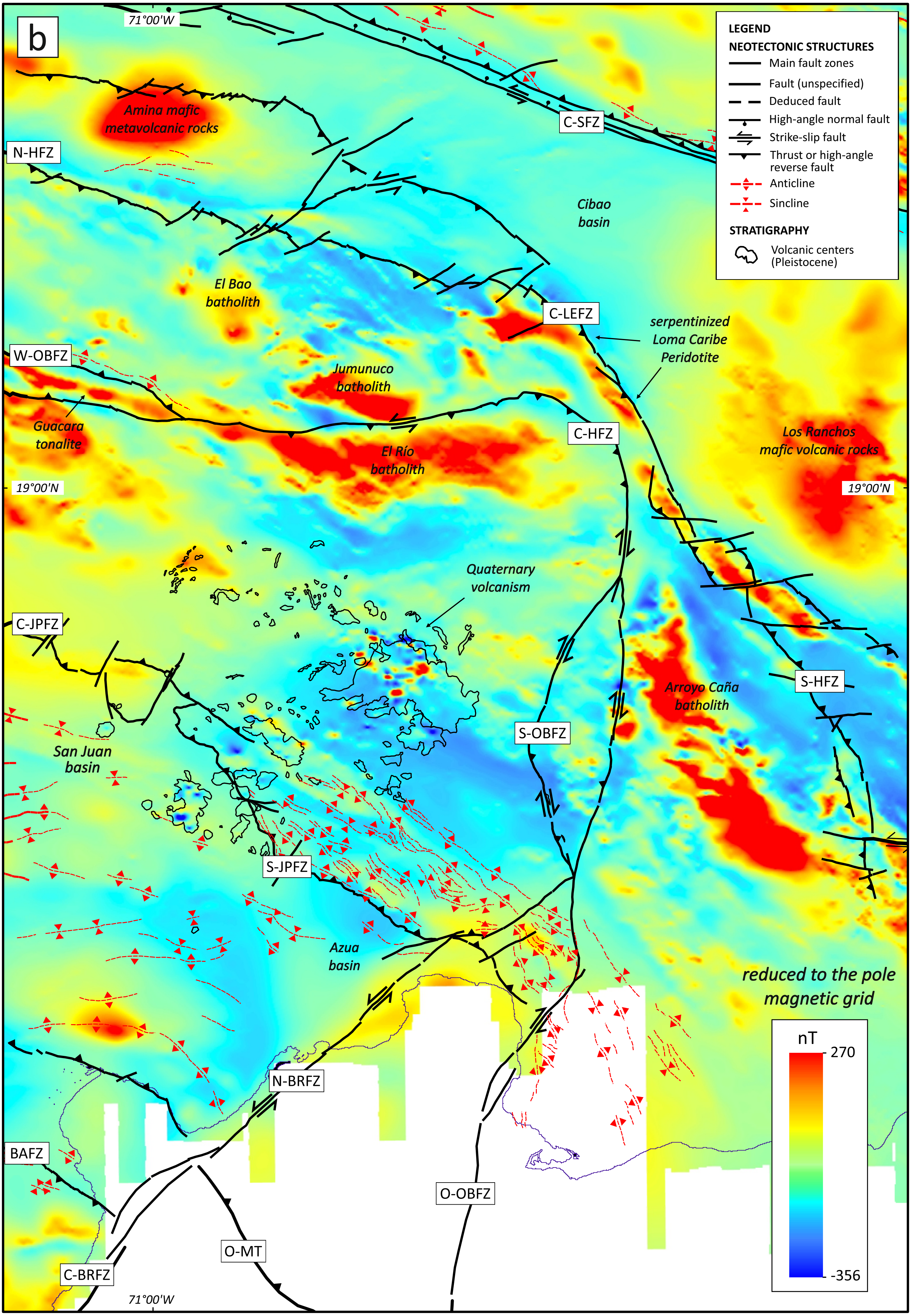

b
71°00'W
LEGEND
NEOTECTONIC STRUCTURES
Main fault zones
Fault (unspecified)
Deduced fault
High-angle normal fault
Strike-slip fault
Thrust or high-angle reverse fault
Anticline
Sincline
STRATIGRAPHY
Volcanic centers (Pleistocene)
Amina mafic metavolcanic rocks
N-HFZ
C-SFZ
Cibao basin
El Bao batholith
C-LEFZ
serpentinized Loma Caribe Peridotite
W-OBFZ
Jumunuco batholith
Guacara tonalite
C-HFZ
El Río batholith
Los Ranchos mafic volcanic rocks
19°00'N
19°00'N
Quaternary volcanism
C-JPFZ
Arroyo Caña batholith
S-HFZ
S-OBFZ
San Juan basin
S-JPFZ
Azua basin
reduced to the pole magnetic grid
nT
270
-356
N-BRFZ
BAFZ
O-OBFZ
O-MT
C-BRFZ
71°00'W

Figure5.

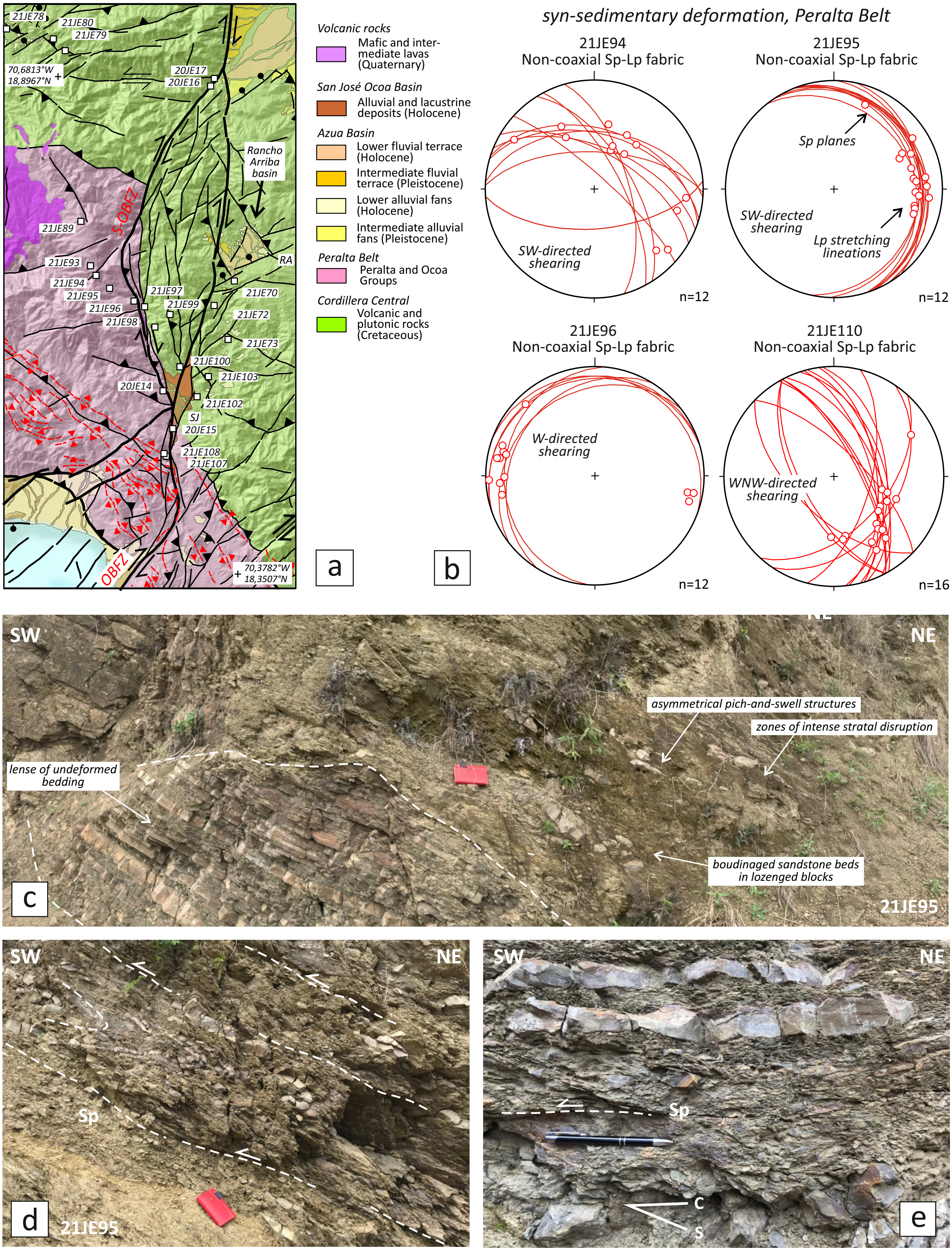
21JE78
21JE80
21JE79
70,6813°W
18,8967°N
20JE17
20JE16
Rancho
Arriba
basin
S-OBFZ
21JE89
RA
21JE93
21JE94
21JE95
21JE97
21JE70
21JE96
21JE99
21JE98
21JE72
21JE73
21JE100
21JE103
20JE14
21JE102
SJ
20JE15
21JE108
21JE107
OBFZ
70,3782°W
18,3507°N
a
Volcanic rocks
Mafic and inter-mediate lavas (Quaternary)
San José Ocoa Basin
Alluvial and lacustrine deposits (Holocene)
Azua Basin
Lower fluvial terrace (Holocene)
Intermediate fluvial terrace (Pleistocene)
Lower alluvial fans (Holocene)
Intermediate alluvial fans (Pleistocene)
Peralta Belt
Peralta and Ocoa Groups
Cordillera Central
Volcanic and plutonic rocks (Cretaceous)
b
syn-sedimentary deformation, Peralta Belt
21JE94
Non-coaxial Sp-Lp fabric
SW-directed shearing
n=12
21JE95
Non-coaxial Sp-Lp fabric
Sp planes
SW-directed shearing
Lp stretching lineations
n=12
21JE96
Non-coaxial Sp-Lp fabric
W-directed shearing
n=12
21JE110
Non-coaxial Sp-Lp fabric
WNW-directed shearing
n=16
SW
NE
asymmetrical pich-and-swell structures
zones of intense stratal disruption
lense of undeformed bedding
boudinaged sandstone beds in lozenged blocks
c
21JE95
SW
NE
Sp
d
21JE95
SW
NE
Sp
C
S
e

Figure6.

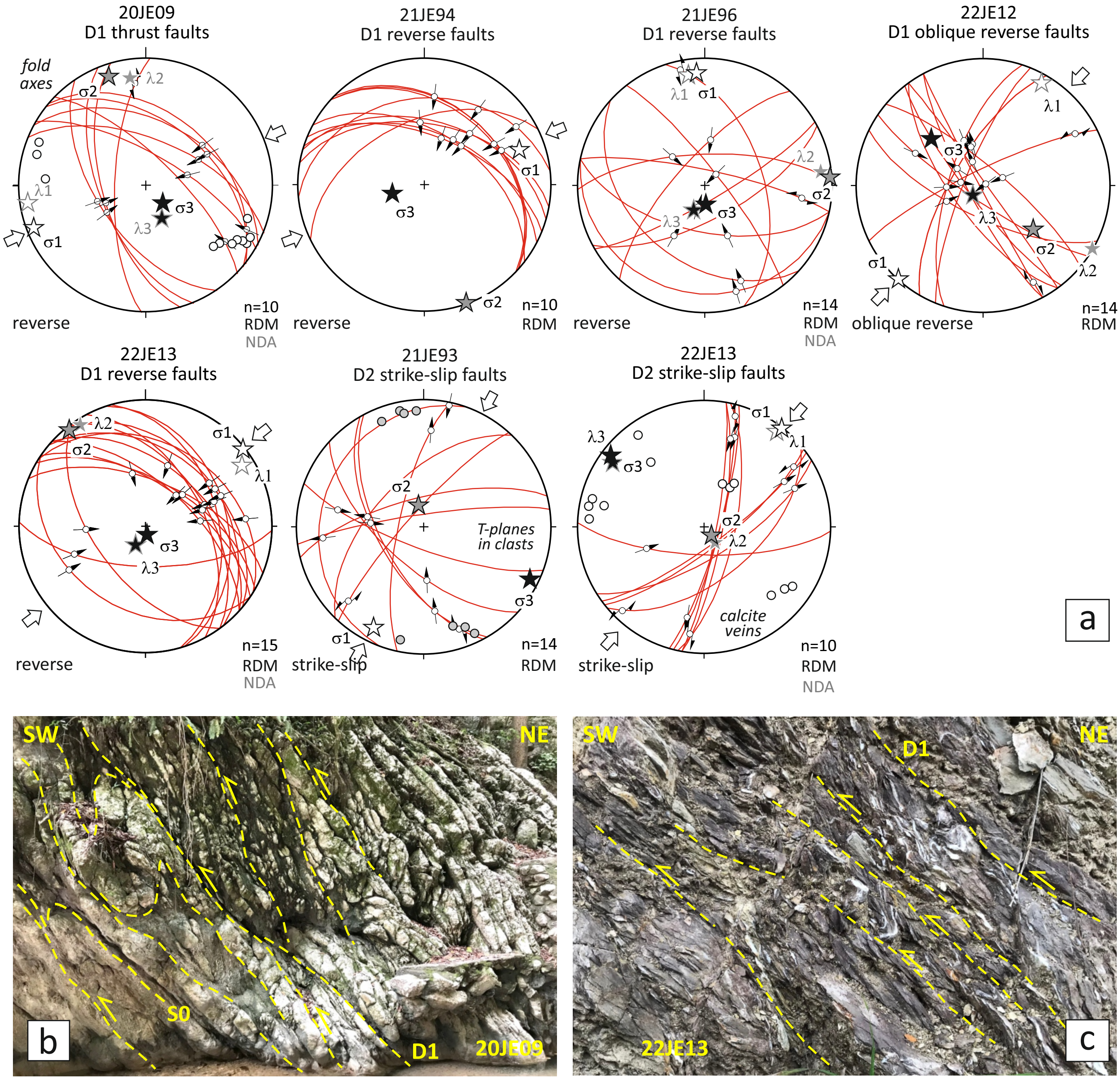

20JE09
D1 thrust faults
fold axes
σ2
λ2
λ1
σ1
σ3
λ3
reverse
n=10
RDM
NDA
21JE94
D1 reverse faults
σ1
σ3
σ2
reverse
n=10
RDM
21JE96
D1 reverse faults
λ1
σ1
λ2
σ2
λ3
σ3
reverse
n=14
RDM
NDA
22JE12
D1 oblique reverse faults
λ1
σ3
λ3
σ2
σ1
λ2
oblique reverse
n=14
RDM
22JE13
D1 reverse faults
λ2
σ2
σ1
λ1
σ3
λ3
reverse
n=15
RDM
NDA
21JE93
D2 strike-slip faults
σ2
T-planes
in clasts
σ3
σ1
strike-slip
n=14
RDM
22JE13
D2 strike-slip faults
σ1
λ3
σ3
λ1
σ2
λ2
calcite
veins
strike-slip
n=10
RDM
NDA
a
SW
NE
S0
D1
20JE09
b
SW
NE
D1
22JE13
c

Figure7.

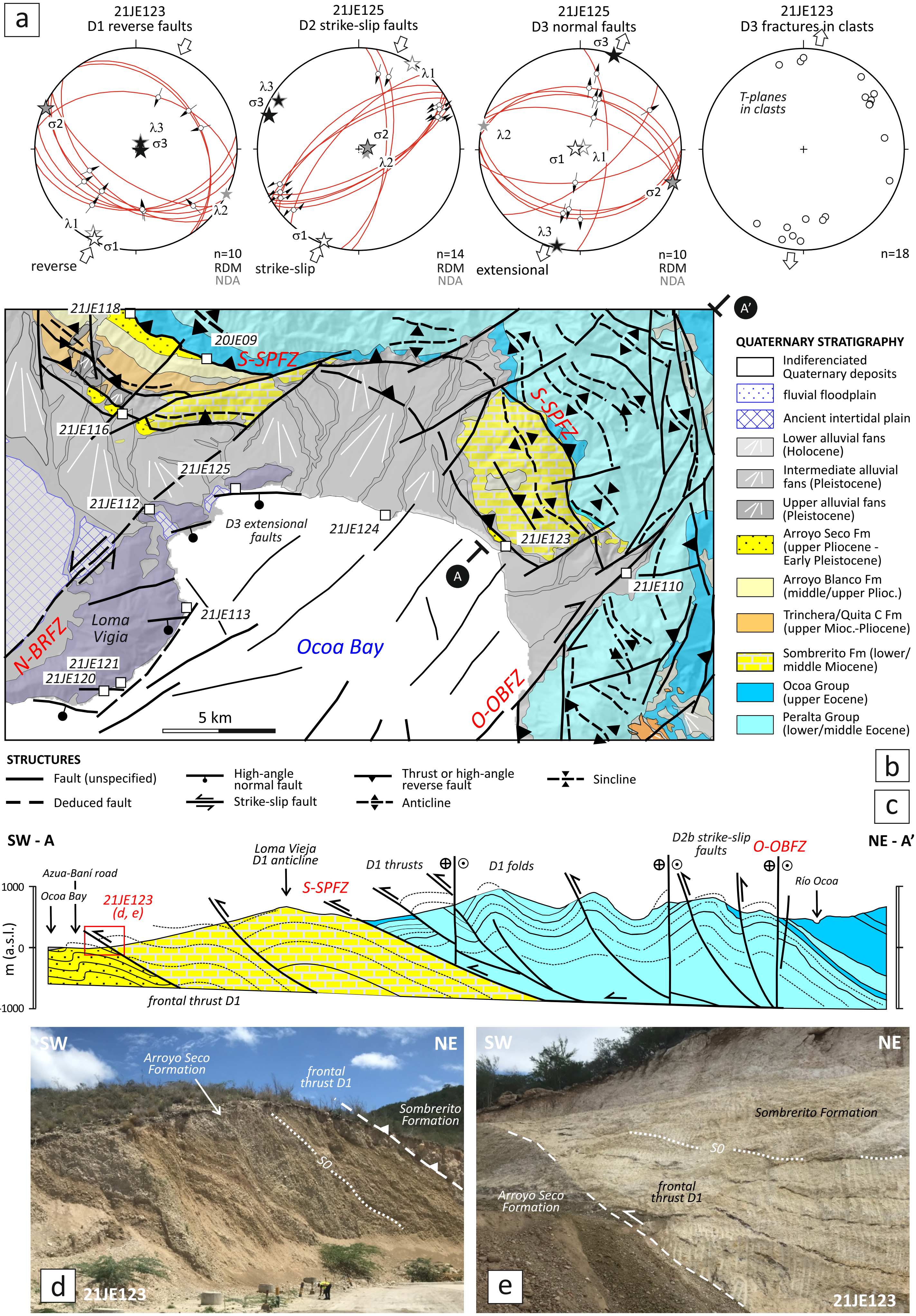

a
21JE123
D1 reverse faults
reverse
n=10
RDM
NDA
21JE125
D2 strike-slip faults
strike-slip
n=14
RDM
NDA
21JE125
D3 normal faults
extensional
n=10
RDM
NDA
21JE123
D3 fractures in clasts
T-planes in clasts
n=18
QUATERNARY STRATIGRAPHY
Indiferenciated Quaternary deposits
fluvial floodplain
Ancient intertidal plain
Lower alluvial fans (Holocene)
Intermediate alluvial fans (Pleistocene)
Upper alluvial fans (Pleistocene)
Arroyo Seco Fm (upper Pliocene - Early Pleistocene)
Arroyo Blanco Fm (middle/upper Plioc.)
Trinchera/Quita C Fm (upper Mioc.-Pliocene)
Sombrerito Fm (lower/middle Miocene)
Ocoa Group (upper Eocene)
Peralta Group (lower/middle Eocene)
21JE118
20JE09
S-SPFZ
21JE116
21JE125
21JE112
D3 extensional faults
21JE124
21JE123
21JE110
21JE113
Loma Vigia
N-BRFZ
21JE121
21JE120
Ocoa Bay
O-OBFZ
5 km
A
A'
b
STRUCTURES
Fault (unspecified)
Deduced fault
High-angle normal fault
Strike-slip fault
Thrust or high-angle reverse fault
Anticline
Sincline
c
SW - A
NE - A'
Azua-Baní road
Ocoa Bay
21JE123 (d, e)
Loma Vieja D1 anticline
S-SPFZ
D1 thrusts
D1 folds
D2b strike-slip faults
O-OBFZ
Río Ocoa
1000
0
-1000
m (a.s.l.)
frontal thrust D1
SW
NE
Arroyo Seco Formation
frontal thrust D1
Sombrerito Formation
S0
d
21JE123
SW
NE
Sombrerito Formation
S0
frontal thrust D1
Arroyo Seco Formation
e
21JE123

Figure8.

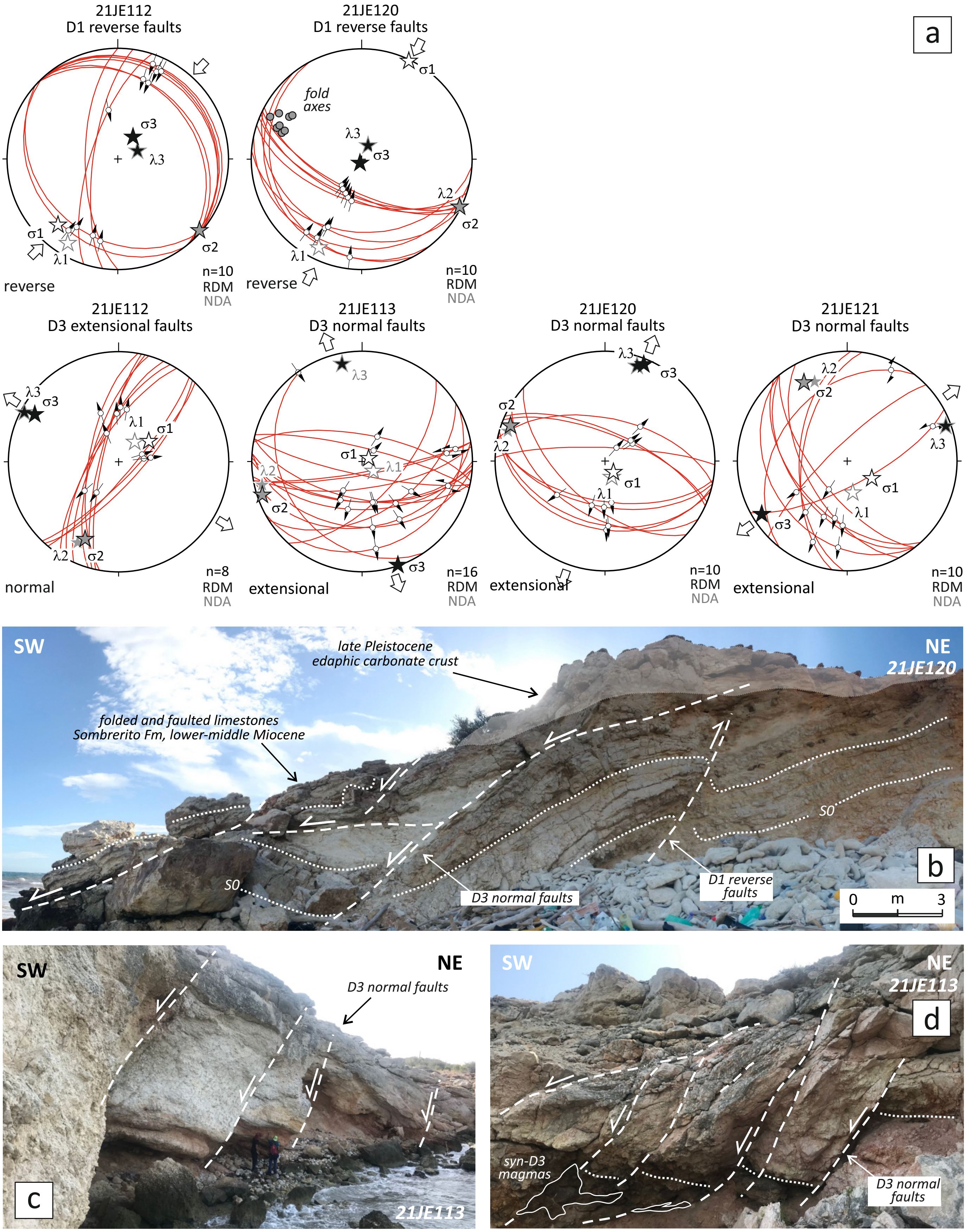

a
21JE112
D1 reverse faults
σ3
λ3
σ1
λ1
σ2
reverse
n=10
RDM
NDA
21JE120
D1 reverse faults
σ1
fold
axes
λ3
σ3
λ2
σ2
λ1
reverse
n=10
RDM
NDA
21JE112
D3 extensional faults
λ3
σ3
λ1
σ1
λ2
σ2
normal
n=8
RDM
NDA
21JE113
D3 normal faults
λ3
σ1
λ1
λ2
σ2
σ3
extensional
n=16
RDM
NDA
21JE120
D3 normal faults
λ3
σ3
σ2
λ2
σ1
λ1
extensional
n=10
RDM
NDA
21JE121
D3 normal faults
λ2
σ2
λ3
σ1
λ1
σ3
extensional
n=10
RDM
NDA
SW
NE
21JE120
late Pleistocene
edaphic carbonate crust
folded and faulted limestones
Sombrerito Fm, lower-middle Miocene
S0
S0
D3 normal faults
D1 reverse
faults
0 m 3
b
SW
NE
D3 normal faults
c
21JE113
SW
NE
21JE113
d
syn-D3
magmas
D3 normal
faults

Figure9.

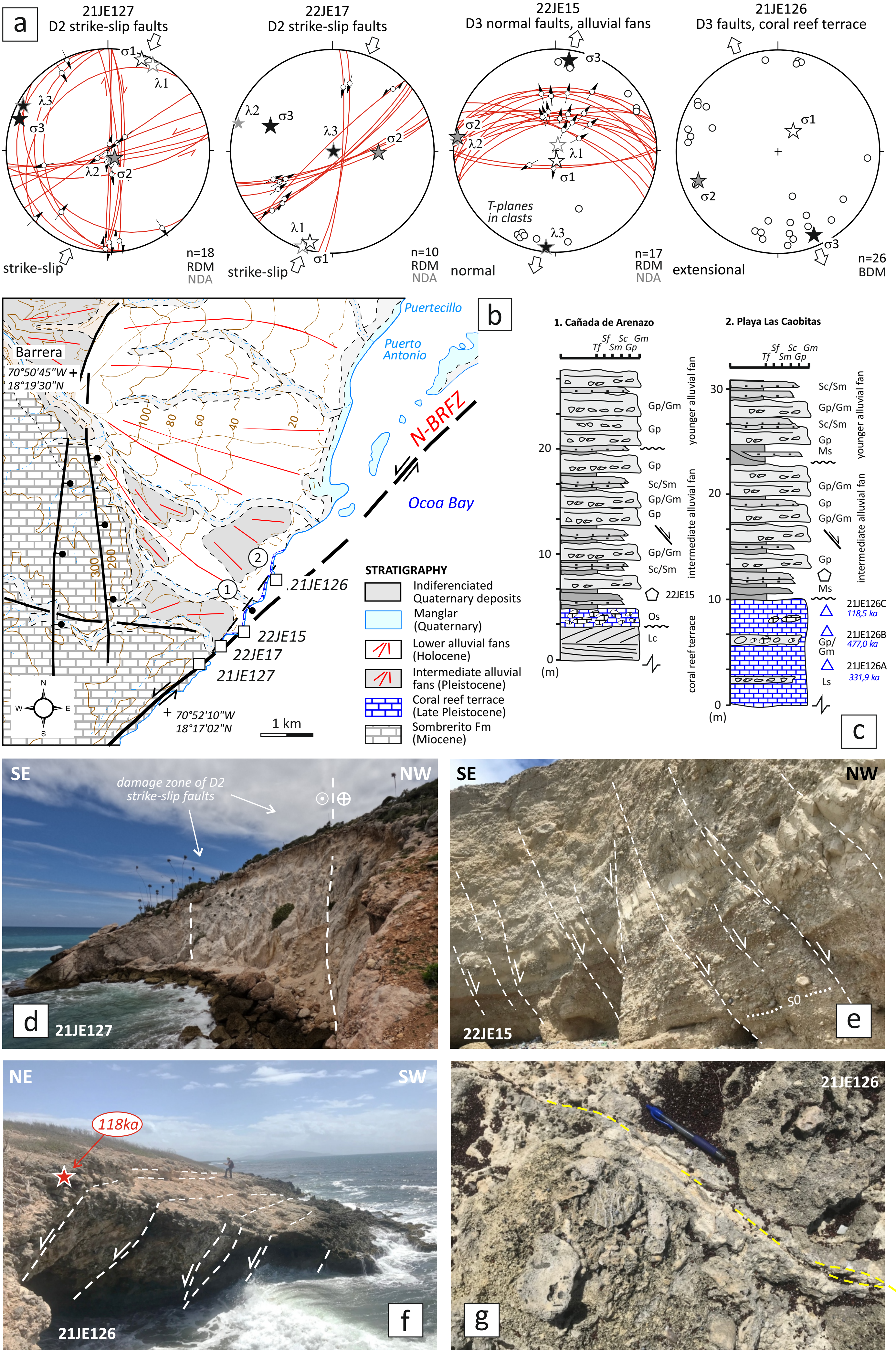

a
21JE127
D2 strike-slip faults
σ1
λ1
λ3
σ3
λ2
σ2
strike-slip
n=18
RDM
NDA
22JE17
D2 strike-slip faults
λ2
σ3
λ3
σ2
λ1
σ1
strike-slip
n=10
RDM
NDA
22JE15
D3 normal faults, alluvial fans
σ3
σ2
λ2
λ1
σ1
T-planes
in clasts
λ3
normal
n=17
RDM
NDA
21JE126
D3 faults, coral reef terrace
σ1
σ2
σ3
extensional
n=26
BDM
b
Puertecillo
Puerto
Antonio
Barrera
70°50'45"W
18°19'30"N
N-BRFZ
Ocoa Bay
21JE126
22JE15
22JE17
21JE127
70°52'10"W
18°17'02"N
1 km
100
80
60
40
20
300
200
STRATIGRAPHY
Indiferenciated Quaternary deposits
Manglar (Quaternary)
Lower alluvial fans (Holocene)
Intermediate alluvial fans (Pleistocene)
Coral reef terrace (Late Pleistocene)
Sombrerito Fm (Miocene)
1. Cañada de Arenazo
2. Playa Las Caobitas
Tf Sf Sm Sc Gp Gm
younger alluvial fan
intermediate alluvial fan
coral reef terrace
Gp/Gm
Gp
Sc/Sm
22JE15
Os
Lc
Ms
Gp/ Gm
Ls
21JE126C
118,5 ka
21JE126B
477,0 ka
21JE126A
331,9 ka
0
10
20
30
(m)
c
SE
NW
damage zone of D2 strike-slip faults
d
21JE127
SE
NW
S0
e
22JE15
NE
SW
118ka
f
21JE126
21JE126
g

Figure10.

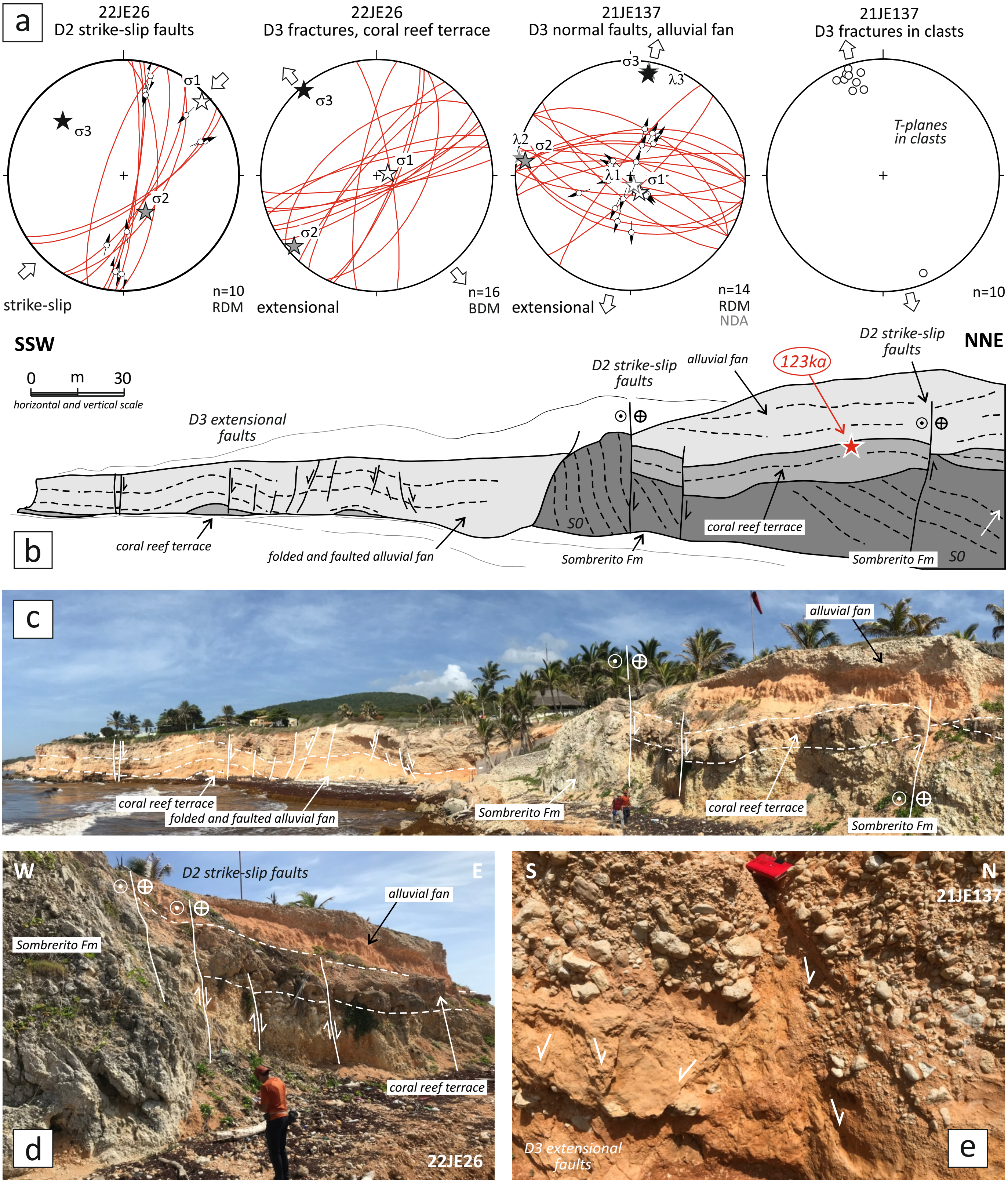
a
22JE26
D2 strike-slip faults
σ1
σ3
σ2
strike-slip
n=10
RDM
22JE26
D3 fractures, coral reef terrace
σ3
σ1
σ2
extensional
n=16
BDM
21JE137
D3 normal faults, alluvial fan
σ3
λ3
λ2
σ2
λ1
σ1
extensional
n=14
RDM
NDA
21JE137
D3 fractures in clasts
T-planes
in clasts
n=10
SSW
NNE
0 m 30
horizontal and vertical scale
D3 extensional
faults
D2 strike-slip
faults
alluvial fan
123ka
D2 strike-slip
faults
S0
coral reef terrace
folded and faulted alluvial fan
Sombrerito Fm
coral reef terrace
Sombrerito Fm
S0
b
c
alluvial fan
coral reef terrace
folded and faulted alluvial fan
Sombrerito Fm
coral reef terrace
Sombrerito Fm
W
D2 strike-slip faults
E
alluvial fan
Sombrerito Fm
coral reef terrace
d
22JE26
S
N
21JE137
D3 extensional
faults
e

Figure11.

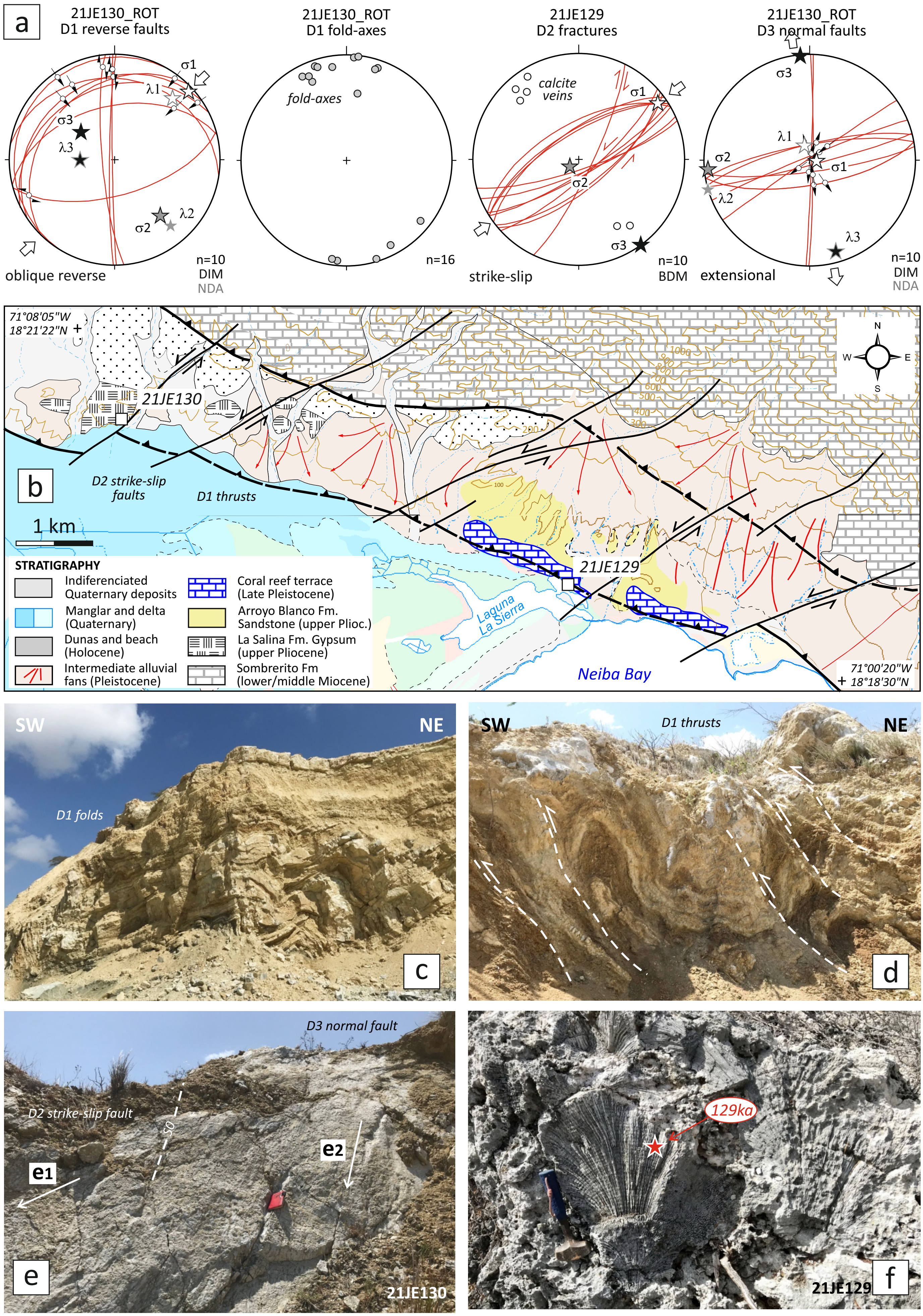
a
21JE130_ROT
D1 reverse faults
σ1
λ1
σ3
λ3
σ2
λ2
oblique reverse
n=10
DIM
NDA
21JE130_ROT
D1 fold-axes
fold-axes
n=16
21JE129
D2 fractures
calcite
veins
σ1
σ2
σ3
strike-slip
n=10
BDM
21JE130_ROT
D3 normal faults
σ3
λ1
σ2
σ1
λ2
λ3
extensional
n=10
DIM
NDA
b
71°08'05"W
18°21'22"N
21JE130
D2 strike-slip
faults
D1 thrusts
1 km
21JE129
Laguna
La Sierra
Neiba Bay
71°00'20"W
18°18'30"N
N
W
E
S
STRATIGRAPHY
Indiferenciated
Quaternary deposits
Manglar and delta
(Quaternary)
Dunas and beach
(Holocene)
Intermediate alluvial
fans (Pleistocene)
Coral reef terrace
(Late Pleistocene)
Arroyo Blanco Fm.
Sandstone (upper Plioc.)
La Salina Fm. Gypsum
(upper Pliocene)
Sombrerito Fm
(lower/middle Miocene)
SW
NE
D1 folds
c
SW
D1 thrusts
NE
d
D3 normal fault
D2 strike-slip fault
S0
e1
e2
e
21JE130
129ka
21JE129
f

Figure12.

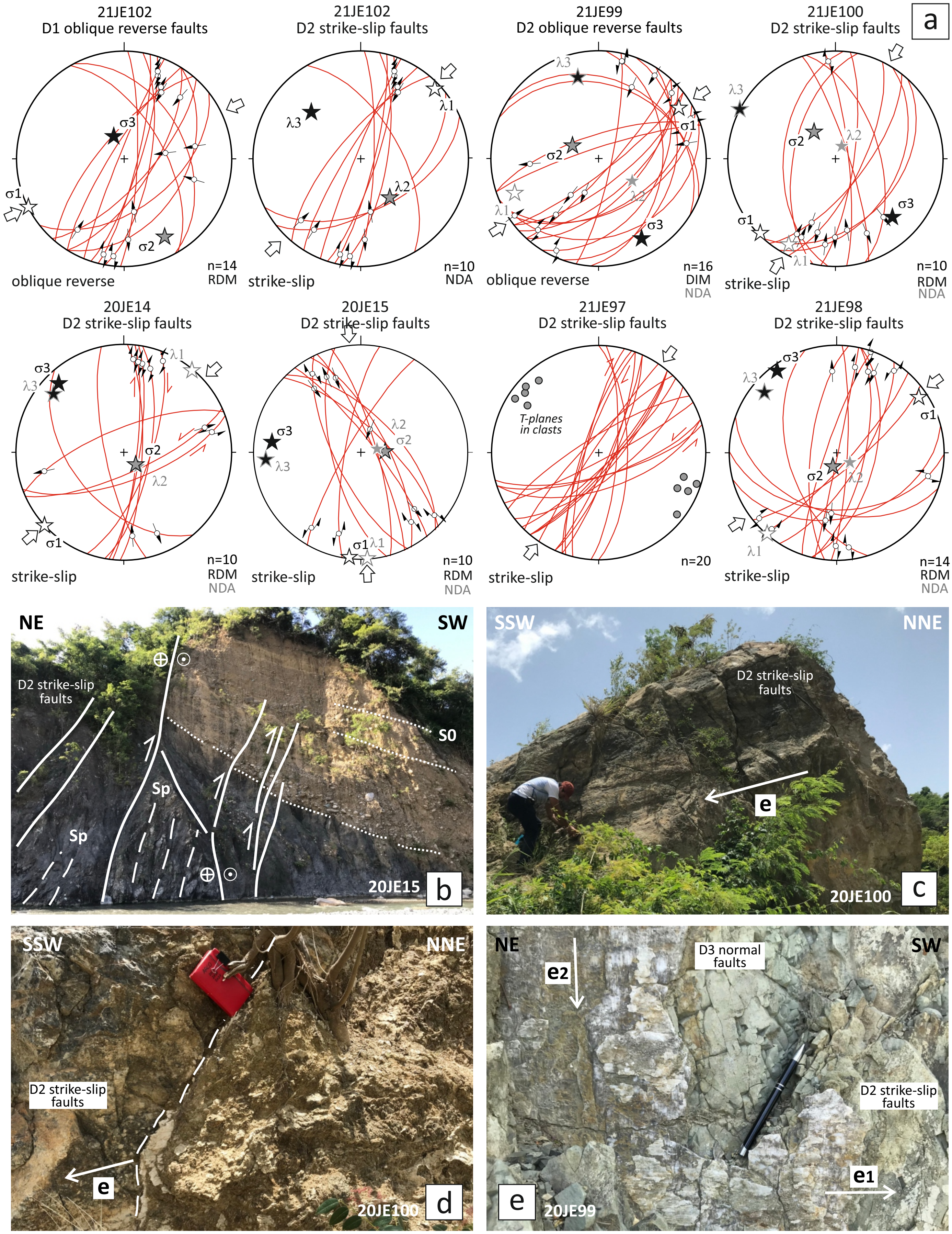

21JE102
D1 oblique reverse faults
σ3
σ1
σ2
oblique reverse
n=14
RDM
21JE102
D2 strike-slip faults
λ3
λ1
λ2
strike-slip
n=10
NDA
21JE99
D2 oblique reverse faults
λ3
σ1
σ2
λ1
λ2
σ3
oblique reverse
n=16
DIM
NDA
21JE100
D2 strike-slip faults
a
λ3
σ2
λ2
σ3
σ1
λ1
strike-slip
n=10
RDM
NDA
20JE14
D2 strike-slip faults
σ3
λ3
λ1
σ2
λ2
σ1
strike-slip
n=10
RDM
NDA
20JE15
D2 strike-slip faults
σ3
λ3
λ2
σ2
σ1
λ1
strike-slip
n=10
RDM
NDA
21JE97
D2 strike-slip faults
T-planes
in clasts
strike-slip
n=20
21JE98
D2 strike-slip faults
σ3
λ3
σ1
σ2
λ2
λ1
strike-slip
n=14
RDM
NDA
NE
SW
D2 strike-slip
faults
S0
Sp
Sp
20JE15
b
SSW
NNE
D2 strike-slip
faults
e
20JE100
c
SSW
NNE
D2 strike-slip
faults
e
20JE100
d
NE
SW
e2
D3 normal
faults
D2 strike-slip
faults
e1
e
20JE99

Figure13.

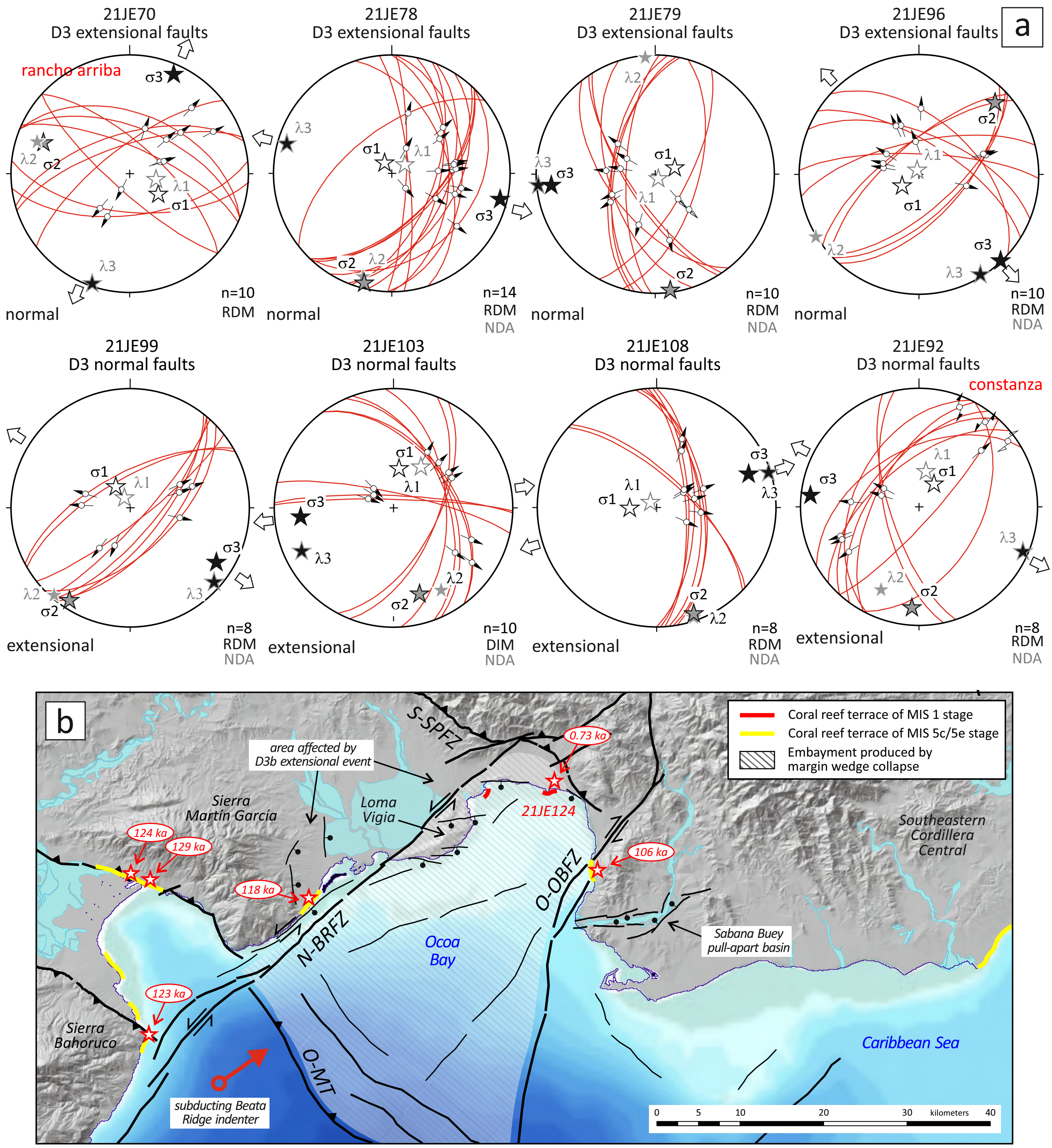

a
21JE70
D3 extensional faults
rancho arriba
normal
n=10
RDM
21JE78
D3 extensional faults
normal
n=14
RDM
NDA
21JE79
D3 extensional faults
normal
n=10
RDM
NDA
21JE96
D3 extensional faults
normal
n=10
RDM
NDA
21JE99
D3 normal faults
extensional
n=8
RDM
NDA
21JE103
D3 normal faults
extensional
n=10
DIM
NDA
21JE108
D3 normal faults
extensional
n=8
RDM
NDA
21JE92
D3 normal faults
constanza
extensional
n=8
RDM
NDA
b
Coral reef terrace of MIS 1 stage
Coral reef terrace of MIS 5c/5e stage
Embayment produced by margin wedge collapse
S-SPFZ
area affected by D3b extensional event
0.73 ka
21JE124
Sierra Martín García
Loma Vigia
124 ka
129 ka
118 ka
106 ka
O-OBFZ
N-BRFZ
Ocoa Bay
Sabana Buey pull-apart basin
Southeastern Cordillera Central
123 ka
Sierra Bahoruco
O-MT
subducting Beata Ridge indenter
Caribbean Sea
0 5 10 20 30 kilometers 40

Figure14.

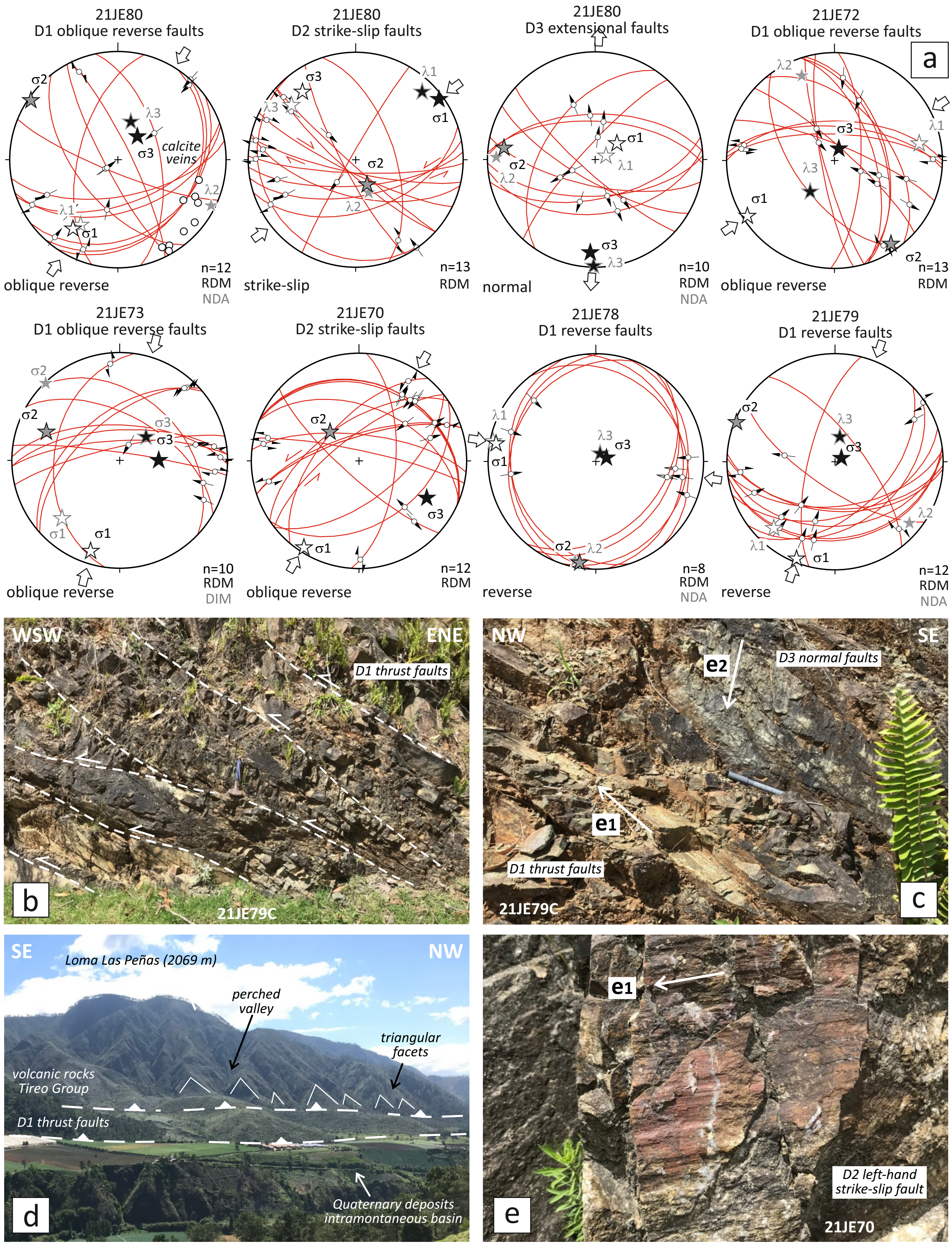

21JE80
D1 oblique reverse faults
calcite veins
oblique reverse
n=12
RDM
NDA
21JE80
D2 strike-slip faults
strike-slip
n=13
RDM
21JE80
D3 extensional faults
normal
n=10
RDM
NDA
21JE72
D1 oblique reverse faults
oblique reverse
n=13
RDM
a
21JE73
D1 oblique reverse faults
oblique reverse
n=10
RDM
DIM
21JE70
D2 strike-slip faults
oblique reverse
n=12
RDM
21JE78
D1 reverse faults
reverse
n=8
RDM
NDA
21JE79
D1 reverse faults
reverse
n=12
RDM
NDA
WSW
ENE
D1 thrust faults
21JE79C
b
NW
SE
D3 normal faults
e2
e1
D1 thrust faults
21JE79C
c
SE
NW
Loma Las Peñas (2069 m)
perched valley
triangular facets
volcanic rocks Tireo Group
D1 thrust faults
Quaternary deposits intramontaneous basin
d
e1
D2 left-hand strike-slip fault
21JE70
e

Figure15.

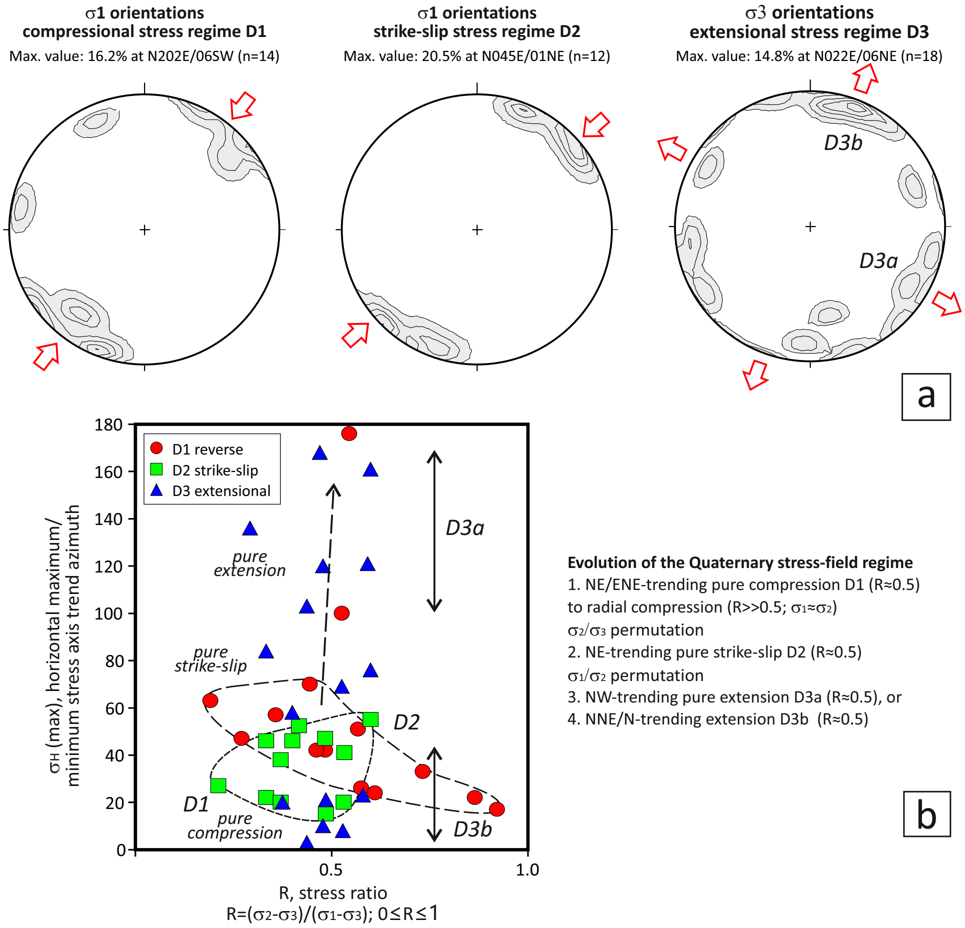
σ1 orientations
compressional stress regime D1
Max. value: 16.2% at N202E/06SW (n=14)
σ1 orientations
strike-slip stress regime D2
Max. value: 20.5% at N045E/01NE (n=12)
σ3 orientations
extensional stress regime D3
Max. value: 14.8% at N022E/06NE (n=18)
D3b
D3a
a
D1 reverse
D2 strike-slip
D3 extensional
pure extension
pure strike-slip
pure compression
D1
D2
D3a
D3b
σH (max), horizontal maximum/ minimum stress axis trend azimuth
R, stress ratio
R=(σ2-σ3)/(σ1-σ3); 0≤R≤1
b
Evolution of the Quaternary stress-field regime
1. NE/ENE-trending pure compression D1 (R≈0.5) to radial compression (R>>0.5; σ1≈σ2) σ2/σ3 permutation
2. NE-trending pure strike-slip D2 (R≈0.5) σ1/σ2 permutation
3. NW-trending pure extension D3a (R≈0.5), or
4. NNE/N-trending extension D3b (R≈0.5)

Figure16.

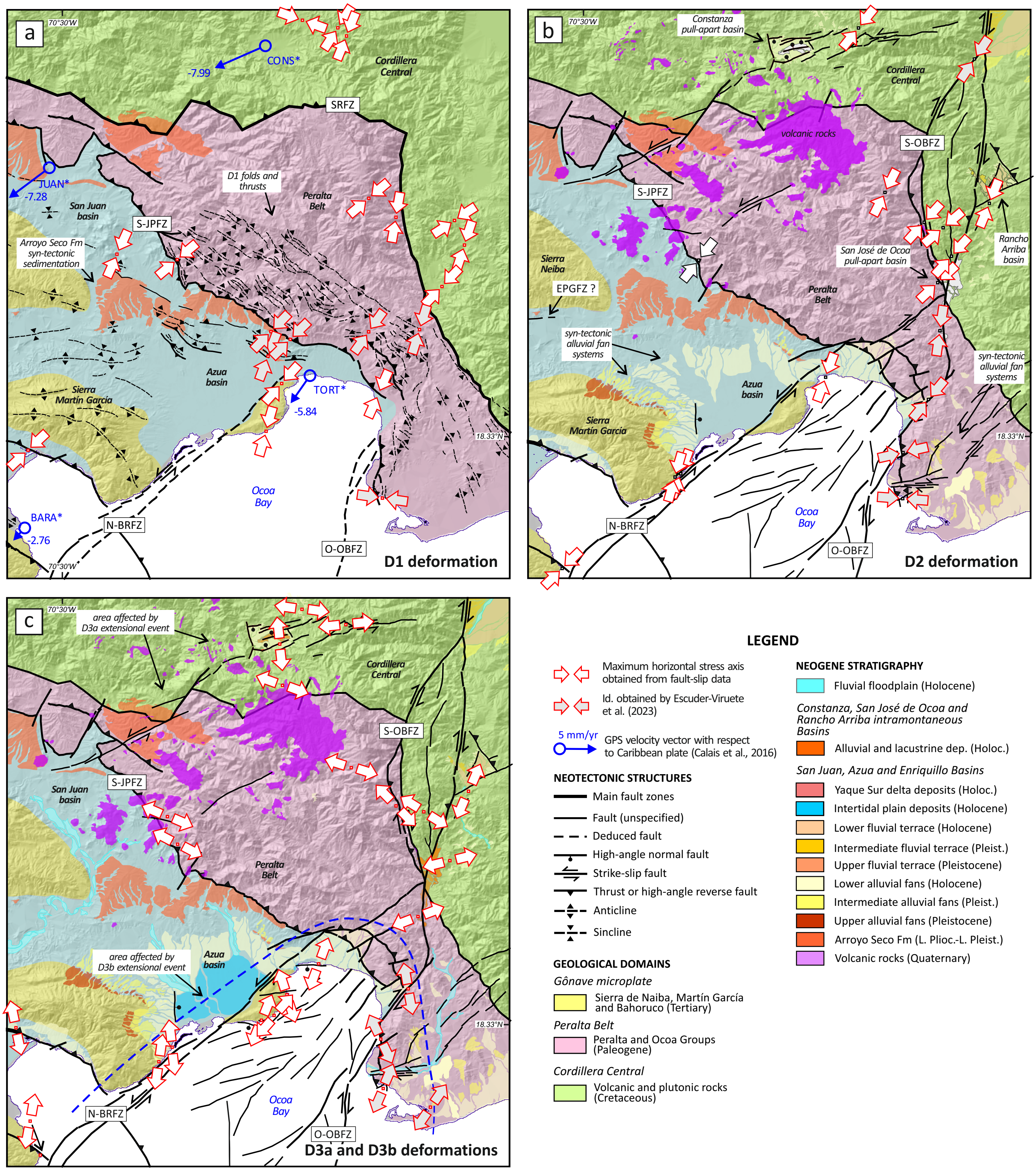
a
70°30'W
CONS*
-7.99
Cordillera Central
SRFZ
JUAN*
-7.28
San Juan basin
D1 folds and thrusts
Peralta Belt
S-JPFZ
Arroyo Seco Fm syn-tectonic sedimentation
Azua basin
TORT*
-5.84
Sierra Martín García
18.33°N
Ocoa Bay
BARA*
-2.76
N-BRFZ
O-OBFZ
D1 deformation
b
Constanza pull-apart basin
Cordillera Central
volcanic rocks
S-OBFZ
S-JPFZ
Rancho Arriba basin
Sierra Neiba
San José de Ocoa pull-apart basin
EPGFZ ?
Peralta Belt
syn-tectonic alluvial fan systems
Azua basin
syn-tectonic alluvial fan systems
Sierra Martín García
N-BRFZ
Ocoa Bay
O-OBFZ
D2 deformation
c
area affected by D3a extensional event
Cordillera Central
S-OBFZ
San Juan basin
S-JPFZ
Peralta Belt
area affected by D3b extensional event
Azua basin
N-BRFZ
Ocoa Bay
O-OBFZ
D3a and D3b deformations
LEGEND
Maximum horizontal stress axis obtained from fault-slip data
Id. obtained by Escuder-Viruete et al. (2023)
5 mm/yr
GPS velocity vector with respect to Caribbean plate (Calais et al., 2016)
NEOTECTONIC STRUCTURES
Main fault zones
Fault (unspecified)
Deduced fault
High-angle normal fault
Strike-slip fault
Thrust or high-angle reverse fault
Anticline
Sincline
GEOLOGICAL DOMAINS
Gônave microplate
Sierra de Naiba, Martín García and Bahoruco (Tertiary)
Peralta Belt
Peralta and Ocoa Groups (Paleogene)
Cordillera Central
Volcanic and plutonic rocks (Cretaceous)
NEOGENE STRATIGRAPHY
Fluvial floodplain (Holocene)
Constanza, San José de Ocoa and Rancho Arriba intramontaneous Basins
Alluvial and lacustrine dep. (Holoc.)
San Juan, Azua and Enriquillo Basins
Yaque Sur delta deposits (Holoc.)
Intertidal plain deposits (Holocene)
Lower fluvial terrace (Holocene)
Intermediate fluvial terrace (Pleist.)
Upper fluvial terrace (Pleistocene)
Lower alluvial fans (Holocene)
Intermediate alluvial fans (Pleist.)
Upper alluvial fans (Pleistocene)
Arroyo Seco Fm (L. Plioc.-L. Pleist.)
Volcanic rocks (Quaternary)

Figure17.

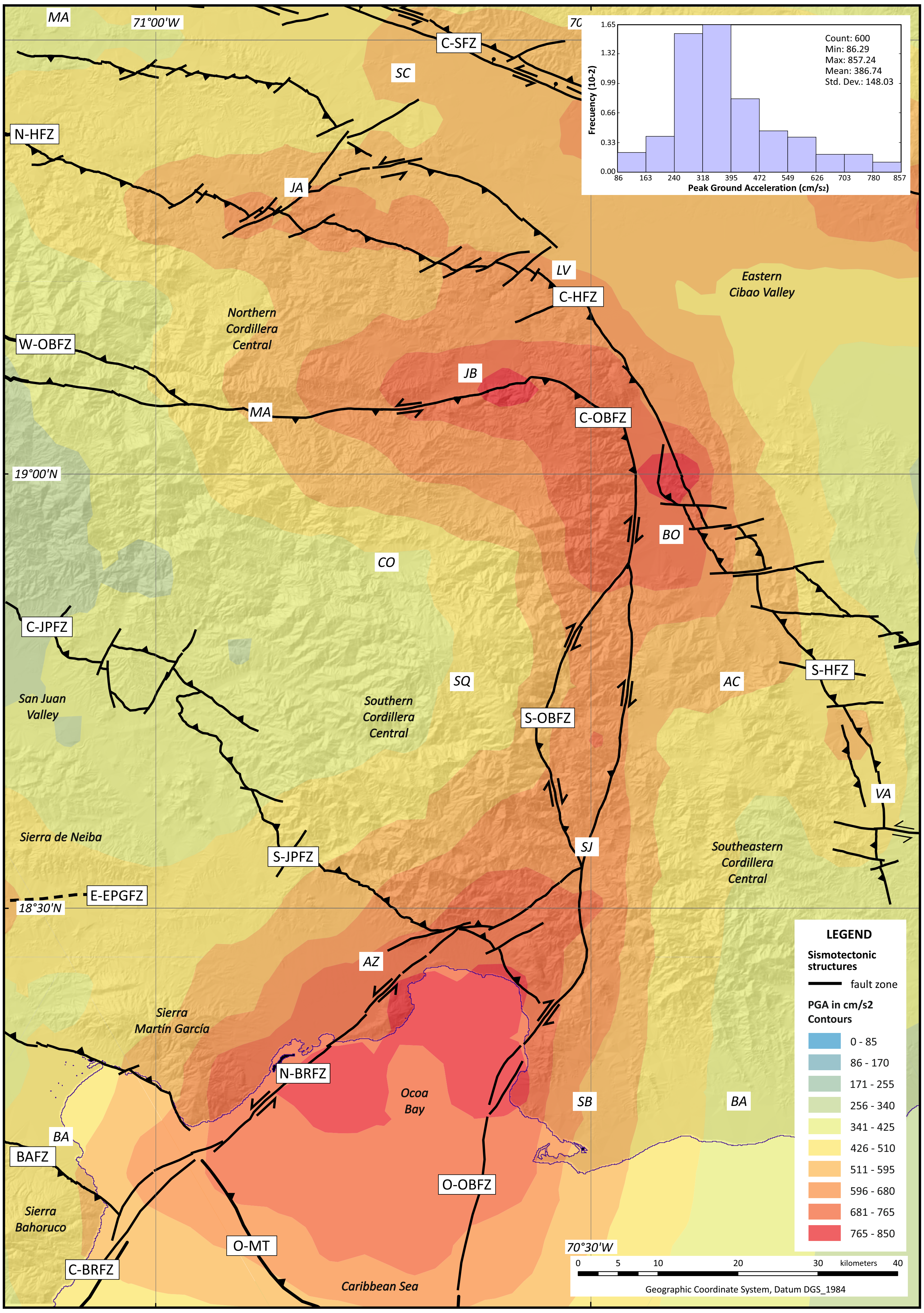

MA
71°00'W
70
C-SFZ
SC
N-HFZ
JA
LV
C-HFZ
Eastern
Cibao Valley
Northern
Cordillera
Central
W-OBFZ
JB
MA
C-OBFZ
19°00'N
BO
CO
C-JPFZ
SQ
AC
S-HFZ
San Juan
Valley
Southern
Cordillera
Central
S-OBFZ
VA
Sierra de Neiba
SJ
Southeastern
Cordillera
Central
S-JPFZ
E-EPGFZ
18°30'N
AZ
Sierra
Martín García
N-BRFZ
Ocoa
Bay
SB
BA
BA
BAFZ
O-OBFZ
Sierra
Bahoruco
O-MT
C-BRFZ
Caribbean Sea
70°30'W
Count: 600
Min: 86.29
Max: 857.24
Mean: 386.74
Std. Dev.: 148.03
Frecuency (10-2)
Peak Ground Acceleration (cm/s2)
LEGEND
Sismotectonic structures
fault zone
PGA in cm/s2 Contours
0 - 85
86 - 170
171 - 255
256 - 340
341 - 425
426 - 510
511 - 595
596 - 680
681 - 765
765 - 850
kilometers
Geographic Coordinate System, Datum DGS_1984

Table 1. Characteristics of the main seismotectonic structures in southern central Hispaniola

Code	*Fault/segment name*	*Deformation mechanism*	*Maximum estimated magnitude (M_w)*	*Major known earthquake and magnitude (M_w)*	*Estimated displacement rate*	*Lenght*	*Azimut and dip of fault zone*
S-OBFZ	Southern Ocoa-Bonao-La Guacara Fault Zone	right-lateral strike-slip	M_{max} 6,5 (± 0,5)	unknown	0.4 (± 0.2) mm/yr	60 (± 10) km	N010°E to N030°E, subvertical dip
C-OBFZ	Central Ocoa-Bonao-La Guacara Fault Zone	oblique reverse	M_{max} 6,5 (± 0,5)	unknown	0.4 (± 0.2) mm/yr	50 (± 10) km	N160°E to N010°E, subvertical dip to 40° (±15) W
W-OBFZ	Western Ocoa-Bonao-La Guacara Fault Zone	left-lateral oblique reverse to strike-slip	M_{max} 6,0 (± 1,0)	1562 earthquake?	0.2 (± 0.1) mm/yr	90 to 120 km	N100°E to N150°E, 45° (±15) SW to subvertical dip
S-HFZ	Southern Hispaniola Fault Zone	righ-lateral strike-slip?	M_{max} 7.1 (± 0.3)	unknown	< 0.2 mm/yr	50 to 70 km	N140°E (±15), subvertical dip
E-MAFZ	Eastern Sierra de Neiba-Matheux thrust	left-lateral oblique reverse to thrust	M_{max} 5.8 (± 0.3)	1942 (Mw 5.8)	0.2 mm/yr	segments of 30 (± 5) km	N120°S (±15), 65° (±10) N
S-JPFZ	Southern San Juan - Pozos Fault Zone	left-lareal oblique revrese to thust	M_{max} 6.5 (± 0.5)	1911 (Mw 6.7)	1.5 (± 1.5) mm/yr	>250 km, including segments and imbrications	N130°E (±15), 45° (±15) NE
BAFZ	Bahoruco Fault Zone or Barahona Thrust	reverse	M_{max} 7.0 (± 0.6)	1963, Mw 5.7; FD 9 km	0.2 mm/yr	50 to 85 km, including segments and imbrications	N100°E (±15), 50° (±15) S
E-EPGFZ	Eastern Enriquillo-Plantain Garden Fault Zone	left-lateral strike-slip to oblique reverse	M_{max} 7.3 (± 0.3)	1751 (Mw 7.5)?, 2010 (Mw 7.0)	8.3 (± 2.0) mm/yr	80 (± 10) km	N080°E (±10), subvertical dip
N-BRFZ	Northern Beata Ridge Fault Zone	left-lateral strike-slip to reverse	M_{max} 6.5 (± 0.1), recorded: 4.3 (12/09/2005) and 4.1 (12/10/2013)	1751 (Mw 7.5-8.0)?, 1691?	0.2 mm/yr, probably	60 (± 5) km	N040°E (±10), subvertical dip
C-BRFZ	Central Beata Ridge Fault Zone	left-lateral strike-slip to normal dip-slip	M_{max} 6.5 (± 0.1), recorded: 4.3 (12/09/2005) and 4.1 (12/10/2013)	1751 (Mw 7.5-8.0)?, 1691?	0.2 mm/yr, probably	100 (± 5) km	N030°E (±10), 70° (±15) E to subvertical dip
W-MT	Western Muertos Trough	reverse to oblique reverse	M_{max} 7.5 (± 0.5)	1673 (Mw 7.3)?; 1691 (Mw 7.7)?; 1751 (Mw 7.5-8.0)?	6.2 (± 1.0) mm/yr	170 km	N100°E (±5), 12° (±5) northward dip
W-DEEP-MT	Western Muertos Trough, deep part	reverse to oblique reverse	M_{max} 7.5 (± 0.5)	1673 (Mw 7.3)?; 1691 (Mw 7.7)?; 1751 (Mw 7.5-8.0)?	6.2 (± 1.0) mm/yr	170 km	N100°E (±5), 40° (±5) northward dip

O-MT	Muertos Trough, Ocoa Bay part	reverse to oblique reverse	M_{max} 7.5 (± 0.5)	1751 (Mw 7.5-8.0)?	6.2 (± 1.0) mm/yr	40 km	N135°E (±5), 15° (±5) northward dip

Width of fault zone
10 ± 5 km
10 ± 5 km
5 ± 2 km
10 ± 5 km
15 ± 5 km
7 ± 5 km
7 ± 5 km
10 ± 5 km
10 ± 5 km
10 ± 5 km
20 ± 15 km
20 ± 15 km

20 ± 15 km